14:30:26 OCA PAD AMENDMENT - PROJECT HEADER INFORMATION MAY 28 1995 05/16/95

Active

Project #: E-20-X66 Cost share #: E-20-355 Rev #: 3
Center # : 10/24-6-R7875-0A0 Center shr #: 10/22-1-F7875-0A0 OCA file #:
Work type : RES
Contract#: BCS-9304897 Mod #: ADM. REVISION Document : GRANT
Prime #: Contract entity: GTRC

Subprojects ? : N CFDA: 47.041
Main project #: PE #: N/A

Project unit: CIVIL ENGR Unit code: 02.010.116
Project director(s):
FROST J D CIVIL ENGR
FROST J D CIVIL ENGR

Sponsor/division names: NATL SCIENCE FOUNDATION / GENERAL
Sponsor/division codes: 107 / 000

Award period: 930801 to 960131 (performance) 970430 (reports)

Sponsor amount	New this change	Total to date
Contract value	0.00	82,589.00
Funded	0.00	47,609.00
Cost sharing amount		14,500.00

Does subcontracting plan apply ?: N

Title: ENERGY PRINCIPLES FOR MONOTONIC & CYCLIC LOADING OF COHESIONLESS SOILS

PROJECT ADMINISTRATION DATA

OCA contact: Jacquelyn L. Bendall 894-4820

Sponsor technical contact

CLIFFORD J. ASTILL
(703)306-1362

NATIONAL SCIENCE FOUNDATION
4201 WILSON BLVD.
ARLINGTON, VA 22230

Sponsor issuing office

CHARLES E. OVERCASH
(703)306-1218

NATIONAL SCIENCE FOUNDATION
4201 WILSON BLVD.
ARLINGTON, VA 22230

Security class (U,C,S,TS) : U ONR resident rep. is ACO (Y/N): N
Defense priority rating : N/A NSF supplemental sheet
Equipment title vests with: Sponsor GIT X
NONE PROPOSED
Administrative comments -
ISSUED TO CHANGE P.I. TO DR. DAVID FROST.

Supply Services Department Y

Energy Principles for Monotonic and Cyclic Loading of Cohesionless Soils
First Year Progress Report: Project CMS-9304897

INTRODUCTION

Significant advances have been made over the past 25 years in improving the understanding of the behavior of saturated cohesionless soils subjected to monotonic and cyclic loading under undrained conditions. Included in these developments are a number of procedures which use the steady state line as a reference state (e.g. Been & Jefferies, 1985; Poulos et al., 1985). The key to the use of these methods is the condition that the steady state line in undrained shear is only a function of void ratio and conflicting evidence on this matter exists in the literature (Poulos et al., 1985; Alarcon and Leonards, 1988; Dennis, 1988a, 1988b; Poulos et al., 1988; Konrad, 1990a, 1990b; Vaid et al., 1990; Frost et al., 1991).

The concept of structural collapse was formulated to explain the behavior of sands in undrained shear (Alarcon et al., 1988). Strain softening behavior during undrained loading is associated with the fact that the structure of contractive sands can be metastable. As a result, in a collapsive skeleton, small shear strains are considered to be sufficient to produce a sudden rearrangement of grains and loss of contact points between neighboring grains. For the case of undrained shearing, collapse of the structure results in the load being suddenly transferred from the sand skeleton to the water and produces a sharp increase in pore-water pressure. The substantial reduction in shear strength leads to large deformations of the sand in a short period of time.

STEADY STATE CONCEPT

The principle of steady state deformation was first formally presented in 1971 (Poulos, 1971) as an extension of the concepts of critical void ratio (Casagrande, 1940) and residual strength (Skempton, 1964). The steady state of deformation for an assembly of particles is that state in which the body is deforming at constant volume, constant normal effective stress, constant shear stress and constant velocity. It is achieved only after all particle re-orientation has reached a statistically steady state condition and after all particle breakage, if any, is complete (Poulos, 1981). If straining of the specimen is stopped, the specimen is no longer in the steady state of deformation.

There are conflicting opinions on the relative influence of the factors (composition, fabric, initial state and method of loading) affecting the stress strain behavior of sands at steady state. These differences in interpretation are based on conceptual issues as well as conflicting test results. It has been suggested (Poulos et al., 1985; Poulos, Robinsky et al., 1985; Castro, 1987; and Poulos et al., 1988) that the steady state line (SSL) is unique for a given soil and is only a function of composition and (a) the normal effective stress for drained tests or (b) the void ratio for undrained tests. However, re-interpretation of data obtained by Castro (Alarcon and Leonards, 1988) shows that the SSL in drained shear is significantly different than that obtained in undrained shear.

It has been argued (Alarcon and Leonards, 1988; Alarcon et al., 1988 and 1989) that the pore pressure response of sand in undrained shear depends not only on the potential volume changes, as determined in drained tests, but also on the tendency of the sand structure to collapse as displayed by the very rapid change in compressibility with respect to shear strain at small strain amplitudes. This collapse potential is a function of composition, fabric, and initial state of stress of the sand and thus these factors all influence the position of the steady state line.

Results presented by Dennis (1988a and 1988b) show significant variations in the slope and

position of the SSL resulting from what were considered minor changes in the preparation procedure. Other test results (Chen et al, 1988; Castro, 1988) show, in general, a unique steady state line even though a range of specimen preparation, initial stress and load methods were used. The effect of the rate and method of loading as well as the applied stress path were also examined by Torrey (1981). The results of that study indicated that the method of loading (incremental versus ramp loading using stress controlled tests) and the total stress path applied influenced the position of the SSL as much, if not more, than the rate of loading. The suggested dependence of the SSL location on the total stress path is of particular interest in view of the current state of practice whereby its position is usually determined from the results of axial compression triaxial tests, while cyclic tests are frequently performed using different devices (such as torsional shear devices which simulate earthquake loading more closely) and hence different stress paths. More recent results (Vaid et al., 1990) also suggest that the steady state line of a given sand is not unique. These tests show that for a given void ratio, the steady state strength is smaller in extension than in compression. Similarly, Konrad (1990a and 1990b) has shown differences in steady state strengths depending on the initial states of the specimens. Frost et al. (1991) presented the results of monotonic and cyclic torsional shear tests which showed the influence of initial fabric on the degree to which specimens collapsed.

STRUCTURAL COLLAPSE CONCEPT

The concept of structural collapse was formulated to explain the behavior of sands in undrained shear (Alarcon, 1986). Strain softening behavior during undrained loading is associated with the fact that the structure of contractive sands can be metastable. In a collapsive skeleton, small shear strains may be sufficient to produce a sudden rearrangement of grains and loss of contact points between neighboring grains. In undrained shearing, collapse of the structure results in the load being suddenly transferred from the sand skeleton to the water, resulting in a sharp increase in pore water pressure. Consequently, the shear strength is reduced substantially and the sand undergoes large deformations. In the process of deformation, the sand grains reach a statistically steady-state orientation after which the shear stress needed to continue deformation eventually reaches a very low, constant (steady state) value (as discussed by Poulos, 1981). In discussing the collapse hypothesis, Alarcon et al. (1988) presented interpretations of the results of torsional shear tests as evidence of the proposed mechanism.

Typical results from an undrained cyclic torsional shear test at constant shear stress amplitude were presented by Alarcon et al. (1988) and are reproduced in Figure 1. First of all, it was noted that strain softening was initiated at a stress ratio (ϕ'_{mob}) that was higher than the stress ratio at the peak monotonic strength ($\phi'_{mob} = 16.6^{o}$ vs 13^{o} obtained in a monotonic test on a replicate specimen). However, more significantly, collapse occurred when the stress state during cyclic loading reached the effective stress path from the monotonic test; thereafter, the two stress paths were essentially the same. The initiation of strain softening behavior was clearly characterized by a sharp increase in pore water pressure and the development of large shear strains (point A in Figure 1). The abrupt increase in the rate of pore pressure generation and the corresponding development of large shear strains was considered to be strong evidence in support of the concept of structural collapse.

Tests performed at different shear stress amplitudes yielded similar results (Alarcon, 1986). At a given void ratio, the monotonic stress path seemed to constitute a collapse boundary that determined the initiation of strain softening behavior under cyclic loading, provided that the stress paths were similar and the cyclic shear stress amplitude was larger than the steady-state strength. Consequently, ϕ'_{mob} at the instant of collapse was not a constant value but a variable one depending upon the cyclic shear stress amplitude.

In torsional shear tests on isotropically consolidated specimens the axis of the major principal

stress changes its orientation from -45° to +45° from the vertical in the course of reversing the shear stress from clockwise to counterclockwise, hence the collapse boundary shown in Figure 1 corresponded to this specific rotation of the principal stresses. For different amounts of rotation of the major principal stresses it was considered likely that this boundary would also change. Evidence for this can also be found in the work by Symes et al. (1984). Accordingly, triaxial tests and torsional shear tests would likely yield different undrained cyclic shear strengths, even in the absence of initial inherent anisotropy of the sand. For the same reasons, the collapse boundary would not be independent of the initial state of stress, since it would be influenced by the magnitude of the rotation of the planes of principal stress and their orientation with respect to the principal axes of anisotropy.

On the basis of the foregoing evidence Alarcon et al. (1988) explained why the undrained steady state strength (F line) might be considerably smaller than the strength obtained from constant volume drained tests (S line) as was shown elsewhere using Castro's data (Alarcon and Leonards, 1988). It was postulated that the pore water pressure response of sand specimens in undrained shear not only depended on the magnitude of the potential volume changes but also on the tendency for very rapid changes in compressibility close to the mobilization of the peak monotonic strength. Thus structural collapse or instability would be of little consequence in drained shear however would result in a sharp increase in pore water pressure in undrained shear and consequently a large decrease in the undrained shear strength.

FURTHER EVIDENCE OF STRUCTURAL COLLAPSE

The results of undrained torsional shear tests were presented by Frost et al. (1991) and are discussed within the framework of structural collapse and its influence on steady state.

Structural Collapse in Cyclic Tests

As discussed earlier, evidence of structural collapse is found in cyclic tests (Figure 1) where the initiation of strain softening behavior is characterized by an increase in the rate of pore pressure generation. This was confirmed by the results of a large number of cyclic torsional shear tests performed at different initial effective confining stresses and void ratios using different specimen preparation techniques. The manner in which the pore pressure generation rate increases for a given void ratio is related to the actual stress state at which the stress path during cyclic loading reaches the effective stress path from the monotonic test (Point A in Figure 1b). This is illustrated by the results in Figure 2, where slopes of pore pressure versus time curves immediately before and immediately after the initiation of collapse are compared. As the stiffness of the sample decreases (larger values of pore pressure ratio), the degree to which the sample collapses is reduced, as evidenced by the change in the rate of pore pressure generation at the initiation of collapse.

Effect of Initial Fabric on Steady State

As noted earlier, there is conflicting evidence in the literature as to the effect of specimen preparation and stress path on steady state. The results of undrained monotonic torsional shear tests performed to determine the steady state line for Ottawa 20-30 sand are summarized in Figures 3 and 4. In particular, Figure 3 compares results from tests performed on specimens at approximately the same void ratio but prepared using different techniques. The specimens exhibit significantly different behavior in terms of both peak strength and post-peak strain softening. The axial strains during isotropic compression were comparable regardless of the method of preparation. It is postulated that differences in non-uniformity of local fabric play a role in the observed behavior, however the small differences in void ratio (0.646 versus 0.653) certainly contributed to these differences as well. It is also noted that the stress-strain curve for

the specimen prepared using the dry tubing method exhibits larger local fluctuations when compared to the specimen prepared with the modified air pluviation method and this is believed to reflect the importance of fabric at a more local level even at shear strain levels approaching steady state.

When the results from these tests are plotted, along with results of other tests on the same sand (Figure 4), the steady state points for specimens prepared with the tubing technique (Tests 64 and 66) are outside the steady state line representative of tests prepared using the modified air pluviation technique, and thus indicate a separate steady state line is appropriate for specimens prepared in this manner. These results agree with data reported by Dennis (1988a and 1988b) and suggest that the steady state during undrained shear is not only a function of void ratio but is also related to the initial structure of the sand. This finding deviates from the usual assumption regarding uniqueness of the steady state line.

The importance of initial structure is further evidenced by the result of tests B36 and B36a shown in Figure 6. A specimen was consolidated initially under an isotropic confining stress of about 50 kPa with a void ratio of 0.659 (Dr = 33%). During loading the specimen reached a quasi-steady state of deformation and was able to sustain a shear stress of about 11.8 kPa at a mean normal stress of 28.1 kPa. The shear stress was then removed from the specimen and it was reconsolidated under the same isotropic confining stress of about 50 kPa to a void ratio of 0.637 (Dr = 43%). On reloading, the denser specimen again reached a quasi-steady state of deformation but was able to sustain a shear stress of only 6.9 kPa at a mean normal stress of 12.1 kPa. On a state diagram (point B36a in Figure 4), the steady state point for the reload test plots far below the steady state line determined for virgin specimens including the initial test. This suggests that the structure of the reloaded specimen, while denser, was more conducive to pore pressure development during undrained loading.

A similar sequence of cyclic undrained torsional shear tests was also performed. A specimen was isotropically consolidated to a mean confining stress of 100 kPa and a void ratio of 0.682 (Dr = 24%). The maximum shear modulus was determined to be 82.4 MPa. The specimen was then subjected to a cyclic shear stress of about 14 kPa. Strain softening behavior was initiated at a shear strain of about 0.3% after the application of 9 cycles as shown in Figure 5, at which stage the rate of pore pressure development increased sharply. A steady state condition was reached at a shear strain of about 5% and the test was terminated at a shear strain of 13%. The shear stress was then removed from the specimen and it was reconsolidated isotropically to a mean effective confining stress of 99.5 kPa. The void ratio at this stage had decreased to 0.641 (Dr = 41%) and the maximum shear modulus was determined to be 77.5 MPa. It is noted that for this combination of confining stress and void ratio for Ottawa 20-30 sand, a G_{max} value of about 90 MPa would have been expected (Frost, 1989). This reduction in G_{max} is attributed to a change in the grain structure during the initial loading, thus while the specimen is denser following reconsolidation, it has a structure which is less stiff in the direction of the applied torsional vibration loading. It was then intended to subject the specimen to a cyclic shear stress of about 14 kPa as in the previous test, however, during the first load cycle, strain softening accompanied by the development of large pore pressure was observed (Figure 6) with the specimen reaching steady state at a shear strain of about 3.5%.

Several aspects of the results in Figures 5 and 6 are of interest. They confirm that the application of large shear strains during the initial loading resulted in a particle arrangement which while denser was more conducive to pore pressure build-up during subsequent undrained loading. During the initial loading, the specimen reached the steady state of deformation at which stage it was able to sustain a shear stress of about 5.2 kPa at a mean normal stress of 15 kPa. Following reconsolidation, the denser specimen was able to sustain a shear stress of only 2.6 kPa at a mean normal stress of 12 kPa. Again, it can be seen on the state diagram that the steady state point

(point B11a in Figure 4) for the reload test plots far below the steady state line determined for virgin specimens (Point B11). This difference is again of interest in view of the fact that it contradicts the assertion that the steady state condition is only a function of initial void ratio for undrained tests. The results of these tests further substantiate that the fabric may also be reflected in the behavior at steady state.

FABRIC QUANTIFICATION

The results of torsional shear tests presented above as evidence of the concept of structural collapse indicate that the degree to which a specimen collapses, and hence its steady state position in the state diagram, is dependent on the loading conditions and the initial fabric of the sand. This finding is consistent with other published test results and suggests that research to quantify the fabric of cohesionless soil specimens is fundamental to the use of energy principles in quantifying failures associated with liquefaction.

A soil mass is essentially composed of discrete soil particles, the mechanical behavior of which is influenced to a great extent by the arrangement of individual particles, particle groups, and pore spaces. This arrangement is usually termed "fabric". Previous work brought recognition of the importance of fabric in the observed response of particulate media under monotonic and cyclic loading. However, most studies on soil fabric still yield results that are more qualitative than quantitative. The reason for this disappointing progress to date is in part due to the fact that the existing quantitative techniques were too laborious. The research being conducted as part of this project is exploring a new, viable procedure of quantifying soil fabric with the aid of image analysis. New procedures which integrate aspects of image analysis, mathematical morphology and stereology are providing valuable insight into the fabric of soil.

The fabric of specimens of granular materials are being quantified by employing image analysis techniques to examine local void ratio distributions, anisotropy (fabric tensor), and uniformity. A new method using image processing and analysis techniques was developed to determine local void ratio distribution (Kuo and Frost, 1994). This method eliminates the operator judgment and the manual work of earlier procedures, and makes local void ratio distribution more viable as a parameter to quantify sand fabric. Typical results are shown in Figures 7 and 8.

The image analysis based measurement techniques are also being used to determine some stereology based fabric tensors: surface area tensor, mean free path tensor, and porosity tensor. Computer algorithms will be developed that will allow for determination of these fabric tensors using image analysis techniques. Experimental examinations of uniformity at a small scale will be conducted by employing the stereological principle, the equivalence between volume fraction and area fraction, on microscopic images of soil specimens. A sampling strategy has been proposed which will allow porosity variations in the vertical direction as well as in the radial direction of soil specimens to be examined.

REFERENCES

Alarcon, A. (1986), "Cyclic Stress-Strain and Liquefaction Characteristics of Sands", Ph.D. Thesis, Purdue University, 591 pp.

Alarcon, A. and Leonards, G. A. (1988), Discussion of "Liquefaction Evaluation Procedure", ASCE, JGED, Vol. 114, No. 2, pp. 232-236.

Alarcon, A., Leonards, G. A. and Chameau, J. L. (1988), "Undrained Monotonic and Cyclic Strength of Sands", ASCE, JGED, Vol. 114, No. 10, pp. 1089-1109.

Been, K., and Jefferies, M. G. (1985), "A State Parameter for Sands", Geotechnique, Vol. 35, No. 2, pp. 99-112.

Casagrande, A. (1940), "Characteristics of Cohesionless Soils Affecting the Stability of Slopes and Earth Fills", reprinted in Contributions to Soil Mechanics, 1925-1940, Boston Society of Civil Engineers, pp. 257-276.

Castro, G. (1987), "On the Behavior of Soils during Earthquakes", Proc. of III International Conference on Soil Dynamics and Earthquake Engineering, Princeton.

Castro, G. (1988), "Reevaluation of the Lower San Fernando Dam", Report submitted to U.S. Army Corps of Engineers, Waterways Experiment Station.

Chen, H. W., and van Zyl, D. J. A. (1988), "Shear Strength and Volume Change Behavior of Copper Tailings under Saturated Conditions", Proceedings ASCE Specialty Conference on Hydraulic Fill Structures, pp. 430-451.

Dennis, N. D. (1988a), Discussion of "Liquefaction Evaluation Procedure" (Poulos, Castro and France, ASCE, JGED, Vol. 111, No. GT6, pp. 772-792), ASCE, JGED, Vol. 114, No. GT2, pp. 241-243.

Dennis, N. D. (1988b), "Influence of Specimen Preparation Techniques and Testing Procedures on Undrained Steady State Shear Strength", ASTM SPT 977, Advanced Triaxial Testing of Soil and Rock, pp. 642-654.

Frost, J. D. (1989), "Studies on the Monotonic and Cyclic Behavior of Sands", Ph.D. Thesis, Purdue University, 333 pp.

Frost, J.D., Chameau, J.L., and Leonards, G.A., (1991), "Structural Collapse Behavior of Sands in Undrained Shear", Proceedings of Second International Conference on Recent Advances in Geotechnical Earthquake Engineering and Soil Dynamics, St. Louis, Vol. 3, pp. 1905-1911.

Konrad, J. M. (1990a), "Minimum Undrained Strength of Two Sands", ASCE, JGED, Vol. 116, No. 6, pp.932-947.

Konrad, J. M. (1990b), "Minimum Undrained Strength Versus Steady State Strength of Sands", ASCE, JGED, Vol. 116, No. 6, pp. 948-963.

Kuo, C.Y., and Frost, J.D., (1994), "Image Processing and Analyisis Techniques for Determining the Distribution of Local Void Ratio", submitted for possible publication in ASTM Geotechnical Testing Journal.

Poulos, S. J. (1971), "The Stress-Strain Curves of Soils", Geotechnical Engineers Inc., Winchester, Massachusetts, 82 pp.

Poulos, S. J. (1981), "The Steady State of Deformation", ASCE, JGED, Vol. 107, No. GT5, pp. 553-562.

Poulos, S. J., Castro, G. and France, J. W. (1985), "Liquefaction Evaluation Procedure", ASCE, JGED, Vol. 111, No. 6, pp. 772-792.

Poulos, S. J., Robinsky, E. I. and Keller, T. O. (1985), "Liquefaction Resistance of Thickened Tailings", ASCE, JGED, Vol. 111, No. GT12, pp. 1380-1394.

Poulos, S. J., Castro, G. and France, J. W. (1988), Closure of "Liquefaction Evaluation Procedure", (Poulos, Castro and France, ASCE, JGED, Vol. 111, No. GT6, pp. 772-792), ASCE, JGED, Vol. 114, No. GT2, pp. 251-259.

Skempton, A. W. (1964), "Long-Term Stability of Clay Slopes", Geotechnique, Vol. 14, No. 2, pp. 77-101.

Symes, M.P.R., Gens, A. and Hight, J. W. (1984), "Undrained Anisotropy and Principal Stress Rotation in Saturated Sand", Geotechnique, Vol. 34, No. 1, pp. 1-27.

Torrey, V. H. (1981), "Some Effects of Rate of Loading, Method of Loading and Applied Critical Stress Path on the Critical Void Ratio of Fine Uniform Sand", Ph.D. Thesis, Texas A&M University, 226 pp.

Vaid, Y. P, Chung, E. K. F., and Kuerbis, R. H. (1990), "Stress Path and Steady State", CGJ, Vol. 27, No. 1, pp. 1-7.

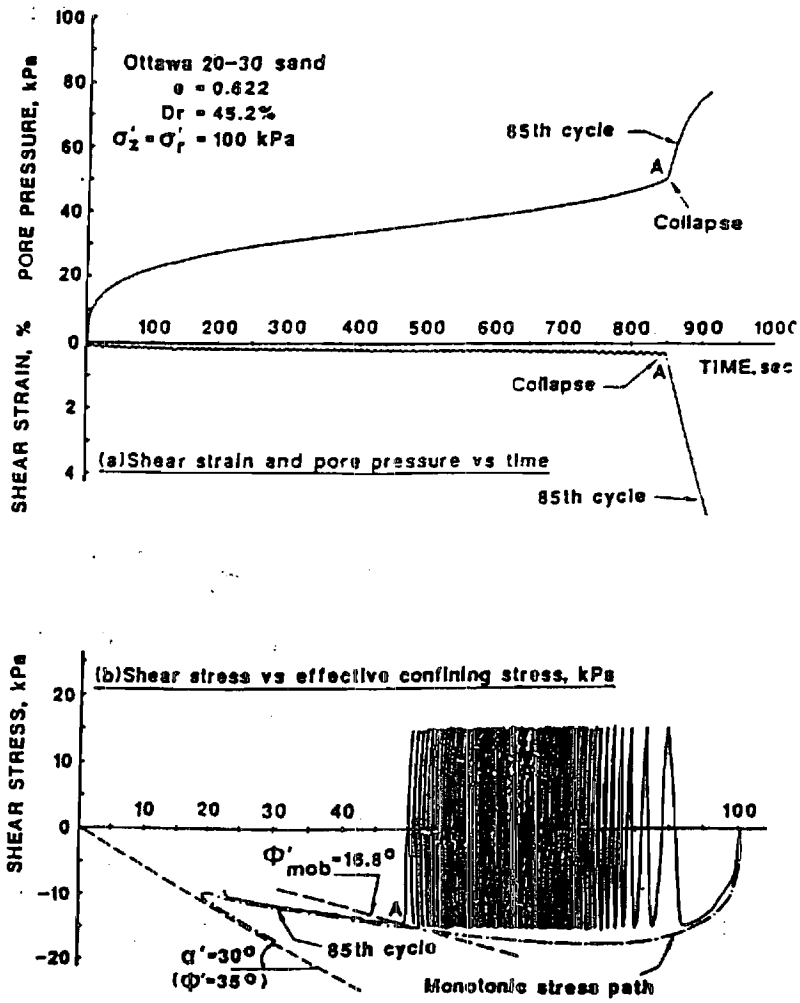

Figure 1 Undrained Cyclic Torsional Shear Test Results

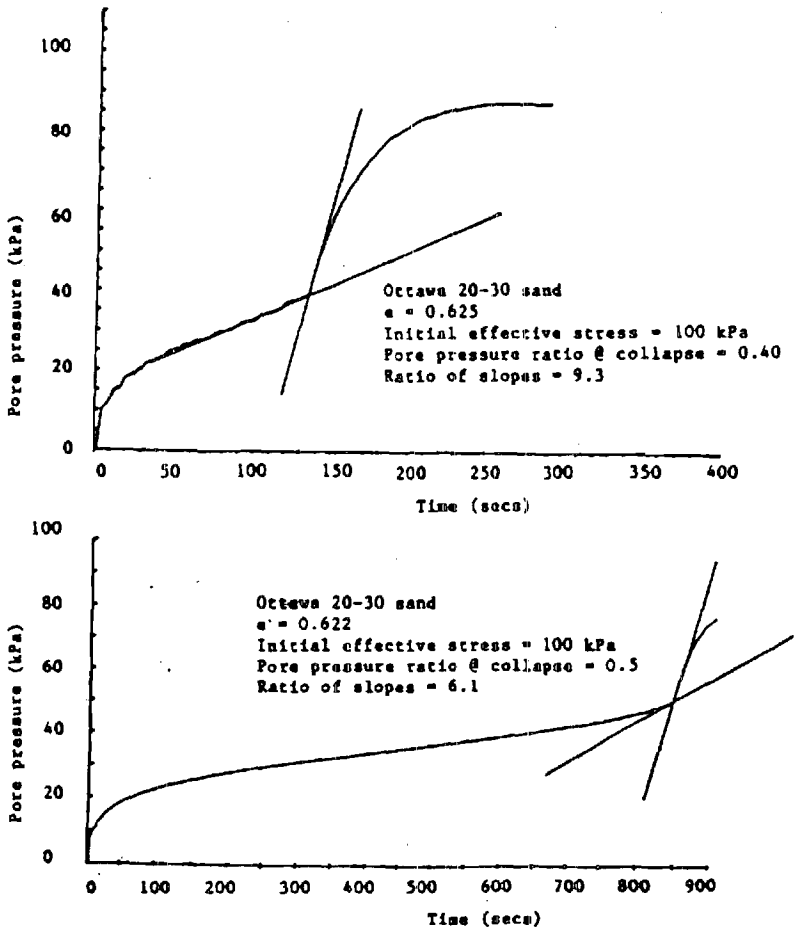

Figure 2 Collapse of Specimens as a Function of Pore Pressure Ratio

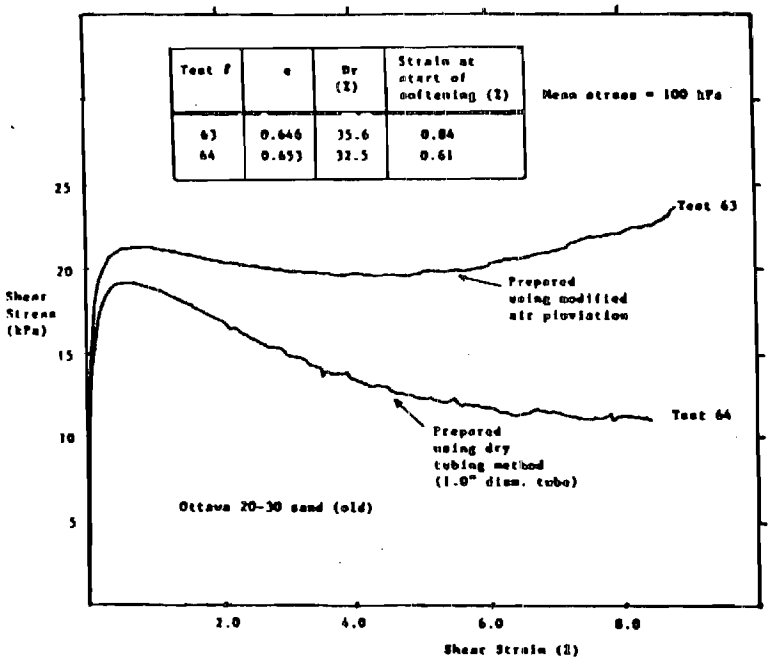

Figure 3 Effect of Method of Preparation

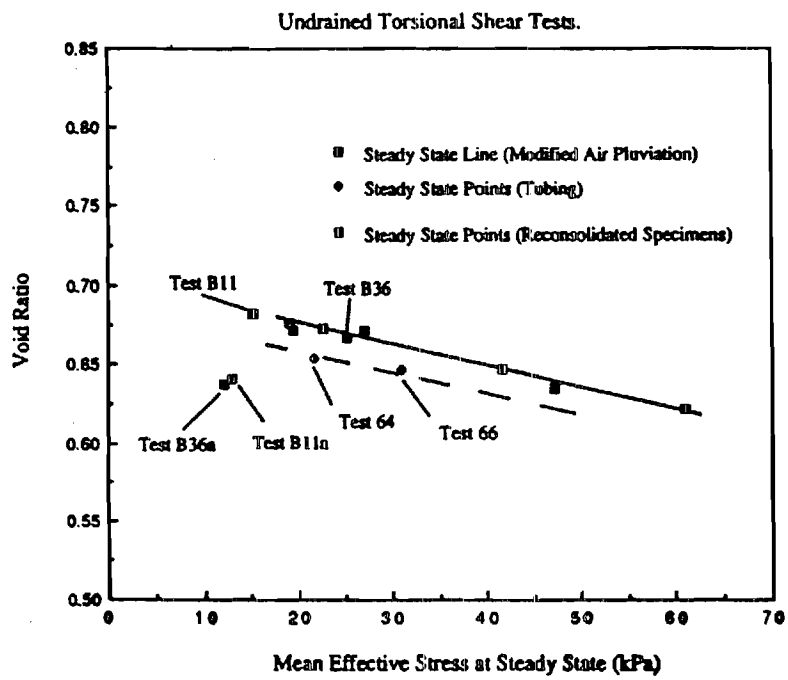

Figure 4 Steady State Line - Ottawa 20-30 Sand

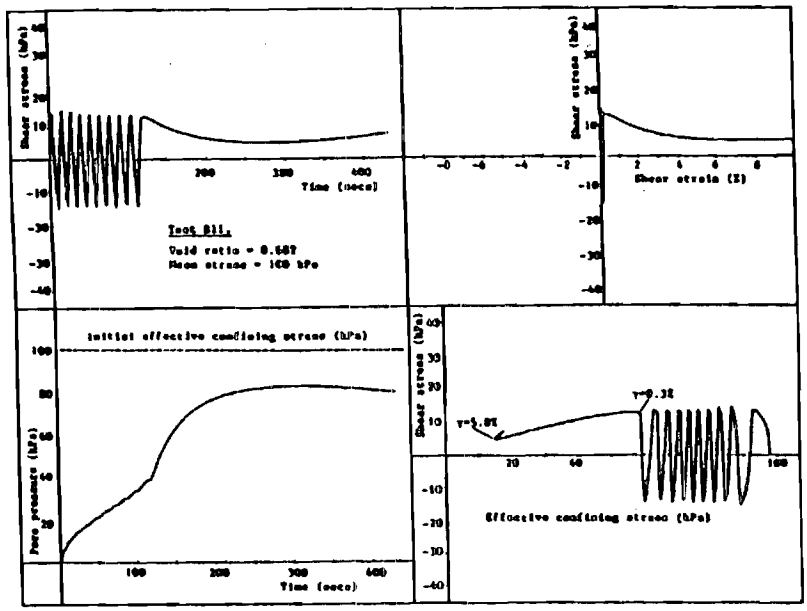

Figure 5 Undrained Cyclic Torsional Shear Test - Initial Loading

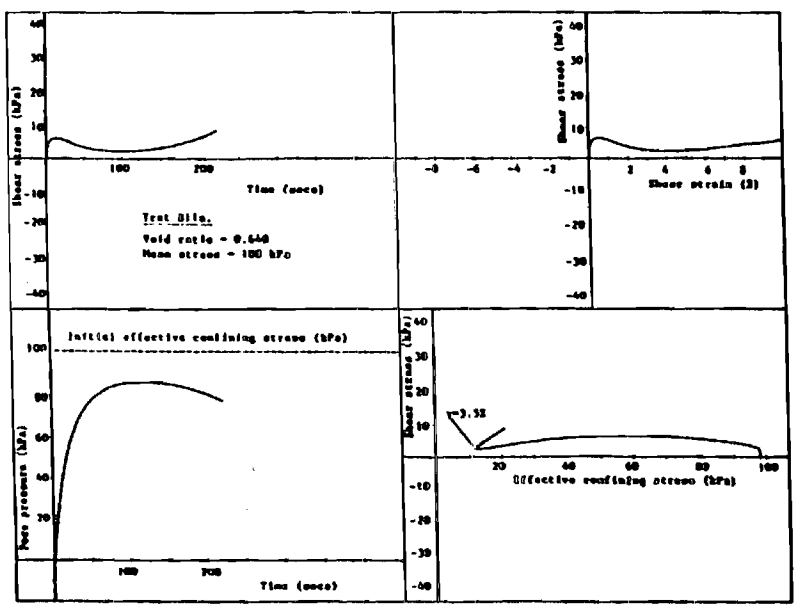

Figure 6 Undrained Cyclic Torsional Shear Test - Reloading

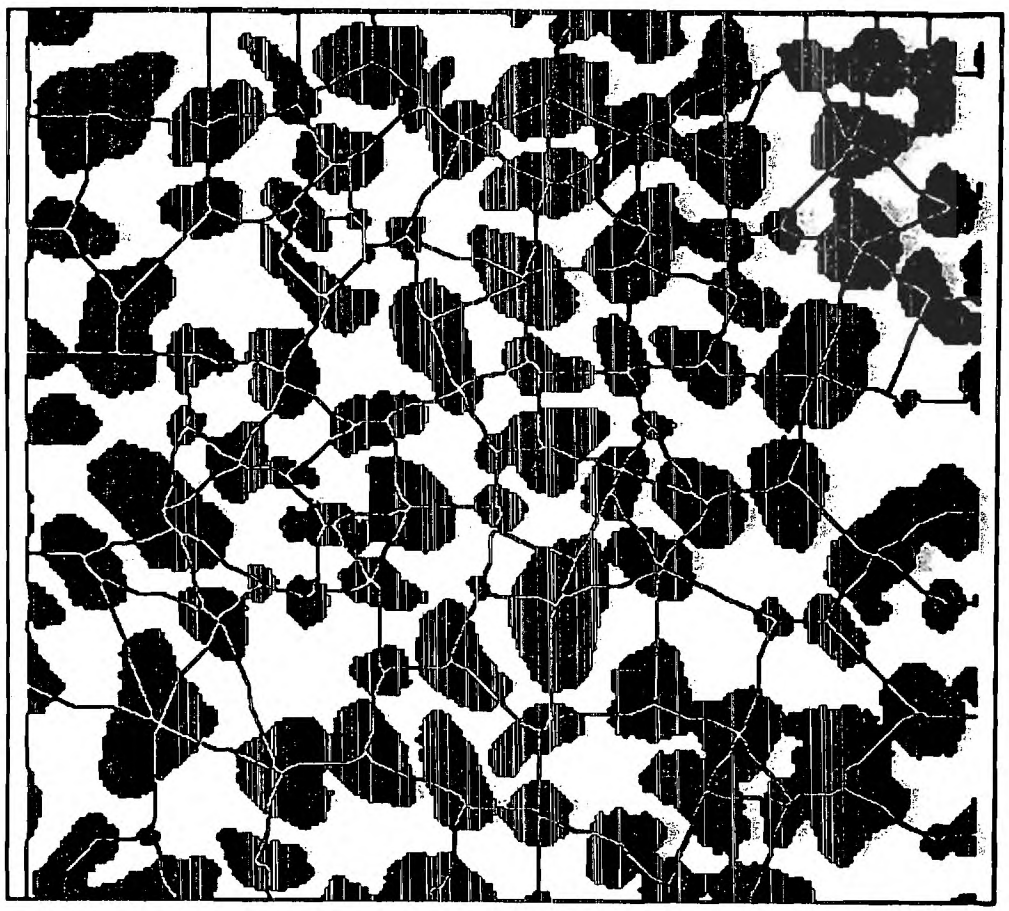

Figure 7 Network of Polygons overlying Sand Particles

E-20-X66 A-2

Georgia Tech

School of Civil & Environmental Engineering

Georgia Institute of Technology
Geotechnical Engineering Program
Atlanta, Georgia 30332-0355
USA
404•894•2282
404•894•2281 FAX

April 25, 1995

Dr. Clifford J. Astill,
Program Director, Siting & Geotechnical Systems
Earthquake Hazard Mitigation Program
National Science Foundation
4201 Wilson Boulevard, Room 545
Arlington
VA 22230

Second Year Progress Report: CMS-9304897, "Energy Principles for Monotonic and Cyclic Loading of Cohesionless Soils"

Dear Dr. Astill,

Please find attached the second year progress report for the project CMS-9304897, "Energy Principles for Monotonic and Cyclic Loading of Cohesionless Soils". The work described in the report has been performed by 2 graduate research assistant at the Georgia Institute of Technology under the direction of Dr. J. David Frost and Dr. Jean-Lou Chameau. In addition, the work has been coordinated with the activities being undertaken by a graduate research assistant at Washington State University under the direction of Dr. Balasingham Muhunthan.

Please do not hesitate to contact the undersigned by phone at (404) 894-2280, fax at (404) 894-2281 or email at dfrost@ce.gatech.edu if you have any questions about the report. We understand that the third year funding of $34,980 as outlined in the proposal budget will be released upon receipt of this report and look forward to continuing this research project with support from the National Science Foundation.

Sincerely,

J. David Frost, Ph.D., P.E., P.Eng.
Associate Professor of Civil Engineering

Energy Principles for Monotonic and Cyclic Loading of Cohesionless Soils
Second Year Progress Report: Project CMS-9304897

Introduction

Significant advances have been made in improving the understanding of the stress-strain behavior of saturated cohesionless soils. Numerous methods of testing and equipment have been developed over the past 30 years in an effort to simulate in situ conditions and characterize the soil's response to undrained static and cyclic loading. Castro (1969) performed extensive stress-controlled tests on a variety of specimens with different gradations, grain sizes and shapes of sands prepared by the moist-tamping method. The steady state line was found to be a unique function of void ratio for each material and thus a potentially useful reference line. However, conflicting evidence regarding this concept of uniqueness exists in the literature (Poulous, 1981; Poulos et al., 1985; Alarcon et al., 1988; Frost, 1989; Konrad, 1990a, 1990b; Vaid et al., 1990; DeGregorio, 1990).

The concept of structural collapse was introduced to explain the sudden increase in pore pressure associated with the initiation of strain softening under either monotonic or cyclic loading (Alarcon et al, 1988). The concept was used to explain why steady state conditions in drained shear are not necessarily the same as in undrained shear. The pore pressure response of sand in undrained shear depends not only on the potential volume changes, as determined in drained tests, but also on the tendency to collapse, i.e. tendency for a sudden change in particle arrangement (fabric). The degree to which a specimen collapses, and hence its steady state position in the state diagram, is dependent of the loading conditions and the initial fabric of the sand (Degregorio, 1990; Frost et al, 1991). Ibrahim and Kagawa (1991) showed the effects of the specimen preparation method on the fabric of sand and the change of sand fabric due to cyclic loading leading to liquefaction. With the help of microscopic measurement it was qualitatively observed that for a "randomly" arranged sand specimen prepared by dry pluviation, cyclic shear tends to line up the arrangement of sand particles, resulting in a less random arrangement of sand particles. In the case of "regularly " arranged sand specimen prepared by wet tamping methods, the opposite trend was observed.

Fabric Effect on the Behavior of Sand

Fabric refers to the arrangement of particles, particle groups, and pore spaces in a soil. Fabric is usually defined as the spatial arrangement of particles, which includes the orientation of each particle, the distribution of the contact normal, and the distribution of void ratios. The characteristics of the fabric depend on the sample preparation method.

Figure 1 compares results from tests performed on specimens at approximately the same void ratio but prepared using different techniques (Frost, 1989). The specimens exhibit significantly different behavior in terms of both peak strength and post-peak strain softening. It is also noted that the stress-strain curve for the specimen prepared using the dry tubing method exhibits larger local fluctuations when compared to the specimen prepared with the modified air pluviation method and this is believed to reflect the importance of fabric at a more local level even at shear strain levels approaching steady state. Figure 2 shows similar variations in stress-strain behavior and stress path for three specimens at almost the same void ratio but prepared by different methods (DeGregorio, 1990).

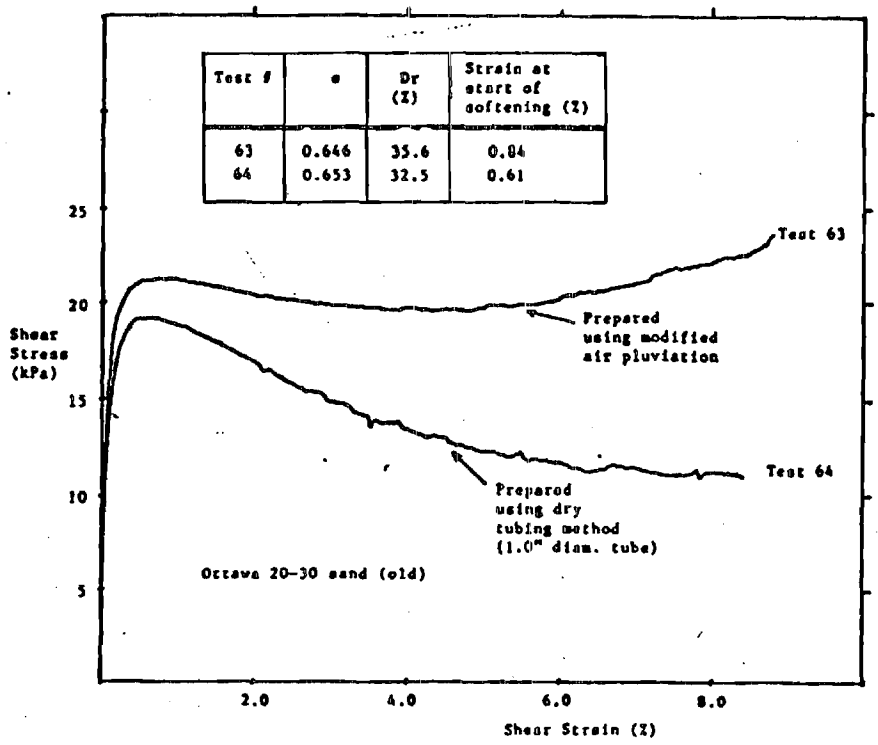

Figure 1. Effect of Method of Preparation on Stress-Strain Behavior (Frost, 1989)

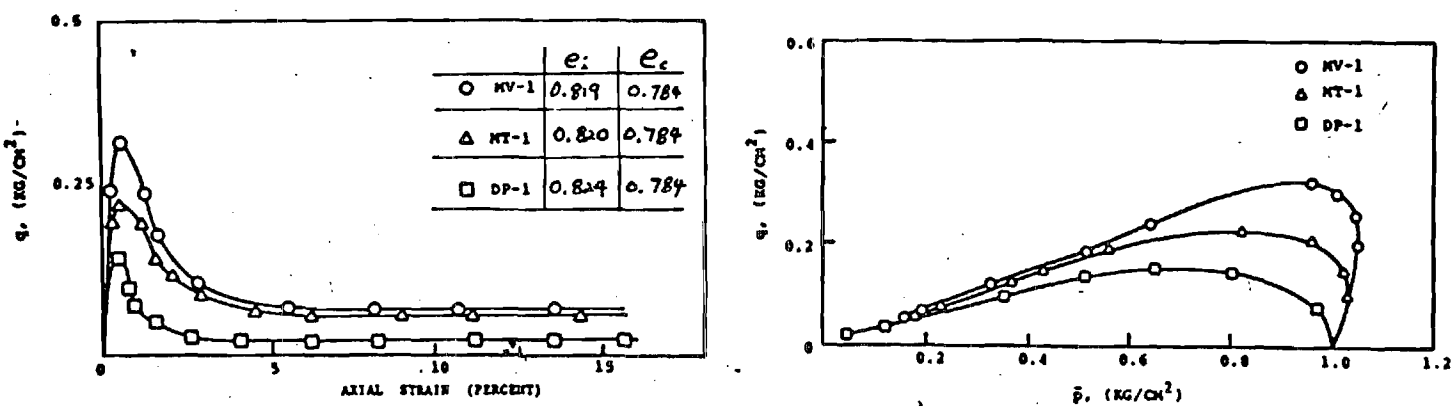

(a) (b)

Figure 2. Effect of Method of Preparation on
(a) Stress -Strain Behavior (b) Effective Stress Path (DeGregorio, 1990)

Structural Collapse in Cyclic Tests

At a given void ratio, the monotonic stress path seemed to constitute a collapse boundary that determines the initiation of strain softening behavior under cyclic loading, provided that the stress paths are similar and the cyclic shear stress amplitude is larger than the steady state strength. The initiation of strain softening behavior is characterized by an increase in the rate of pore pressure generation. The manner in which the pore pressure generation rate increases for a given void ratio is related to the actual stress state at which the stress path during cyclic loading reaches the effective stress path from the monotonic test (point C, C' in Figure 3)

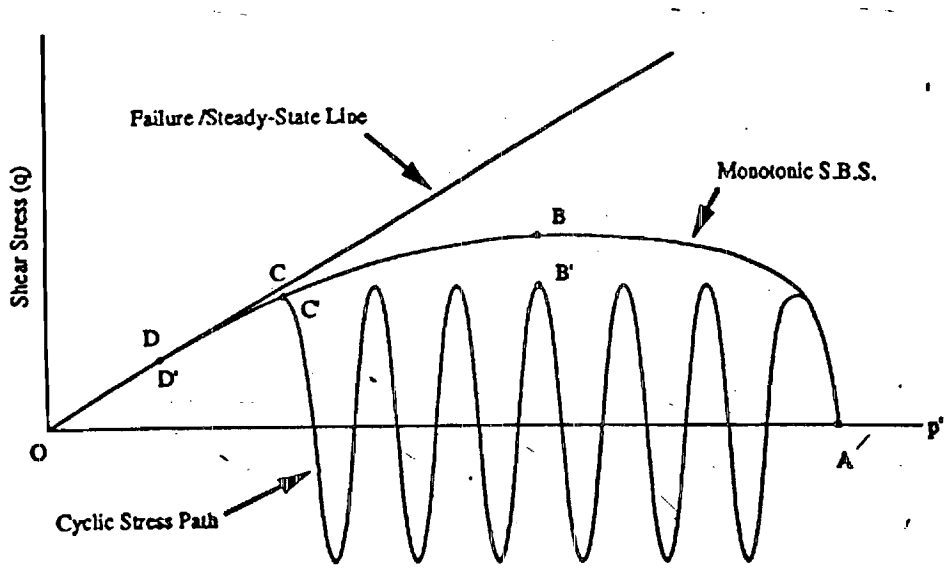

Figure 3 Schematic Stress Path for Monotonic and Cyclic (after Alarcon et al, 1988)

Fabric Quantification

The importance of fabric was noted earlier in the behavior of saturated sand under monotonic and cyclic loading. Research during the current period has resulted in the development of image analysis based methods to quantify the fabric of specimens of granular materials. Techniques to examine local void ratio distributions, anisotropy (fabric tensor), and uniformity have been developed (Kuo, 1994 - Attachment #1). The method and results are presented in detail in 2 papers that has been submitted to Geotechnique for possible publication (Attachments #2 and #3).

Now that the methodologies have been developed, they will be used during the remainder of this research effort to study the evolution of fabric in cohesionless soils under monotonic and cyclic loading and relate this to the observed collapse behavior. Accordingly, the initial and post-consolidation fabric of specimens (point O and A in Figure 3) prepared by 2 different sample preparation methods will be quantified with the help of new methodology. Further, changes in the

fabric will be observed particularly at points B, C, and D under monotonic loading and B', C', and D' under cyclic loading. Points B and B' are on the monotonic and cyclic stress paths respectively at an effective stress level corresponding to the peak strength point on the monotonic curve. Points C and C' are at the effective stress level where the cyclic effective stress path reaches the monotonic effective stress path. The steady state position is indicated as point D and D'. A summary of the tests to be performed is given in Table 1.

Table 1. Summary of Tests for 1 Sample Prepration Method

Sample Preparation	Void Ratio	Monotonic or Cyclic	Where the fabric will be examined
Method 1	e1	-	point O in Fig.4
		-	A
		Mono	B
		Mono	C
		Mono	D
		Cyclic	B'
		Cyclic	C'
		Cyclic	D'
	e2	-	O
		-	A
		Mono	B
		Mono	C
		Mono	D
		Cyclic	B'
		Cyclic	C'
		Cyclic	D'

References

Alarcon, A., Leonards, G. A., and Chameau, J. L. (1988), "*Undrained Monotonic and Cyclic Strength of Sands*", Journal of Geotechnical Engineering, ASCE, Vol. 114, No. 10, pp. 1089-1109.

Castro, G. (1969), "*Liquefaction of sands*", Harvard Soil Mechanics series, 81, Harvard University, 112 pp.

DeGregorio V. B. (1990), "*Loading Systems, Sample Preparation, and Liquefaction*", Journal of Geotechnical Engineering, ASCE, Vol. 116, No. 5, pp 805-821.

Frost, J. D. (1989), "*Studies on the Monotonic and Cyclic Behavior of Sands*", Ph. D. Thesis, Purdue University, 333 pp.

Frost, J. D., Chameau, J. L. and Leonards, G. A. (1991), "*Structural Collapse Behavior of Sands in Undrained Shear*", Proceedings 2nd International Conference on Recent Advances in Geotechnical Earthquake Engineering and Soil Dynamics, St. Louis, MIssouri, Vol. 3, pp. 1905-1911.

Ibrahim, A. A. and Kagawa, T.(1991), "*Microscopic Measurement of Sand Fabric from Cyclic Tests Causing Liquefaction*", Geotechnical Testing Journal, GTJODJ, Vol. 14, No. 4, pp. 371-382.

Konrad, J. M. (1990a), "*Minimum Undrained Strength of Two Sands*", Journal of Geotechnical Engineering, ASCE, Vol. 116, No. 6, pp. 932-947.

Konrad, J. M. (1990b), "*Minimum Undrained Strength Versus Steady State Strength of Sands*", Journal of Geotechnical Engineering, ASCE, Vol. 116, No. 6, pp. 948-963.

Kuo, C. Y. (1994), "Quantifying the Fabric of Granular Materials - An Image Analysis Approach", Ph. D. Thesis, Georgia Institute of Technology, 254 pp.

Poulos, S. J. (1981), "*The Steady State of Deformation*", Journal of Geotechnical Engineering, ASCE, Vol. 107, No. 5, pp. 553-562.

Poulos, S. J. Castro G. and France, J. W.(1985), "*Liquefaction Evaluation Procedure*", Journal of Geotechnical Engineering, ASCE, Vol. 111, No. 6, pp. 772-792.

Vaid, Y. P., Chung, E. K. F., and Kuerbis, R. H.(1990), "*Stress Path and Steady State*", Canadian Geotechnical Journal, Vol. 27, No. 1, pp. 1-7.

Attachment # 1

QUANTIFYING THE FABRIC OF GRANULAR MATERIALS - AN IMAGE ANALYSIS APPROACH

A Thesis
Presented to
The Academic Faculty

by

Chun-Yi Kuo

In Partial Fulfillment
of the Requirements for the Degree
Doctor of Philosophy in Civil and Environmental Engineering

Georgia Institute of Technology

August 1994

TABLE OF CONTENTS

SUMMARY

A soil mass is essentially composed of discrete soil particles, the mechanical behavior of which is influenced to a great extent by the arrangement of individual particles, particle groups, and pore spaces. This arrangement is usually termed "fabric". Previous work on fabric analysis brings recognition of the importance of fabric in the observed response of particulate media under monotonic and cyclic loading. However, most studies on soil fabric still yield results that are more qualitative than quantitative. The reason for this disappointing progress to date is clearly that the existing quantitative techniques were too laborious. This research explores a new, viable procedure of quantifying soil fabric with the aid of an image analysis system. New procedures which integrate aspects of image analysis, mathematical morphology and stereology have provided valuable insight into the fabric of soil.

The fabric of granular materials is quantified by employing image analysis techniques to examine its local void ratio distribution, its anisotropy (fabric tensor), and its uniformity. A new method using image processing and analysis techniques was developed to determine local void ratio distribution. This method eliminates the operator judgment and the manual work of earlier studies, and makes local void ratio distribution more viable as a parameter to quantify sand fabric. The definitions and measurement techniques for some stereology based fabric tensors: surface area tensor, mean free path tensor, and porosity tensor are introduced. Those measurement techniques are then implemented using an automated image analysis system. Computer algorithms are developed that allow determination of these fabric tensors easily using image analysis techniques. Experimental examinations of uniformity at a small scale are

conducted by employing the stereological principle, the equivalence between volume fraction and area fraction, on microscopic images of soil specimens. A sampling strategy is proposed which allows porosity variations in the vertical direction as well as in the radial direction of soil specimens to be examined. The proposed methods are applied to examine the uniformity and initial fabric of an actual sand specimen and demonstrate that the procedures developed in this research are viable and efficient in quantifying the fabric of granular materials.

Attachment # 2

STEREOLOGY BASED FABRIC TENSORS - PART I : DEFINITIONS AND MEASUREMENT TECHNIQUES

Chun-Yi Kuo[1], J. David Frost[1], and Jean-Lou A.Chameau[2]

Abstract

Increased recognition of the importance of fabric in the observed response of particulate media under monotonic and cyclic loading has led to the development of new procedures to quantify this role. Fabric tensors which characterize the distribution of directional data (anisotropy) from microscopic observations are considered to be a useful measure of fabric in addition to porosity for granular materials. This paper reviews several stereology based fabric tensors where formulations in three dimensions can be obtained with observations on three mutually perpendicular planes. The definitions and measurement techniques for those fabric tensors are discussed. Fabric tensors are directly usable in design applications as they can be used explicitly in continuum models to describe the discrete granular medium in a continuum sense .

A companion paper presents the implementations of these measurement techniques using image analysis.

---

1 Postdoctoral Fellow and Associate Professor, respectively, School of Civil & Environmental Engineering, The Georgia Institute of Technology, Atlanta, Georgia 30332, USA.

2 President, Golder Associates, 3730 Chamblee-Tucker Road, Atlanta, Georgia 30341, USA.

Fabric Tensors and Soil Modeling

There is increasing evidence that the mechanical behavior of granular materials depends to a great extent on the relative arrangement of voids and particles which is usually termed "fabric". Some attempts have been made to develop a fabric tensor which describes the packing of granular materials. Fabric tensors which characterize distribution of directional data are measures of the anisotropy of the microstructure and are considered to be a useful measure of fabric in addition to porosity for granular materials. Moreover, they can be used explicitly in a continuum model thus allowing the discrete granular medium to be described in a continuum sense. Some of the efforts in developing the constitutive formulation of granular materials taking the fabric tensor into account are reviewed in this section.

Oda et al. (1984) theoretically formulated elastic compliance for cracked materials like rocks and rock masses in term of the generalized fabric tensor which explicitly expressed the crack geometry. On the assumption that the elastic interaction between cracks is negligibly small, Oda concluded the principal axes of a fabric tensor of second-rank exactly coincide with the symmetry axes of the elastic compliance tensor of fourth-rank. He also found that the supersonic wave velocity is closely related to the character of the fabric tensor and is useful to estimate the fabric tensor of in situ rock masses.

Cowin (1985) developed the relationship between the fourth rank elasticity tensor, the tensor that relates the stress tensor to strain tensor, and the fabric tensor. Cowin (1986) also developed a strength criterion with a dependence on fabric tensor. Sedegh et al. (1991) further extended Cowin's work and established a stress-strain-fabric relationship which is an extension of the anisotropic form of Hooke's law to include a dependence of the elastic coefficients upon a second-rank fabric tensor. The inversions related to the stress-strain-fabric relationship were considered. They showed that it is possible to construct the stress-strain-fabric relation from the strain-

stress-fabric relation and vice versa. They also showed a semi-inversion of the relationship between the fourth-rank tensor of elastic coefficients and the fabric tensor. This permits the determination of the fabric tensor by measurement of anisotropic elastic constants of materials.

Tobita (1989) carefully examined the constitutive formulation including the fabric tensors as internal variables. He pointed out that a granular mass subjected to a general stress path including the rotation of principal stress axes shows less symmetry (more anisotropy) that orthotropic symmetry, which is a consequence of the fact that there are, at least, two fabric tensors showing completely different evolution modes (Figure 1). The experimental foundations for the different evolution modes for orientation tensor and contact tensor were given by Oda et al. (1985). As a result, the combined fabric tensor $H^*_{ij}, H^*_{ij} = H^{(1)}_{ik} H^{(2)}_{kj}$, may be a good candidate for a generalized fabric tensor which preserves important features stemming from the introduction of two independent fabric tensors. Tobita also concluded that in two dimensions, the introduction of fabric tensor being non-coaxial with the stress tensor is essential to describe the non-coaxial and dilatant behavior under the rotation of principal stress axes.

Muhunthan (1991) proposed to use the second invariant of the fabric tensor , J_f, to be a fabric parameter. He then proposed that :" soil particles, irrespective of their insitu nature of structural arrangement, tend towards an ultimate arrangement characterized by a value of the fabric invariant $(J_f)_{ult}$ specific to a certain type of loading". He further proposed a fabric state parameter ψ_f along the lines of the existing state parameter ψ (Been and Jefferies, 1985) based on the distance to the $(J_f)_{ult}$ line ($\psi_f = (J_f)_{initial} - (J_f)_{ult}$). The classical three dimensional space state variables (p,q,e) of Critical State Soil Mechanics (CSSM) were also extended to four dimensional space (p,q,e,J_f) including the fabric parameter. Muhunthan (1991) then developed a simple stress-strain model with inclusion of the fabric tensor along the

lines of Modified Cam-Clay model by using the theory of thermodynamics. The model incorporates an additional parameter β related to fabric. β is a parameter relating the rate of change of the fabric tensor ($\dot{\phi}_{ij}$) to the rate of the change of the deviatoric strain tensor ($\dot{\varepsilon}_{ij}$). The model reduces to the Modified Cam Clay with $\beta = 1$.

Recently, Oda and Ohnishi (1992) generalized the Cam-clay model for isotropically hardening soils to include the plasticity for anisotropically hardening soils by simply substituting a modified stress tensor T_{ij} for stress tensor σ_{ij} in which $T_{ij} = \frac{1}{3}F_{ik}^{-1}\sigma_{kj}$, and F_{ij} is the fabric tensor. Nakai and Funada (1992) extended an elastoplastic model for sand (kinematic t_{ij}-sand model, Nakai, 1989) to describe the behavior of sand with inherent anisotropy. In the formulation of the model, only the stress ratio tensor x_{ij} is replaced by $\overline{x_{ij}}$ which is modified by a fabric tensor b_{ij}. Only one soil parameter, the ratio of principal values of b_{ij} (b_1 / b_3), is added. The validity of the proposed model was then confirmed by the results of isotropic compression tests, triaxial tests and plane strain tests.

Review of Methodologies for Quantifying Fabric Tensors

The spatial distribution of various micromechanical quantities such as contact normals, the orientation of the long axis of particles and the shape of associated voids (see Figure 2) have been used to define a fabric tensor. The concept of " fabric tensor" evolved as a means to describe the discrete granular medium in a continuum sense. The most fundamental second order fabric tensor is given in a mathematical form as (Tobita, 1989):

$$H_{ij} = \frac{1}{4\pi}\int_{\Omega} H(\Omega) n_i n_j d\Omega \qquad (1)$$

where $H(\Omega)$ denotes the spatial distribution with respect to a specified geometrical quantity; and is defined by $H(\Omega) = \overline{H}E(\Omega)$ where $\overline{H} = \int_{\Omega} H(\Omega)d\Omega$ and $E(\Omega)$: the probability density function, n_i denotes the unit normal of an elementary solid angle $d\Omega$. The term Ω is the whole surface of the unit sphere.

Oda (1982) defined a fabric tensor F_{ij} for discontinuous geological materials by taking into account: (1) the position and density of cracks; (2) the shape and dimension of cracks; and (3) the orientation of cracks. The fabric tensor can then be calculated through the number of cracks which cross scanning lines. A similar fabric tensor was proposed for granular materials in which an assembly of particles is represented by an assembly of branches, lines connecting the centers of adjacent connecting particles. The density, dimension and orientation of branches is then used to define fabric tensor in the same manner as in the treatment of cracks.

Oda et al. (1985) further proposed to characterize the anisotropy of granular materials by : (1) the distribution of contact normals; (2) the orientation of non-spherical particles; and (3) the shape of the voids. The two-dimensional illustrations of orientation of a particle, contact normal, and branch of a particle are shown in Figure 3. Oda et al. (1985) actually characterized the orientation and shape of voids by the mean free path, the mean edge-to-edge distance between particles, $\bar{l}(\mathbf{p})$, where $\mathbf{p}$ is the unit vector of scanning lines. When lines pass through both solid particles and voids, $\bar{l}(\mathbf{p})$ is the mean path length through the voids in the direction $\mathbf{p}$. Konishi and Naruse (1988) introduced an alternative approach to quantify the shape, size and orientation of voids where a void with n curved segments is replaced by a polygon with n vectors along the chords (Figure 4).

As reviewed, the spatial distribution of various micromechanical quantities such as contact normals, the orientation of long axis of particles and the shape of associated voids have been used to define the fabric tensor. However, it is almost impossible to identify contact normals or the particle orientation for each particle in three dimensions. In practice, two dimensional equivalent tensors that can be determined by measuring contact normal distribution (or particle orientation) from vertical and horizontal sections are introduced. Then, the two dimensional equivalent tensors ($\bar{F}_{ij}$) are extended to one three dimensional fabric tensor (F_{ij}) under assumptions of (1) axial symmetry and (2) the principal values of $\bar{F}_1$ and $\bar{F}_2$ in two dimensions are proportional to the principal values F_1 and F_2 in three

dimensions (Oda & Nakayama, 1989). Furthermore, the determinations of contact normal, or branch (Figure 3) , or void polygon (Figure 4) all rely on the contact of particles in 2-D sections. However, for particles which contact in three dimensional, they may or may not show contact in a two dimensional section. In fact, most of them will show separately in a 2-D section since the probability of intercepting the contacts in a 2-D section is generally very small.

This paper employs different fabric measure for granular materials in which fabric tensors are formulated in three dimensions based on the principle of stereology. Stereological methods are precise tools for obtaining quantitative information about three dimensions based mainly on observations made on sections. Hilliard (1962, 1967) has provided a mathematical framework for the quantitative description of anisotropic structures. He dealt with the orientation distribution of lines in a plane, of surfaces in space, and of lines in space and related them to the number of intersections per unit length of test line, P_L, and the number of interactions per unit area of test plane, P_A. If intersections are counted for each different orientation of the probe line or plane, then the "structure anisotropy", i.e. the distribution of the curves or surfaces can be determined. Hilliard's method was further formulated into Cartesian tensor by Kanatani (1984a & b, 1985). Kanatani described distribution densities of directional data in terms of what he called fabric tensors. He first generalized Hilliard's method for different types of problems into a single mathematical framework called the Buffon transform, Then, he derived its inverse transform in term of Cartesian tensor equations which made it possible to determine the fabric tensors directly from the data of intersection counting.

Based on the analysis of Kanatani, stereological based fabric tensors such as surface area tensors (S_{ij}) or mean free path tensor (λ_{ij}) could be determined experimentally from microscopic observations. Muhunthan (1991) and Muhunthan and Chameau (1992b) have also outlined an experimental technique for determining the components of a void tensor from microscopic observations which makes use of classical stereology principles

and the analysis by Kanatani (1984a & b, 1985). However, Muhunthan's scheme has shown to introduce bias into the results of analysis. A revised methodology (Kuo and Frost, 1993) was then proposed to minimize bias in determine the porosity and porosity tensor (N_{ij}).

This paper reviews the analysis of Kanatani and discusses the definitions and measurement techniques of stereological based fabric tensors such as surface area tensors (S_{ij}), mean free path tensor (λ_{ij}) and porosity tensor (N_{ij}).

The measurement techniques presented in this paper to determine fabric tensors of granular materials are very efficient when they are implemented using an automated image analysis system. Implementations of these technique using image analysis are presented in a companion paper.

Stereological Approach to Evaluating Anisotropy

Before introducing the Hilliard's and Kanatani's analysis for the quantitative description of anisotropic structures, it is necessary to clearly understand the concept of angular orientation of lines and surfaces in three dimensional space.

Angular Orientation of Lines

Consider a line of any arbitrary geometry, the angular orientation of this line is different at different positions. Focusing on a small segment dl of this line, the orientation of this segment is specified by its tangent vector $\bar{t}$ and is completely defined by the angles θ and ϕ with respect to the XYZ frame of reference (see Figure 5). The different segments of this line have different (θ,ϕ) values associated with them, and hence have different orientations.

Angular Orientation of Integral Boundary Surfaces (or Interfaces)

Consider microstructure containing α and β phases, the boundaries between α and β regions are thus $\alpha\beta$ internal surfaces (or interfaces). Focusing on a small element δS of $\alpha\beta$ interface, the angular orientation of δS is equal to the angular

orientation of the normal vector $\bar{N}$ to this surface element and is specified by the angles θ and ϕ with respect to the XYZ frame of reference (see Figure 6).

Orientation Distribution Function

Suppose the angular orientation of each small element δS of all $\alpha\beta$ interfaces in a specimen is measured. Let $dN(\theta,\phi)$ be the number of surface elements having orientations in the range ϕ to $\phi + d\phi$ and θ to $\theta + d\theta$. The total area of these elements $ds(\phi,\theta)$ is equal to $dN(\phi,\theta)\cdot\delta S$. Let S_0 be the sum of area of all $\alpha\beta$ interfaces in the specimen. An orientation distribution function, is defined such that $f(\phi,\theta)$ reports the fraction of $\alpha\beta$ interface area in the orientation range ϕ to $(\phi + d\phi)$ and θ to $(\theta + d\theta)$. In other word, $f(\phi,\theta) = dN(\phi,\theta)\cdot\delta S/S_0$.

Anisotropy and stereology

The orientation of $\alpha\beta$ interface elements are said to be random if the orientation distribution function $f(\phi,\theta)$ is constant. When the orientation distribution function $f(\phi,\theta)$ is constant , the structure is considered statistically isotropic.

However, anisotropy usually exists for most materials. Thus, one major challenge facing stereologists is how to estimate stereological properties in an unbiased and efficient manner since isotropic, uniformly random (IUR) planes are difficult to achieve in practice. The development of vertical sections for surface area (S_v) estimation (Baddeley et al., 1986) and vertical slices from projected images for length (L_v) estimation (Gokhale, 1990 & 1992) are among the important developments for estimating stereological properties for anisotropic structures.

Another challenge resulting from the anisotropic nature of materials is how to quantify the anisotropy. As noted earlier, Hilliard (1962, 1967) has provided a mathematical framework for the quantitative description of anisotropic structures. Hilliard's analysis for orientation distribution of surfaces in space is summarized as follows : (after Underwood 1970)

The total area of a system of surfaces per unit volume is defined as

$$S_V = \int_0^{2\pi} \int_0^{\pi/2} S_v(\psi,\omega)\sin\psi d\psi d\omega \qquad (2)$$

where the angles ψ and ω refer to normals to the boundary elements. $S_v(\psi,\omega)$is the orientation distribution of the system of surfaces in spaces.

The analysis of orientation distribution of the system of surfaces uses a test array of parallel straight lines whose orientation is referred to the same axes as for the system of surfaces. Referring to Figure 7, and focusing on one surface element δS of $\alpha\beta$ interface, if one considers a test array of (say M) test lines all parallel to the Z axis and of length L. The probability of intersection of a test line with the surface element δS is $\delta S_{proj}/L^2$, where δS_{proj} is the projected area of δS on the XY plane and $\delta S_{proj} = |\cos\gamma| \cdot \delta S$, where γ is the angle between line segments and the normals to areal elements. The number of intersections of test lines with the surface element δS is thus $\delta S \cdot |\cos\gamma| \cdot M / L^2$. The number of intersections per unit test line length of test lines with all the surface elements having orientations in the range ψ to $\psi + d\psi$ and ω to $\omega + d\omega$ is $\delta S(\psi,\omega) \cdot |\cos\gamma| / L^3$ which is $S_V(\psi,\omega) \cdot |\cos\gamma|$. So, at a specified angular position,

$$P_L(\phi,\theta) = \int_0^{2\pi} \int_0^{\pi/2} S_V(\psi,\omega)|\cos\gamma|\sin\psi d\psi d\omega \qquad (3)$$

where $P_L(\phi,\theta)$ is the expected number of intersections per unit length of the test lines.

Buffon Transform and Fabric Tensors

Hilliard's (1962, 1967) analysis of the orientation distribution of lines in a plane, surfaces in space, and lines in space were generalized into a single mathematical framework called the Buffon transform by Kanatani (1984a & b, 1985) as :

$$N(\mathbf{m}) = \int |\mathbf{m}\cdot\mathbf{n}| f(\mathbf{n})\, d\mathbf{n} \tag{4}$$

Where f(**n**) is the distribution density with unit normal **n**, and N(**m**) is the expected number of intersections of directional **m**. Note that eqn. 3 for the case of distributed surfaces in space is equivalent to eqn. 4. In particular, $|\mathbf{m}\cdot\mathbf{n}|$ is equivalent to $|\cos\gamma|$. For the case of distributed surfaces in the space, f(**n**) is the distribution density of surface density with unit normal **n**, i.e. f(**n**) d**n** is the " total area " of those surface elements whole normal vector is lying in the differential solid angle dn per unit volume. Obviously, f(**n**)= f(-**n**) and $\int f(\mathbf{n})d\mathbf{n}$ is the total area of the surfaces per unit volume. If a line of direction **m** (a unit vector) is randomly placed in space, then N(**m**) will be the expected number of intersections with the surface per unit length.

Kanatani (1984a & b, 1985) expanded the distribution density into a polynomial in **n** in such a way that each term is orthogonal to the rest. In other words, it is a Cartesian tensor expression of the spherical harmonics expansion in the 3-dimensional case and the Fourier series expansion in the 2-dimensional case. He called the coefficient tensors fabric tensors. A symmetric distribution density f(**n**) is expressed in the form

$$f(\mathbf{n}) = \frac{C}{4\pi}\left[1 + D_{ij}n_i n_j + D_{ijkl}n_i n_j n_k n_l + \ldots.\right] \tag{5}$$

where C and the fabric tensor $D_{i_1\ldots i_n}$ are given respectively by

$$C = \int f(\mathbf{n})d\mathbf{n} \tag{6}$$

$$D_{i_1\ldots i_n} = \frac{2n+1}{2^n}\binom{2n}{n} N_{i_1\ldots i_n} \tag{7}$$

and $N_{i_1\ldots i_n}$ is the moment tensor defined by

$$N_{i_1 \ldots i_n} = \frac{1}{C} \int n_{i_1} \ldots . n_{i_n} f(\mathbf{n}) d\mathbf{n} \tag{8}$$

It was also shown that

$$\int |\mathbf{m} . \mathbf{n}| \, n_{i_1} \ldots . n_{i_n} d\mathbf{n} = \frac{2\pi}{a_n} m_{i_1} \ldots . m_{i_n} \tag{9}$$

$$a_n = \frac{(-1)^{\frac{n}{2}-1} 2^{n-1} (n-1)(n+2)}{\binom{n}{n/2}} \tag{10}$$

For example, $a_0 = 1$, $a_2 = 4$, $a_4 = -24$, $a_6 = 64$ etc....

Hence, the Buffon transform of equation (5) is

$$N(\mathbf{m}) = \frac{2\pi C}{4\pi} \left[1 + \frac{1}{4} D_{ij} m_i m_j - \frac{1}{24} D_{ijkl} m_i m_j m_k m_l + \ldots \right] \tag{11}$$

Conversely, if N(**m**) is given in the form

$$N(\mathbf{m}) = \frac{C}{4\pi} \left[1 + D_{ij} m_i m_j + D_{ijkl} m_i m_j m_k m_l + \ldots \right] \tag{12}$$

then, its inverse Buffon transform is given by

$$f(\mathbf{n}) = \frac{C/2\pi}{4\pi} \left[1 + 4 D_{ij} n_i n_j - 24 D_{ijkl} n_i n_j n_k n_l + \ldots \right] \tag{13}$$

Suppose high order fluctuations of the distribution density f(**n**) can be neglected, and f(**n**) is described by

$$f(\mathbf{n}) = \frac{C'}{4\pi}\left[1 + D'_{ij} n_i n_j\right] \tag{14}$$

and the observed data by

$$N(\mathbf{m}) = \frac{C}{4\pi}\left[1 + D_{ij} m_i m_j\right] \tag{15}$$

Comparing eqn. 13 and eqn. 14, one gets

$$C' = C/2\pi,\ D'_{ij} = 4D_{ij} \tag{16}$$

Consider a sample cut with a plane whose unit normal is I. Drawn on the cross section are lines of different orientation (h) orthogonal to I. Consider the following quantities:

$$M(I) = \int_{C(I)} N(\mathbf{m})d\mathbf{m} \tag{17}$$

$$M_{ij}(I) = \int_{C(I)} m_i m_j N(\mathbf{m})d\mathbf{m} \tag{18}$$

where C(I) is a unit circle encircling I perpendicularly, $\int_{C(I)} ds$ the line integral along C(I) (Figure 8) normalized to 2π. These quantities represent the zero moment and second skew symmetric moment respectively of the quantity N(**m**) in the plane I, with respect to the pole p.

If the experimental observations are based on three perpendicular planes with basis vectors e_1=(1,0,0), e_2=(0,1,0), e_3=(0,0,1). It can be shown that:

$$M(e_i) = \frac{C}{2}\left(1 - \frac{1}{2}D_{ii}\right) \quad (\text{i not summated}) \tag{19}$$

and
$$M_{ij}(e_k) = \frac{C}{8}D_{ij} \tag{20}$$

where
$$C = \frac{2}{3}[M(e_1) + M(e_2) + M(e_3)] \tag{21}$$

From equation (19) , an expression for D_{ii} can be obtained as:

$$D_{ii} = 2 - \frac{4M(e_i)}{C} \tag{22}$$

From equation (20) , an expression for D_{ij} can be obtained as:

$$D_{ij} = \frac{8M_{ij}(e_k)}{C} \tag{23}$$

In the 2-dimensional case, a symmetric distribution f(**n**) is expressed in the form

$$f(\mathbf{n}) = \frac{C}{2\pi}\left[1 + D_{ij}n_in_j + D_{ijkl}n_in_jn_kn_l + \ldots\right] \tag{24}$$

The Buffon transform of eqn (24) is given by

$$N(\mathbf{m}) = \frac{4C}{2\pi}\left[1 + \frac{1}{3}D_{ij}m_im_j - \frac{1}{15}D_{ijkl}m_im_jm_km_l + \ldots\right] \tag{25}$$

Conversely, if N(**m**) is given in the form

$$N(\mathbf{m}) = \frac{C}{2\pi}\left[1 + D_{ij}m_i m_j + D_{ijkl}m_i m_j m_k m_l + \ldots\right] \tag{26}$$

then its inverse Buffon transform is given by

$$f(\mathbf{n}) = \frac{C/4}{2\pi}\left[1 + 3D_{ij}n_i n_j - 15D_{ijkl}n_i n_j n_k n_l + \ldots\right] \tag{27}$$

Stereological Based Fabric Tensors : Their Definitions and Determinations

Kanatani's analysis offers a unified tensorial formulation for fabric parameters. Based on the analysis of Kanatani, stereological based fabric tensors such as surface area tensors (S_{ij}), mean free path tensor (λ_{ij}), or porosity tensor (N_{ij}) could be determined experimentally from microscopic observations. The definitions of those stereological based fabric tensors and the experimental techniques for determining surface area tensors (S_{ij}), mean free path tensor (λ_{ij}) and porosity tensor (N_{ij}) are discussed as follows:

Surface Area Tensor:

As shown, the orientation distribution function $S_v(\phi,\theta)$ which is defined as the fraction of surface area per unit volume which has a unit normal vector in the range ϕ to $(\phi + d\phi)$ and θ to $(\theta + d\theta)$ can be used as a quantitative descriptor of anisotropy. The total surface area density, S_v, is given by simply integrating this function over a unit sphere.

Let $$S_v(\mathbf{n}) = \frac{S_v}{4\pi}\left[1 + S_{ij}n_i n_j\right] \tag{28}$$

where $$S_v = \int S_v(\mathbf{n})d\mathbf{n} \tag{29}$$

and S_{ij} is called the surface area tensor.

Based on Kanatani's (1984a & b, 1985) analysis, S_v and S_{ij} can be obtained by observing $P_L(\mathbf{m})$, the number of intersections with the surface per unit length of test line at direction **m**.

Let
$$P_L(\mathbf{m}) = \frac{C}{4\pi}\left[1 + D_{ij}\mathbf{m}_i\mathbf{m}_j\right] \tag{30}$$

From equation (16),
$$S_v = C/2\pi \text{ and } S_{ij} = 4D_{ij} \tag{31}$$

The experimental procedures to obtain S_v and S_{ij} can be summarized as :

Step 1: Fix a Cartesian coordinate system in the soil specimen. Prepare thin sections of the soil specimen parallel to the three different ij-planes.

Step 2: A grid of parallel test lines is laid over a cross section in a given direction θ_m (see, for example, Figure 9), and the number of intercepts per unit length $P_L(\theta_m)$ is measured. Measurement are repeated for test lines oriented in several directions $\theta_m = m\ \pi/N$, $m=0,1,2,...,N-1$.

Step 3: Compute $M(e_k)$ and $M_{ij}(e_k)$ from:

$$M(e_k) = 2\pi \sum_{m=0}^{N-1} \frac{P_L(\theta_m)_{ij}}{N} \tag{32}$$

$$M_{ij}(e_k) = \pi \sum_{m=0}^{N-1} \frac{P_L(\theta_m)_{ij}\,\mathrm{Sin}(\frac{2\pi m}{N})}{N} \tag{33}$$

Where i,j,k is a permutation of 1,2,3 and ij refer to the plane of observation.

Step 4: Repeat steps 2 and 3 for the three orthogonal planes. Calculate the coefficient C using equation (21) and calculate the components of D_{ij} using equations (22) and (23). Obtain S_v and S_{ij} from $S_v = C/2\pi$ and $S_{ij} = 4D_{ij}$.

Mean Free Path Tensor:

Mean free path, λ, between particles is a spatial parameter of great importance in a particulate system. Mean free path, λ, is essentially a mean edge-to-edge distance. It represents the uninterrupted interparticle distance through the matrix averaged between all possible pairs of particles and given the true three-dimensional distance between particles. The directional variation of lineal measure mean free path $\lambda(\phi,\theta)$ also gives a quantitative description of anisotropy.

The orientation distribution $\lambda(\mathbf{n})$ is described by the "mean free path" λ and the mean free path tensor λ_{ij}.

Let
$$\lambda(\mathbf{n}) = \frac{C}{4\pi}\left[1+\lambda_{ij}\mathbf{n}_i\mathbf{n}_j\right] = \lambda\left[1+\lambda_{ij}\mathbf{n}_i\mathbf{n}_j\right] \tag{34}$$

The experimental procedures to obtain λ and λ_{ij} can be summarized as :

Step 1: Fix a Cartesian coordinate system in the soil specimen. Prepare thin sections of the soil specimen parallel to the three different ij-planes.

Step 2: A grid of parallel test lines is laid over a cross section in a given direction θ_m , and the mean free path $\lambda(\theta_m)$ is measured. Measurement are repeated for test lines oriented in several directions $\theta_m = m\ \pi/N$, m=0,1,2,...,N-1 .

Step 3: Compute $M(e_k)$ and $M_{ij}(e_k)$ from:

$$M(e_k) = 2\pi\sum_{m=0}^{N-1}\frac{\lambda(\theta_m)_{ij}}{N} \tag{35}$$

$$M_{ij}(e_k) = \pi\sum_{m=0}^{N-1}\frac{\lambda(\theta_m)_{ij}\,\mathrm{Sin}(\frac{2\pi m}{N})}{N} \tag{36}$$

Where i, j, k is a permutation of 1,2,3 and ij refer to the plane of observation.

Step 4: Repeat steps 2 and 3 for the three orthogonal planes. Calculate the coefficient C using equation (21) and calculate the components of λ_{ij} using equations (22) and (23). Obtain λ from $\lambda = \frac{C}{4\pi}$.

Porosity Tensor:

An idealized Representative Element Volume (REV), specified by spherical coordinates ϕ and θ, with shaded voids is shown in Figure 10. The orientation distribution function $N(\phi,\theta)$ is defined as the porosity, the ratio of void volume to the total volume, of the volume element in the orientation range ϕ to $(\phi + d\phi)$ and θ to $(\theta + d\theta)$. This function is described by the porosity of the specimen n_0 and porosity tensor N_{ij} as

$$N(\mathbf{n}) = n_0\left[1 + N_{ij}n_i n_j\right] \tag{37}$$

Muhunthan (1991) considered the lineal fraction of void $l_p(\phi,\theta)$ as an estimator of volume fraction of void (porosity), $N(\phi,\theta)$, and used test lines with different orientations that passed through the same center point (see Fig.11), in an attempt to account for the anisotropic distribution of void phases. However, this procedure introduces bias in the estimation of porosity (Kuo and Frost, 1993). As a limiting condition, consider the two synthetic cases shown in Figure 12. Both cases will have the same estimated porosity of 0.5 using Muhunthan's method. However, their actual porosities are 0.25 and 0.75, respectively. This bias is further illustrated in the two identical photos of elastic rods shown in Figure 13. The left-hand photo shows the measurement center point located in a grain while the other has the center point located in a void just to the right of this grain. The measurements show a significant difference in the estimated porosity and fabric tensor. For example, the difference in estimated porosity for these two cases is about 20% (0.168 versus 0.201). A revised method was proposed by considering the concept of representative element circle, REC, as shown schematically in Figure 14. In this revised

scheme, the measurement of lineal fraction of void $l_p(\theta_m)$ is made on segments of the lines which are fully located within the region between two RECs as shown in Figure 15.

The experimental procedures to obtain n_0 and N_{ij} based on the revised method are summarized as follows:

Step 1 : Fix a Cartesian coordinate system in the soil specimen. Prepare thin sections of the soil specimen parallel to the three different ij-planes.

Step 2 : For each cross section, measure the porosity for different size of measurement fields and determine the regions of stable RECs .

Step 3 : Select radii of inner REC(r_1) and outer REC(r_2).

Step 4 : Draw test line within the region between the two RECs in a given direction θ_m, measure the fraction $l_p(\theta_m)$ occupied by voids. Measurement are repeated for test lines oriented in several directions $\theta_m = m\ \pi/N$, m=0,1,2,...,N-1 .

Step 5: Compute $M(e_k)$ and $M_{ij}(e_k)$ from:

$$M(e_k) = 2\pi \sum_{m=0}^{N-1} \frac{l_p(\theta_m)_{ij}}{N} \tag{38}$$

$$M_{ij}(e_k) = \pi \sum_{m=0}^{N-1} \frac{l_p(\theta_m)_{ij} \mathrm{Sin}(\frac{2\pi m}{N})}{N} \tag{39}$$

where i, j, k is a permutation of 1,2,3 and ij refer to the plane of observation.

Step 6: Repeat steps 2 through 5 for the three orthogonal planes. Calculate the coefficient C using equation (21) and calculate the components of N_{ij} using equations (22) and (23). Obtain n_0 from $n_0 = \frac{C}{4\pi}$.

Simplified Procedure for Two Dimensional Observations

If only a single plane section is available, the formulations and measurements for two dimensional tensors: length tensor (L_{ij}), mean free path tensor (λ_{ij}), and area fraction tensor (A_{ij}) are also available. In 2-D, an orientation distribution function $f(\theta)$ reduces to a simple Fourier series in θ with period 2π as (Kanatani, 1984a & b; Muhunthan, 1991):

$$f(\theta) = \frac{C}{2\pi}\left[1 + \sum_{n=2}^{\infty}{}' (A_n \cos n\theta + B_n \sin n\theta)\right] \tag{40}$$

$$C = \int_0^{2\pi} f(\theta) d\theta \tag{41}$$

$$\begin{bmatrix} A_n \\ B_n \end{bmatrix} = \frac{2}{C}\int_{\theta=0}^{2\pi} f(\theta) \begin{bmatrix} \cos n\theta \\ \sin n\theta \end{bmatrix} d\theta \tag{42}$$

where ' denotes summation with respect to even indices. This distribution can also be represented in Cartesian tensors (Kanatani, 1984a), and keeping terms up to a second rank tensor ϕ_{ij} being written explicitly as :

$$\phi_{ij} = \begin{bmatrix} A_2 & B_2 \\ B_2 & -A_2 \end{bmatrix} \tag{43}$$

As reviewed previously, the orientation distribution of lines in a plane $L_A(\theta)$, is related to the orientation distribution of number of intersections per unit length of test line, $P_L(\theta)$.

If $$P_L(\mathbf{m}) = \frac{C}{2\pi}(1 + \phi_{ij} m_i m_j) \tag{44}$$

From Eq. 27, one can get

$$L_A(\mathbf{n}) = \frac{C/4}{2\pi}(1 + 3\phi_{ij}\mathbf{n}_i\mathbf{n}_j) = \frac{L_A}{2\pi}(1 + L_{ij}\mathbf{n}_i\mathbf{n}_j) \tag{45}$$

Similarly, structural anisotropy can be quantified in 2-D by observing the orientation distribution of mean free path $\lambda(\theta)$, or length fraction of pore $l_p(\theta)$ as described previously for 3-D. Now, Let

$$\lambda(\mathbf{m}) = \frac{C}{2\pi}(1 + \lambda_{ij}\mathbf{m}_i\mathbf{m}_j) = \lambda(1 + \lambda_{ij}\mathbf{m}_i\mathbf{m}_j) \tag{46}$$

and

$$l_p(\mathbf{m}) = \frac{C}{2\pi}(1 + A_{ij}\mathbf{m}_i\mathbf{m}_j) = A_A(1 + A_{ij}\mathbf{m}_i\mathbf{m}_j) \tag{47}$$

Substituting $f(\theta)$ with $P_L(\theta)$, or $\lambda(\theta)$, or $l_p(\theta)$, results in the simplified expressions for two dimensional observations for experimental techniques introduced above. For $\theta_m = m\pi/N$, $m=0,1,2,...,N-1$, A_n, B_n and C can be computed as:

$$C = 2\pi\sum_{m=0}^{N-1}\frac{f(\theta_m)}{N} \tag{48}$$

$$\begin{bmatrix} A_n \\ B_n \end{bmatrix} = 2\sum_{m=0}^{N-1} f(\theta_m)\begin{bmatrix} \cos(n\pi m/N) \\ \sin(n\pi m/N) \end{bmatrix} \Big/ \sum_{m=0}^{N-1} f(\theta_m) \tag{49}$$

For a second order tensor, n=2, resulting in the calculation of A_2 and B_2.

The corresponding mean fabric descriptor (L_A, or λ, or A_A) and fabric tensor can then be calculated.

Conclusions

Anisotropy of granular materials is quantified by using fabric tensors which characterize the distribution of directional data. It is shown that the stereological approach, Kanatani's analysis, offers a unified tensorial formulation for fabric tensors in which the structure of granular materials can be modeled via two measures : a scalar measure giving the mean value of a fabric descriptor and a tensor giving its directional distribution in space. Specifically, the directional distributions of surface area density, mean free path, and porosity were modeled by their mean value and associated tensor. The measurement techniques to determine such mean fabric descriptors and their associated tensor are presented. These measurement techniques could be implemented using digital image analysis (as discussed in companion paper) which make the determinations of mean fabric descriptor and its associated tensor very efficient. The mean values of surface area density, mean free path, or porosity play a key role in most current granular media models. Hence, their associated fabric tensors are useful to extend these models. The introduction of a fabric tensor in a continuum model will permit the discrete nature of granular materials to be accounted for in a continuum sense.

Acknowledgments

The work reported in this paper was supported by National Science Foundation Grant No.'s MSS-9011232, MSS-9007581 and BCS-9304897. This support is gratefully acknowledged.

Sedegh, A. M., Cowin, S. C., and Luo, G. M., (1991), "Inversions Related to the Stress-Strain-Fabric Relationship", Mechanics of Materials, Vol. 11, pp. 323-336

Tobita, Y., (1989), "Fabric Tensors in Constitutive Equations for Granular Materials", Soils and Foundations, Vol. 29, No. 4, pp. 91-104

Underwood, E. E., (1970), Quantitative Stereology, Addison-Wesley Publishing Company. 274 pp.

LIST OF FIGURES

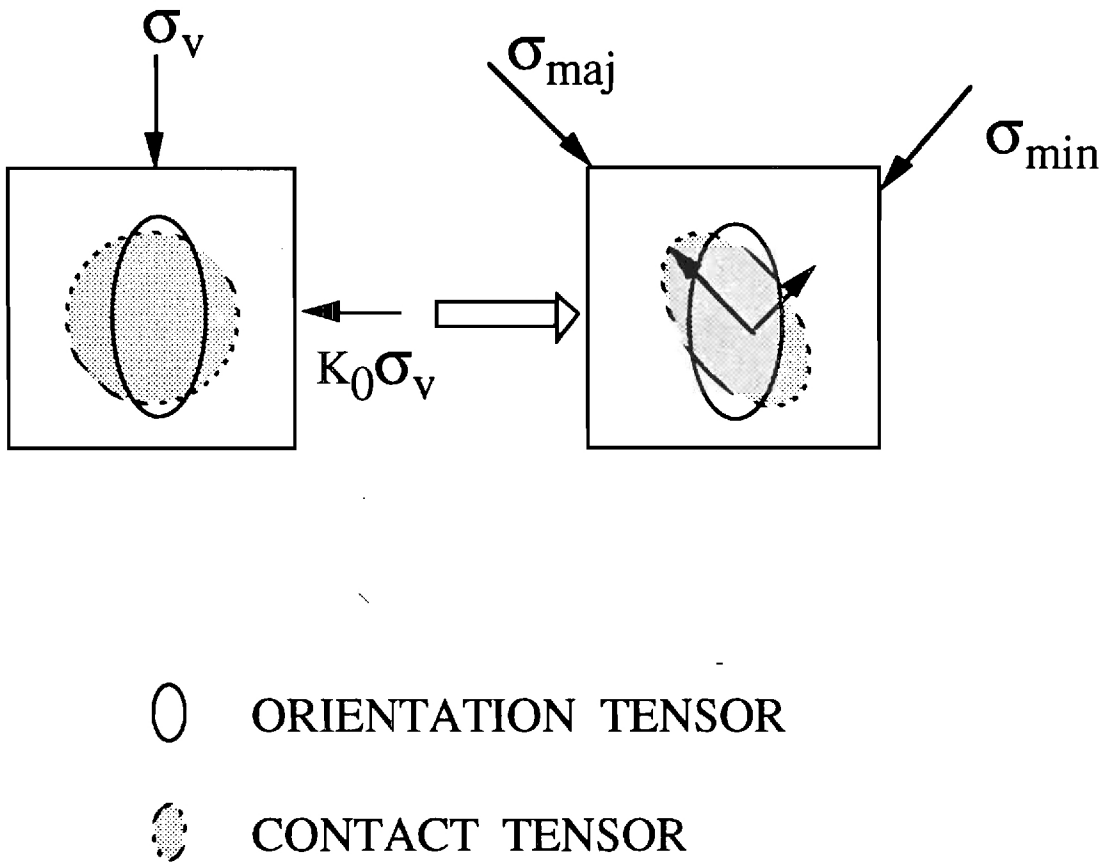

Figure 1 Two fabric tensors showing completely different evolution modes (after Tobita, 1989)

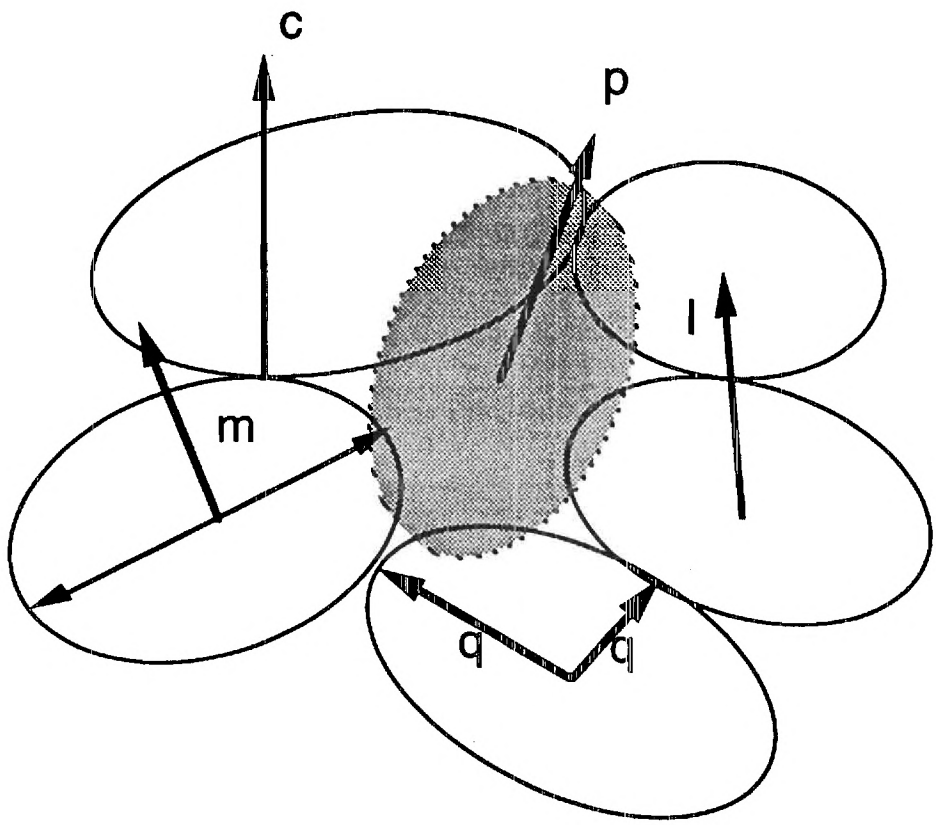

Note : c denotes a contact normal,
l denotes a branch vector,
q denotes a vector from the center of particles to contacts,
m denotes a normal unit vector to the long axis of particles,
p denotes a vector relating to void shape and volume.

Figure 2 Various micromechanical quantities in a granular mass (after Tobita, 1989)

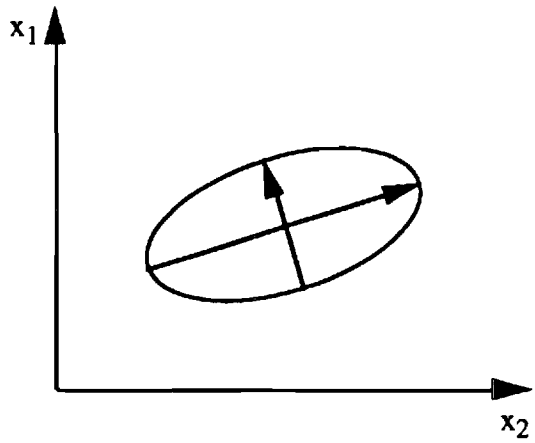

(a) orientation of a particle

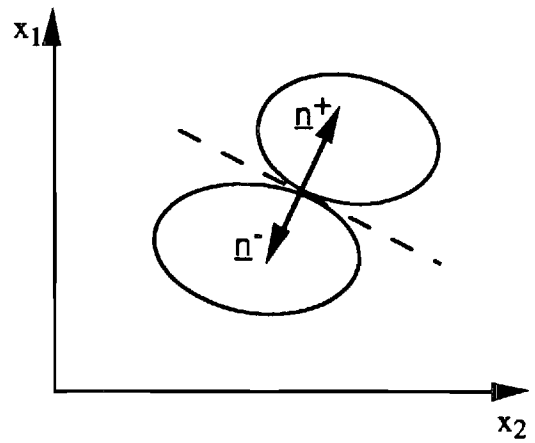

(b) contactnormal

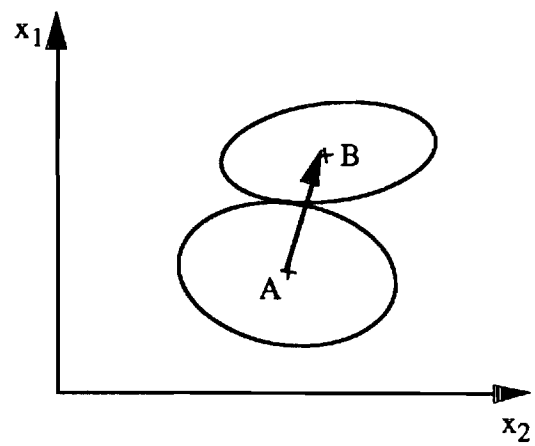

(c) branch vector

Figure 3 Fabric measures associated with solid particles (Konishi and Naruse, 1988)

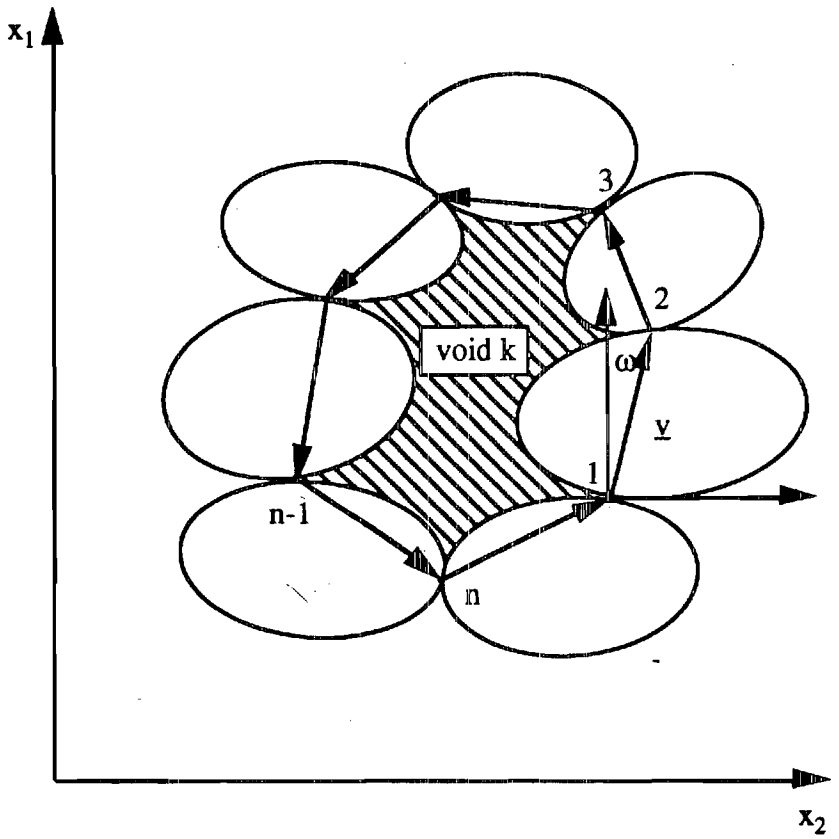

Figure 4 A void k with the associated n particles and a replaced polygon (after Konishi and Naruse, 1988)

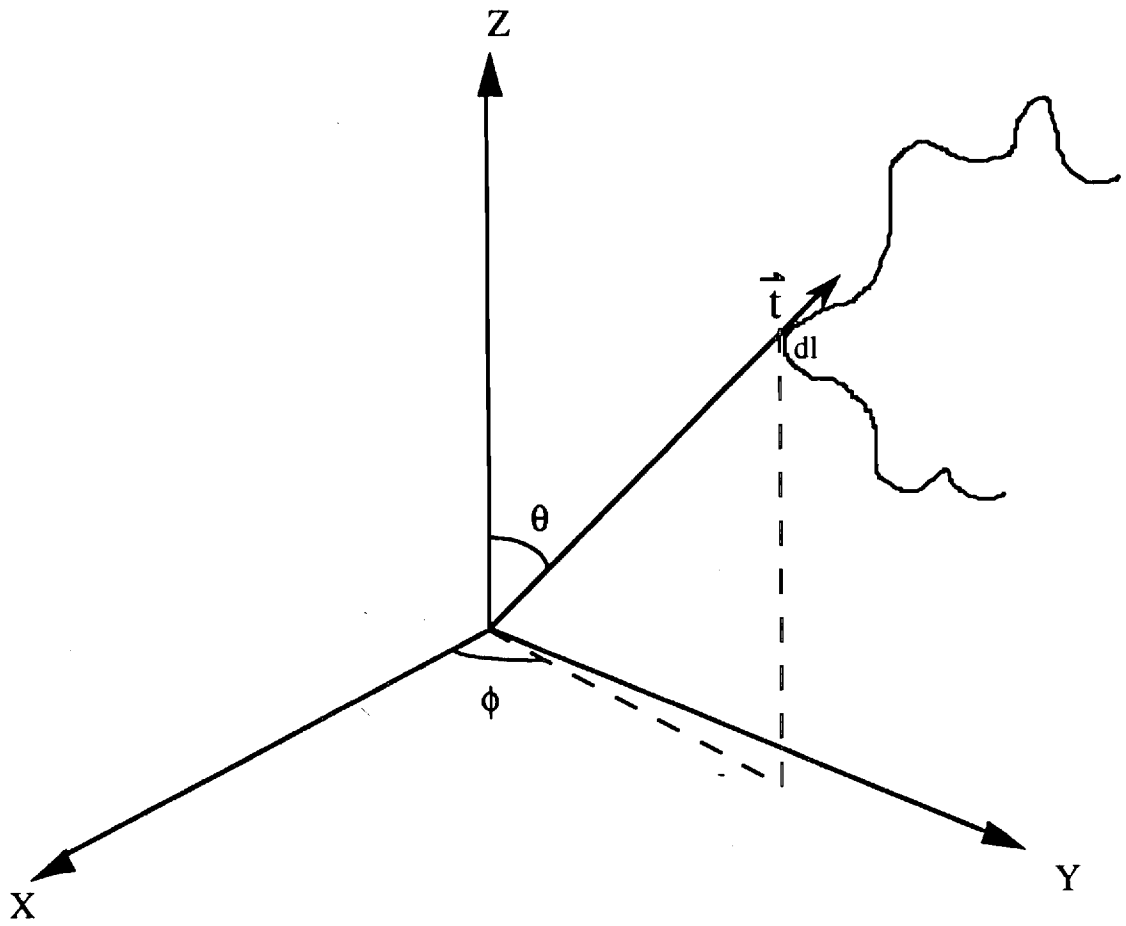

Figure 5 Angular orientation of lines

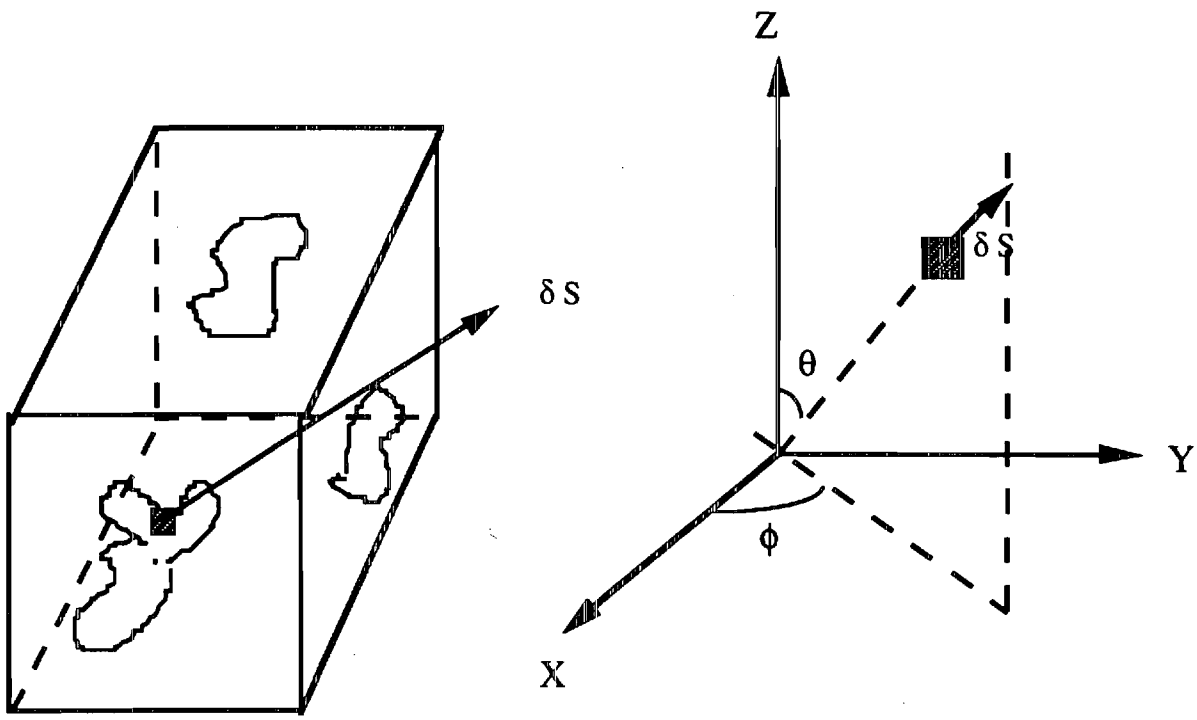

Figure 6 Angular orientation of surfaces

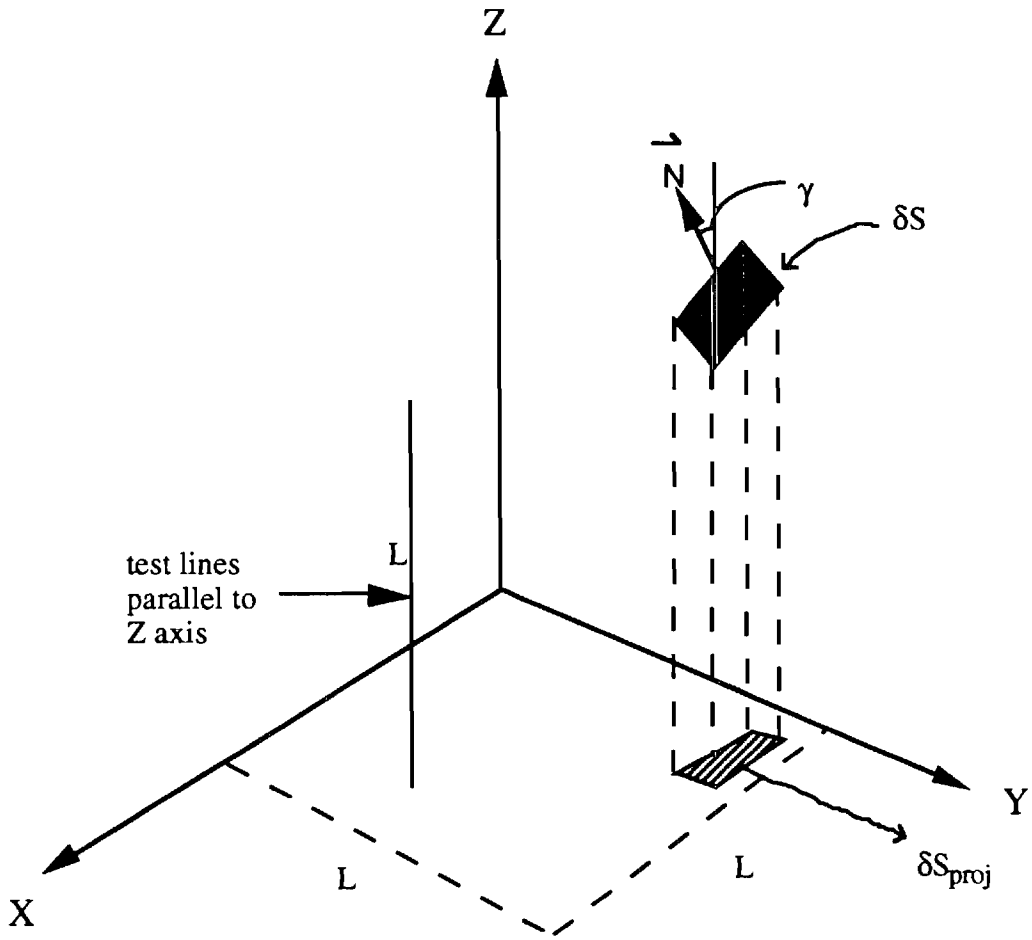

Figure 7 The probability of intersection of test lines with areal element is proportional to the projected area of areal element on the plane normal to test lines

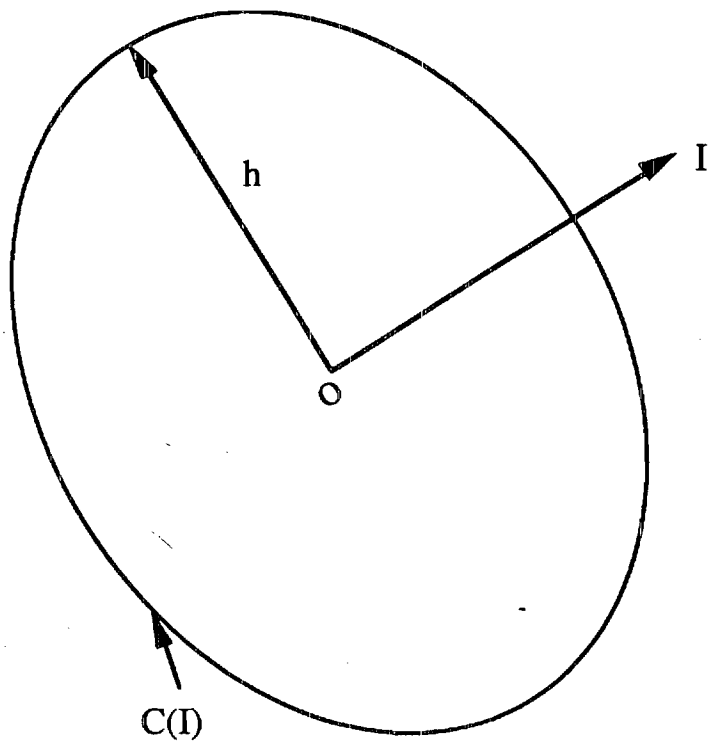

Figure 8 Illustration of unit vector on circle C(I) (after Muhunthan 1991)

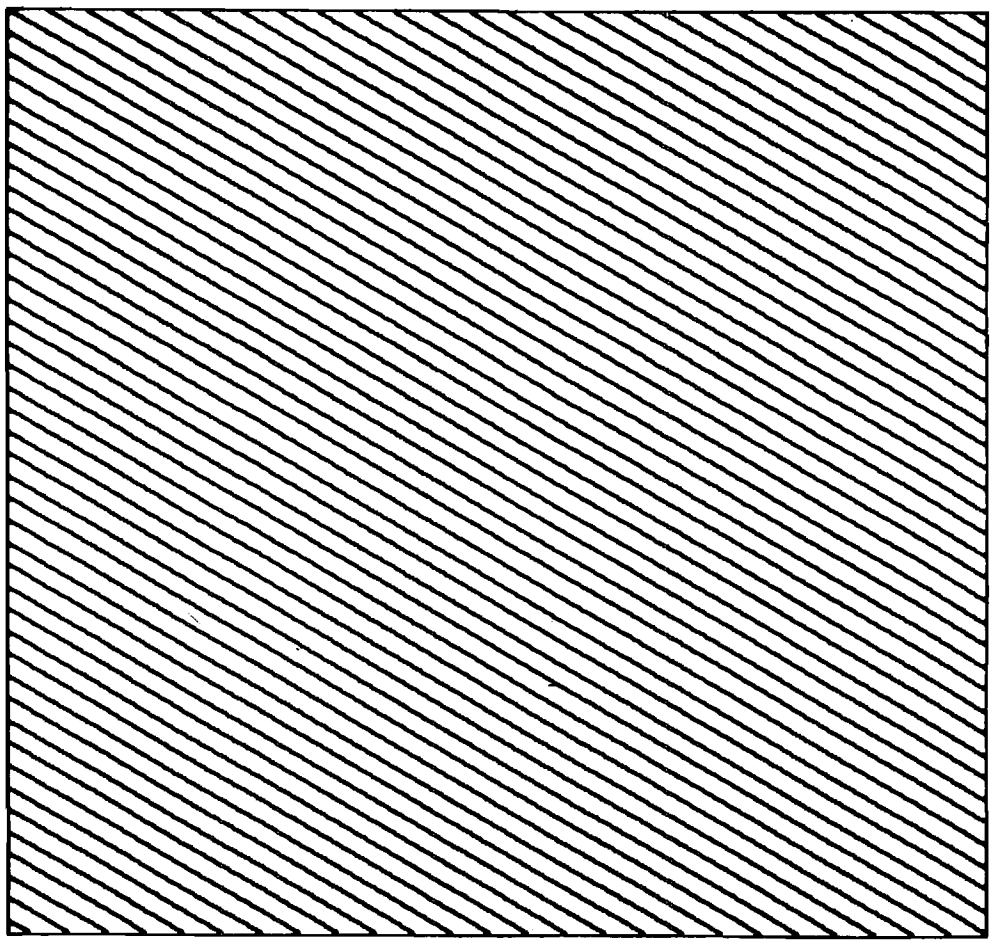

Figure 9 A grid of parallel test lines

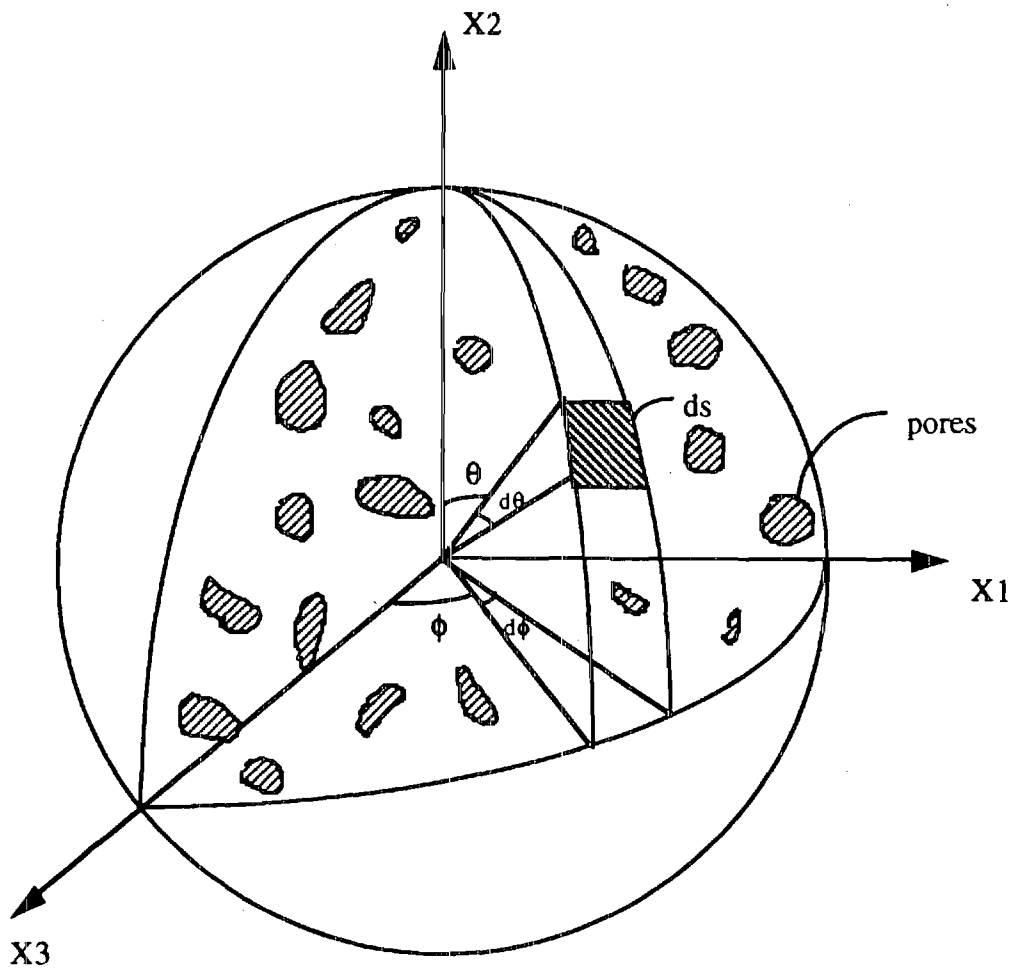

Figure 10 Spherical REV enclosing particles (adapted from Muhunthan, 1991)

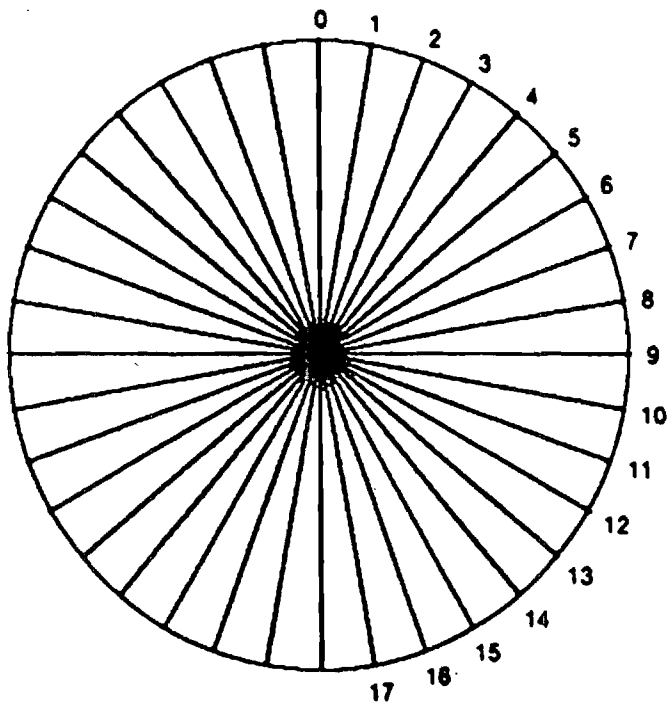

Figure 11 REA with radial lines of observation (after Muhunthan, 1993)

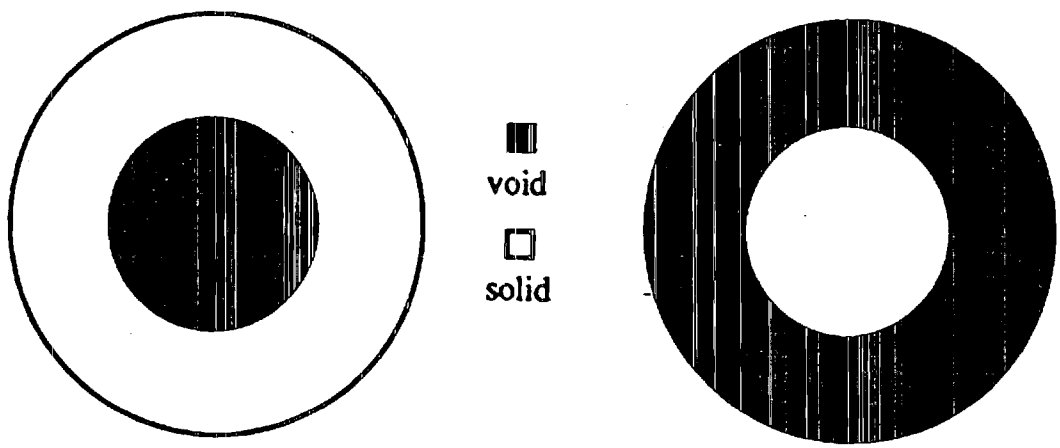

Figure 12 Synthetic cases showing potential error in estimated porosity using Muhunthan's method

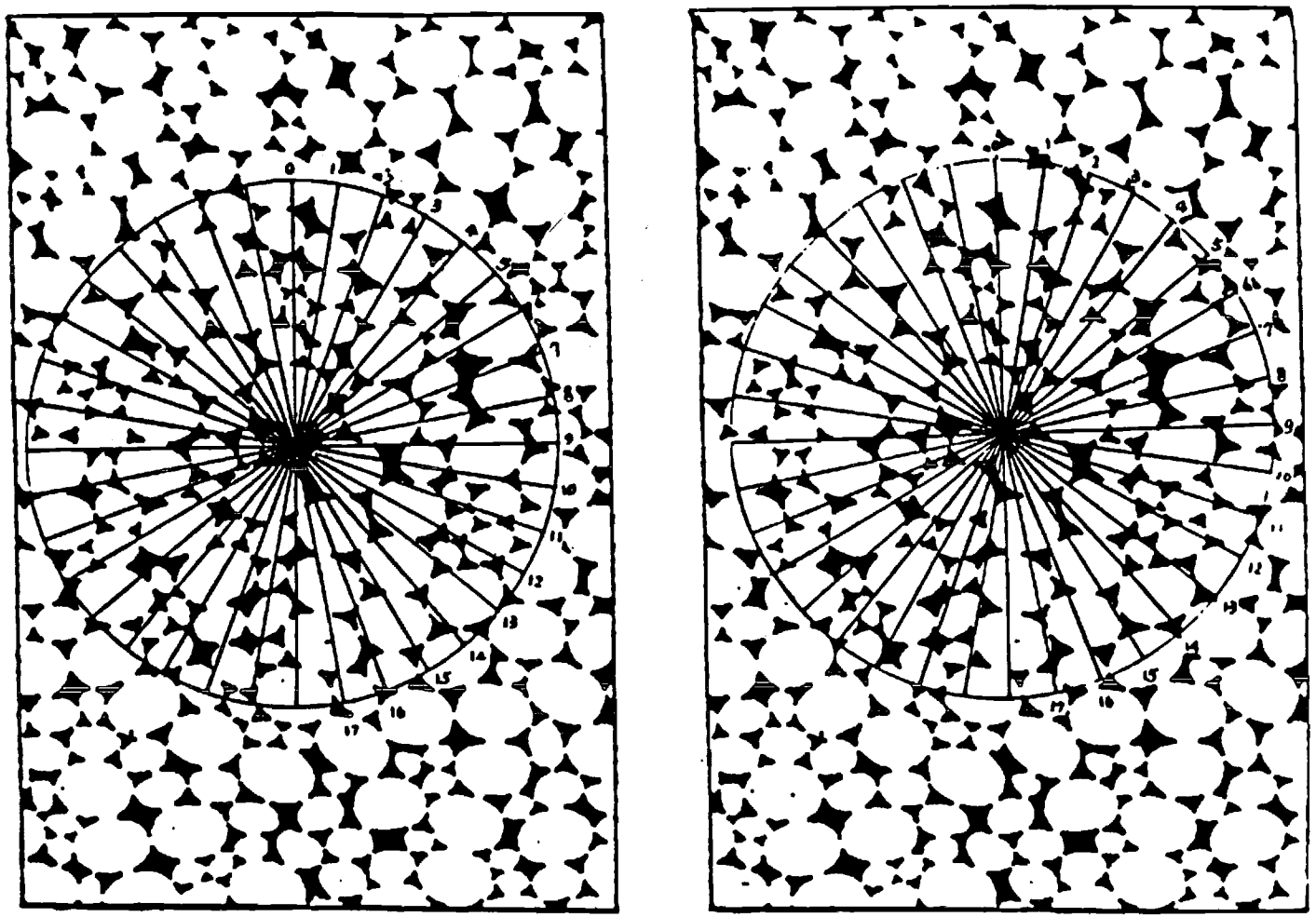

Figure 13 Same Photo elastic rods data employing Muhunthan's method at slightly different location of centers

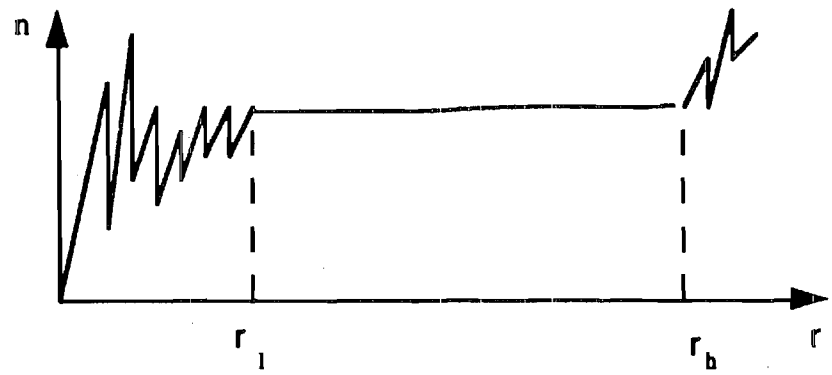

Figure 14 Variation in estimated porosity as a function of measurement field radius.

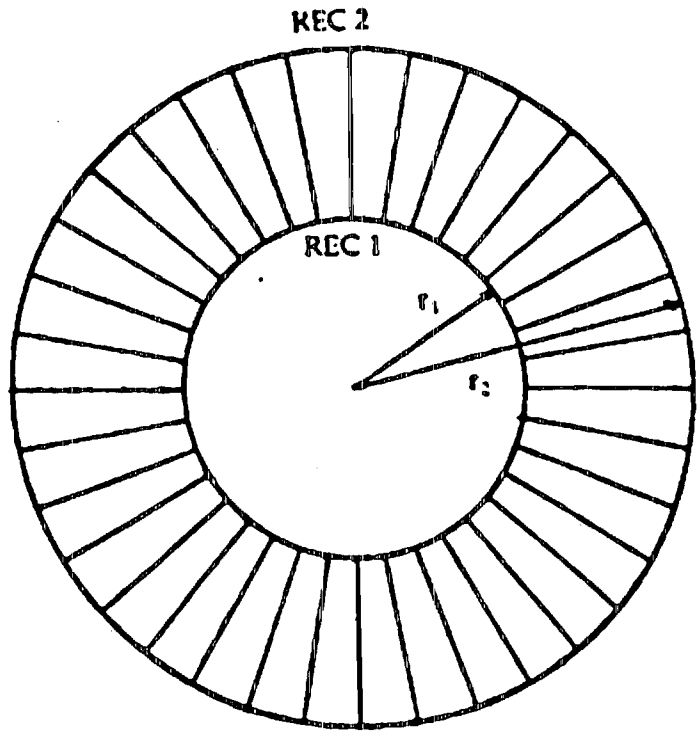

Figure 15 Effective measurement field for revised procedure to minimize bias

Attachment # 3

STEREOLOGY BASED FABRIC TENSORS - PART II : IMAGE ANALYSIS IMPLEMENTATION

Chun-Yi Kuo[1], J. David Frost[1], and Jean-Lou A. Chameau[2]

Abstract

On the basis of Kanatani's analysis, stereological based fabric tensors such as a surface area tensor (S_{ij}) or a mean free path tensor (λ_{ij}) or a porosity tensor (N_{ij}) could be determined experimentally from microscopic observations. The definitions and measurement techniques for these stereological based fabric tensors were discussed in the companion paper to this. It was shown that the structure of granular materials can be modeled via two measures : a scalar measure giving the mean value of a fabric descriptor and a tensor giving its directional distribution in space. This paper describes how measurement techniques can be implemented using an automated image analysis system. Computer algorithms were developed that permit the determination of mean fabric descriptors and their associated tensors possible using image analysis techniques. The implementation of these techniques are illustrated using example images. Both two-dimensional and three-dimensional cases are presented. The effect of test grid interline spacing and orientation increment on the resulting mean fabric descriptors and their associated tensor are examined. Two tremendously different images were used for this parametric study, the results support that the current settings of line spacing and orientation increment are adequate. Besides that, the generality, practical implications and limitations of these techniques are discussed.

---

1 Postdoctoral Fellow and Associate Professor, respectively, School of Civil & Environmental Engineering, The Georgia Institute of Technology, Atlanta, Georgia 30332, USA.

2 President, Golder Associates, 3730 Chamblee-Tucker Road, Atlanta, Georgia 30341, USA.

Introduction

Fabric tensors which characterize the distribution of directional data from microscopic observations are considered to be good quantitative measures of the structural anisotropy of granular materials. The introduction of fabric tensors in continuum models (e.g., Tobita, 1989; Muhunthan, 1991; Oda and Ohnishi, 1992) permits the underlying micromechanical features of granular materials to be accounted for in a continuum sense. As shown in the companion paper (Kuo, Frost, and Chameau, 1995), the stereological approach offers a unified tensorial formulation for fabric tensors in which the structure of granular materials can be modeled via two measures : a scalar measure giving the mean value of a fabric descriptor and a tensor giving its directional distribution in space. Specifically, the directional distributions of surface area density, mean free path, and porosity were modeled by their mean value and associated tensor. The measurement techniques to determine such mean fabric descriptors and their associated tensor were presented. Based on observations on three mutually perpendicular planes, mean value and associated tensor of directional distribution could be obtained from the zero moment M(I) and second skew symmetric moment $M_{ij}(I)$ respectively of the observed quantity. In this paper, these measurement techniques are implemented using digital image analysis which make the determinations of mean fabric descriptor and its associated tensor very efficient. The mean values of surface area density, mean free path, or porosity play a key role in most current granular media models. Hence, their associated fabric tensors are useful to extend these models.

Image Analysis Implementations

As shown the companion paper (Kuo, Frost, and Chameau, 1995), the measurement techniques for determining surface area tensor (S_{ij}), mean free path tensor

(λ_{ij}), and porosity tensor (N_{ij}) are very similar to one another and can be readily implemented by using an image analysis system. The use of image analysis allows an efficient means of determining fabric tensors.

The work reported herein was performed using a Cambridge Instruments Quantimet Q570 Image analysis system although any system of similar capabilities could be used to program the algorithms described herein. Unlike many other image analysis systems which contain preset functions but do not allow for user customization of these features, the Quantimet Q570 allows users to develop new applications by accessing a range of powerful processing commands using simple, intuitive menus . It also permits the user to assemble image analysis routines with the Quantimet Q570's built-in Basic-like Macro-language-QBasic. This feature was used extensively in this study.

There are two types of measurement on binary images: Field Measurements - one total value per parameter for each field; and Feature Measurements - one individual value per parameter for each isolated object (feature) in the field. Basic parameters such as area, perimeter, horizontal intercept number, vertical intersect number and number of features are measured which allows complete quantitative description of the image.

The general procedure for their implementation in an image analyzer is summarized in Figure 1. The "Image pre-processing" stage is to enhance the image to be analyzed and is case specific depending on the specimen illumination and capture conditions and is not discussed further herein. Starting with a good binary image (Figure 2), the procedure for image analysis implementation is explained as follows:

Surface Area Tensor :

As shown in the companion paper, based on Kanatani's (1984a & b, 1985) analysis, the total surface area density, S_V, and surface area tensor, S_{ij}, can be obtained by observing $P_L(\mathbf{m})$, the number of intersections with the surface per unit length of test line at direction $\mathbf{m}$.

For $$P_L(\mathbf{m}) = \frac{C}{4\pi}\left[1 + D_{ij}\mathbf{m}_i\mathbf{m}_j\right] \quad (1)$$

It has been shown $$S_v = C/2\pi \text{ and } S_{ij} = 4D_{ij} \quad (2)$$

The test probe for determining surface area tensor (S_{ij}) is a grid of parallel test lines in a given direction θ_m (see Figure 3). To determine surface area tensor (S_{ij}), the number of intercepts per unit length in a given direction θ_m , $P_L(\theta_m)$, is to be measured. To identify the intercepts of test lines and soil particles, the image processing operation "outline" and logical operation "C=A and B" were used. Figure 4 shows the outline of the example image (Figure 2). Figure 5 shows the intercepts of test lines and soil particles of the example image for one given direction. The intercept count $P(\theta_m)$ of Figure 5 can be obtained from "feature number" by applying the "feature measurement" to Figure 5. The length of test lines is obtained from the coordinates of the two end pixels of each test line. For a test line with two end pixels (x_0, y_0) and (x_1, y_1), the length of this test line in pixels is calculated as :

$$L = ((x_1 - x_0)^2 + (y_1 - y_0)^2)^{0.5} + 1 \quad (3)$$

The number of intercepts per unit length $P_L(\theta_m)$ is simply the ratio of the intercept count $P(\theta_m)$ to the total length of all parallel test lines on a given direction, $TL(\theta_m)$. When the desired quantity $P_L(\theta_m)$ is available, it is a simple task to compute $M(e_k)$ and $M_{ij}(e_k)$ from the corresponding equations as shown in the companion paper. Similarly, the mean descriptor and fabric tensor (S_v and S_{ij}) can be calculated from appropriate equations .

Mean Free Path Tensor:

Mean free path, λ, between particles is a spatial parameter of great importance in a particulate system. Mean free path, λ, is essentially a mean edge-to-edge distance. It represents the uninterrupted interparticle distance through the matrix averaged between all possible pairs of particles and given the true three-dimensional distance between particles. The directional variation of lineal measure mean free path $\lambda(\phi,\theta)$ also gives a quantitative description of anisotropy.

The orientation distribution $\lambda(\mathbf{n})$ is described by the "mean free path" λ and the mean free path tensor, λ_{ij}.

Let
$$\lambda(\mathbf{n}) = \frac{C}{4\pi}\left[1 + \lambda_{ij}\mathbf{n}_i\mathbf{n}_j\right] = \lambda\left[1 + \lambda_{ij}\mathbf{n}_i\mathbf{n}_j\right] \qquad (4)$$

The test probe for determining mean free path tensor (λ_{ij}) is a grid of parallel test lines in a given direction θ_m also (see Figure 3). To determine the mean free path tensor (λ_{ij}), the free paths between particles (Figure 6) can be obtained by simply applying the logical operation "C=A and B" to the test grid and the inverse of the example image. To calculate the mean free path at a given direction $\lambda(\theta_m)$, the number and the total length of free paths are needed. The number of free paths is obtained from "feature number" by applying "feature measurement" to Figure 6. The total length of free paths is obtained from the "pixel number (area)" by applying "field measurement" to Figure 6. Since the width of all test lines (free paths) is 1 pixel, the number of total pixels of free paths is the total length of free paths if all lines are "straight". However, except for horizontal and vertical directions, lines have a saw-tooth appearance in a digitized image (see Figure 3). For a given direction (θ_m), there will be a factor $k(\theta_m) \geq 1$ which is the ratio of pixels number to the true length of lines for a given direction (θ_m) on a digital image. By applying

"field measurement" to the test grid (Figure 3), the total number of pixels of test lines can be measured. The true length of lines is obtained by using equation 3 as described previously for $TL(\theta_m)$. By knowing the factor $k(\theta_m)$, the total length of free paths is then simply equal to the total pixel numbers $/k(\theta_m)$. When the desired quantity $\lambda(\theta_m)$ is available, it is a simple task to compute $M(e_k)$ and $M_{ij}(e_k)$ from corresponding equations. Similarly, the mean free path, λ and mean free path tensor, λ_{ij} , can be calculated from corresponding equations .

Porosity Tensor :

The orientation distribution function $N(\phi,\theta)$ is defined as the porosity, the ratio of void volume to the total volume, of the volume element in the orientation range ϕ to $(\phi + d\phi)$ and θ to $(\theta + d\theta)$. This function is described by the porosity of the specimen n_0 and the porosity tensor, N_{ij} , as

$$N(\mathbf{n}) = n_0\left[1 + N_{ij}\mathbf{n}_i\mathbf{n}_j\right] \tag{5}$$

The test probe for determining the porosity tensor (N_{ij}) is a test line within the region between two REC's in a given direction θ_m. Before the test line can be drawn, the regions of representative element circles (RECs) needs to be determined. A Q-Basic program was written to measure the porosities of a image with different sizes of square measure frame. For the image of Figure 2, the measured porosities with different size of measure frame are shown in Figure 7. It is shown that the measured porosities become stable after the width of measure frame is larger than about 50 pixels. Based on this information, the radius of inner REC(r_1) and outer REC(r_2) could be selected as 40 pixels and 230 pixels (see Figure 8, $r_1 \geq \frac{\sqrt{2}}{2} w_1$ and $r_2 \leq 0.5 \cdot w_2$). Note that this value is related to the size of the particles in the image and thus should be computed for each experimental

configuration. This issue is discussed further later in this paper. The test line within the region between the two RECs in a given direction θ_m is shown as Figure 9.

To determine the porosity tensor (N_{ij}), the portions of test line occupied by voids $l_p(\theta_m)$ (Figure 10) can easily be obtained by applying a logical operator to the test probe and the inversion of the example image. The fraction of the test line occupied by voids $l_p(\theta_m)$ can be determined by the ratio of number of pixels measured when "Field Measurement" is applied to the test line (Figure 9) and the portions of the test line occupied by voids (Figure 10). When the desired quantity $l_p(\theta_m)$ is available, it is a simple task to compute $M(e_k)$ and $M_{ij}(e_k)$ from the corresponding equations. Similarly, the mean descriptor and fabric tensor, n_0 and N_{ij}, can be calculated from corresponding equations.

Similarly, if only a single plane section is available, the implementation of measurement techniques for two dimensional tensors: length tensor (L_{ij}), mean free path tensor (λ_{ij}), and area fraction tensor (A_{ij}) can also be programmed using the Q 570 built-in Basic-like Macro-language-QBasic.

Illustration of the Techniques

Two examples are considered to illustrate the application of the above procedures. One shows the typical application to two dimensional tensors. The other illustrates the application to three dimensional tensors.

Applications to Two Dimensional Tensors

For the binary image shown in Figure 2, the resulting mean fabric descriptors and fabric tensors using the measurement techniques described above are

$$L_A = 0.067 \text{ / pixel}, \qquad L_{ij} = \begin{bmatrix} -0.0092 & -0.0075 \\ -0.0075 & 0.0092 \end{bmatrix} \tag{6}$$

and $\lambda = 23.905$ pixel, $\lambda_{ij} = \begin{bmatrix} -0.0054 & 0.0032 \\ 0.0032 & 0.0054 \end{bmatrix}$ (7)

and $A_A^v = 0.478$, $A_{ij} = \begin{bmatrix} 0.0316 & 0.0440 \\ 0.0440 & -0.0316 \end{bmatrix}$ (8)

The results of "field measurement" of the binary image (Figure 2) are shown in Table 1. From Table 1, the area fraction of solids is 0.511 which implies that the area fraction of voids is 0.489. It is evident that the proposed measurement technique gives a very good approximation of the area fraction of void which is 0.478 measured using the stereology based method versus the value of 0.489 obtained directly from the field measurement. Similarly, the total length per unit area, L_A, can be obtained from results of field measurement as perimeter/ frame area which is 0.065/pixel. The proposed stereological measurement technique estimates the value of L_A as 0.067/ pixel which is very close to 0.065/pixel from the field measurement. The results of "field measurement" offer an independent check to the proposed measurement techniques. The close agreement between the results of proposed measurement techniques and of "field measurement" confirms the correctness of the measurement techniques and their implementation.

Applications to Three Dimensional Tensors

For example images of three orthogonal planes, the surface area density and surface area tensor are obtained as:

$$S_V = 0.076 \text{ / pixel} \qquad S_{ij} = \begin{bmatrix} 0.0320 & -0.0819 & 0.0193 \\ -0.0819 & 0.1958 & 0.0120 \\ 0.0193 & 0.0120 & -0.2278 \end{bmatrix} \quad (9)$$

The mean free path and mean free path tensor are obtained as:

$$\lambda = 23.44 \text{ pixels} \qquad \lambda_{ij} = \begin{bmatrix} -0.2429 & 0.0061 & -0.0010 \\ 0.0061 & 0.1036 & -0.0048 \\ -0.0010 & -0.0048 & 0.1393 \end{bmatrix} \tag{10}$$

The porosity and porosity tensor can be obtained from Q570 as previously described by varying the size of measure frame, and the inner and outer radii were chosen as $r_1 = 40$ pixels and $r_2 = 230$ pixels respectively. The results show that

$$n_0 = 0.434, \qquad N_{ij} = \begin{bmatrix} -0.3123 & 0.0013 & -0.0441 \\ 0.0013 & 0.1187 & -0.0198 \\ -0.0441 & -0.0198 & 0.1935 \end{bmatrix} \tag{11}$$

Theoretically, there are interrelationships between surface area density S_v, mean free path λ, and porosity n_0. It can be shown that

$$\lambda = \frac{4 \cdot n_0}{S_v} \tag{12}$$

For $n_0 = 0.434$ (Eq. 11) and $S_v = 0.076$/pixels (Eq. 9), the calculated mean free path (from Eq. 12) is 22.75 pixels. This value is reasonably close to 23.44 pixels obtained with the programmed program (Eq. 10).

Discussion

Parametric Study

For the illustrations described above, the test grid (Figure 3) had interline spacing of 10 pixels and was rotated for every 10 degrees of orientation. It is interesting to know

the sensitivity of the proposed methods to different line spacing and orientation increments. Figure 11 shows the resulting mean free path and second invariant of the mean free path tensor, J_f, for the example image (Figure 2) with different line spacing for the test grid oriented at every 10 degrees. Figure 11a shows the mean free path obtained is insensitive to the line spacing in the test grid as it rotates at every 10 degrees (values range from 23.04 pixels to 24.46 pixels). Even with only a single test line at the center (line spacing > 240 pixels), the estimated mean free path is not significantly different from the others. It is considered that since the test grid is rotated every 10 degrees, even a single test line gives a reasonable coverage of the image and yields a reasonable estimation of the mean free path. However, the estimation of mean free path is more consistent with the line spacing between 5 and 20 pixels which yields values in the range of 23.86 pixels to 23.91 pixels. Figure 11b shows the second invariant of the mean free path tensor, J_f, obtained ranges from 2.2×10^{-5} to 1.4×10^{-2} and indicates that the anisotropy of the example image is very weak. Again, the estimation of J_f is more consistent with the line spacing between 5 and 20 pixels which yields values ranging from 2.2×10^{-5} to 9.8×10^{-5}.

Figure 12 shows the effect of orientation increment for the resulting mean free path and the second invariant of the mean free path tensor, J_f, for the cases of a single test line (spacing > 240 pixels) and a test grid with line spacing of 10 pixels. The results show that for the case of a single test line, the increment of orientation should be equal to or smaller than 10 degrees to get reasonable estimations of mean free path and the second invariant of the mean free path tensor, J_f. For the case of 10 pixels spacing test grid, the increment of orientation should be equal to or smaller than 20 degrees to get reasonable estimations.

A similar analysis was also applied to an anisotropic synthetic image (Figure 13). The effects of line spacing and increment of orientation on the resulting mean free path and the second invariant of the mean free path tensor, J_f, are shown in Figures 14 and 15,

respectively. The results support that the current settings of 10 pixels spacing and 10 degree orientation increment are adequate for two tremendously different images (Figure 2 & Figure 13). It is believed that this setting will be adequate for most soil images in practice, although this factor should be routinely verified.

The effect of the increment of orientation on the measured area fraction and area fraction tensor (or porosity and porosity tensor for 3D) was examined also. Current setting uses a 5 degree increment for the orientation. Figure 16 shows the effect of orientation increment to the resulting area fraction and the second invariant of area fraction tensor for the example image shown in Figure 2. It shows that the increment of orientation should be less than or equal to 10 degrees to obtain a reasonable estimate of area fraction and associated fabric tensor. A similar analysis was also applied to the anisotropic synthetic image of Figure 13. The results (Figure 17) indicate that when the orientation increment is less than or equal to 5 degrees, the estimation of area fraction and the second invariant of area fraction tensor become stable.

The above analyses show that the current settings for the line spacing and orientation increment are adequate. However, the appropriate setting of line spacing and orientation increment is case dependent. Since the determinations of mean fabric descriptor and its associated tensor can be efficiently performed with an image analysis system (less than 3 minutes for current setting), it is worth performing a few trials for set-up purpose before the extensive usage of certain type of images.

Generality of Methodology

The formulations of fabric tensors introduced in the papers are based on the principle of stereology. The attraction of these proposed stereology based fabric tensors is that there are no assumptions on the shape or size of particles/ voids. Thus, the methods developed here can generally be applied to any materials of interest. Even though the illustrations of the methods are made on sandy materials, the methods can be applied to

clayey soils . They can be applied to study cracks in rock also. The generality of these proposed methods make them superior than previous fabric formulations that use distribution of contact normal or particle orientation, because the proposed methods provide unified treatment for quantifying the anisotropy of materials.

Practical Implications and Limitations

In general, in order to formulate the fabric tensor in three dimensions, three orthogonal planes are needed. However, if axial symmetry is assumed, only one horizontal and one vertical plane are required. It is found that the axial symmetry characteristic is common in artificially deposited sands. However, this characteristic disappears in many undisturbed natural sands. This is probably because water (or air) flow at the time of sedimentation may have an effect on the particle orientation.

In obtaining the surface area density and surface area tensor or mean free path and mean free path tensor from three orthogonal planes, it is crucial to know the magnification and keep the same magnification for each plane observed. For porosity and porosity tensor, since the quantities examined are dimensionless, the magnification can be unknown. The magnifications of the three planes observed can also be slightly different. Of course, keeping the same magnification is preferable.

The information on distribution of porosity versus frame width provides guidelines for selecting a suitable sample size for analyzing porosity and porosity tensors. It is desired that the radius of inner REC(r_1) is smaller than 1/3 of the radius of outer REC(r_2) such that over 90% of the area inside the outer REC is analyzed. For the maximum image size of many analyzers (512 pixels x 480 pixels), it is desirable to have the radius of the outer REC(r_2) as large as possible (230 or 240 pixels). Thus, the radius of inner REC(r_1) should be kept smaller than 80 pixels if possible. So, if the distribution of porosity does not stabilize at frame widths of up to 110 pixels, it indicates that the sample size may be too small. Decrease the magnification and observe larger sample sizes

will allow the porosity distribution be stable within a frame width of 110 pixels. Figure 18 shows an image of insufficient sample size that is not suitable for analysis of porosity and porosity tensor at the current magnification.

Surface area density S_v, mean free path λ, and porosity n_0 are important structural parameters in practice. The behavior of soils are closely related to these parameters. For example, by knowing surface area and porosity, permeability can be estimated through Kozeny - Carman relation. Blair et. al. (1993) have utilized the Kozeny - Carman relation to estimate the permeability of porous materials where porosity and specific surface area are provided from image analysis measurements.

As discussed before, there are interrelationships between surface area density S_v, mean free path λ, and porosity n_0, so only two independent parameters exist among these three parameters. Similarly, they will be some interrelationships between surface area tensor, mean free path tensor and porosity tensor. But among these three tensors, any two among them are expected to be independent. To fully quantify the anisotropy of the material, at least two such fabric tensors may be needed.

Conclusion

A stereological approach was used to determine fabric tensors of granular materials. The stereological approach, Kanatani's analysis, offers a unified tensorial formulation for fabric tensors. Based on Kanatani's analysis, fabric tensor formulations in three dimensions can be obtained with observations on three mutually perpendicular planes.

On the basis of Kanatani's analysis, stereological based fabric tensors such as a surface area tensors (S_{ij}) or a mean free path tensor (λ_{ij}) and a porosity tensor (N_{ij}) could be determined experimentally from microscopic observations. It was shown that the structure of granular materials can be modeled via two measures : a scalar measure giving the mean value of a fabric descriptor and a tensor giving its directional distribution in space. Those measurement techniques were implemented using an automated image analysis

system. Computer algorithms were developed to permit the determinations of mean fabric descriptors and their associated tensors efficiently using image analysis techniques. Furthermore, the attraction of these proposed stereology based fabric tensors is that there are no assumptions on the shape or size of particles/ voids. Thus, the methods described here can generally apply to any materials of interest.

The effect of test grid interline spacing and orientation increment on the resulting mean fabric descriptors and their associated tensor was examined. Two tremendously different images were used for this parametric study. The results support that the current settings of line spacing and orientation increment are adequate. However, the appropriate setting of line spacing and orientation increment is case dependent. Since the determinations of mean fabric descriptor and its associated tensor are very efficient when performed with an image analyzer, it is recommended that a few trials be performed for set-up purpose before the extensive usage of certain type of images.

Acknowledgments

The work reported in this paper was supported by National Science Foundation Grant No.'s MSS-9011232, MSS-9007581 and BCS-9304897. This support is gratefully acknowledged.

References

Kanatani, K., (1984a), "Distribution of Directional data and Fabric Tensors", Int. J. Engng. Sci., Vol. 22, No. 2, pp. 149-164.

Kanatani, K., (1984b), "Stereological determination of Structural Anisotropy", Int. J. Engng. Sci., Vol. 22, No. 5, pp. 531-546.

Kanatani, K., (1985), "Procedures for Stereological Estimation of Structural Anisotropy", Int. J. Engng. Sci., Vol. 23, No. 5, pp. 587-598.

Leica Cambridge Ltd., (1991), "Quantimet 570 - QUIC Menu System Operators Manual".

Muhunthan, B., (1991), "Micromechanics of Steady State, Collapse and Stress-Strain Modeling of Soils", Ph.D. dissertation, Purdue University, IN., 222 pp.

Oda, M., Ohnishi, A. (1992) "Plasticity Theory for Granular Soils with Induced Anisotropy" Advances in Micromechanics of Granular Materials H. H. Shen et al. (Editors), pp. 193-202.

Tobita, Y., (1989), "Fabric Tensors in Constitutive Equations for Granular Materials", Soils and Foundations, Vol. 29, No. 4, pp. 91-104.

Kuo, C.-Y., Frost, J. D., and Chameau, J. L., (1995), "Stereology based Fabric Tensors - Part I : Definitions and Measurement Techniques", paper submitted for possible publication in Geotechnique.

LIST OF TABLES

LIST OF FIGURES

Table 1 Field measurement of example image (Figure 2)

	FIELD 1	NORMALIZED	ACCUMULATED
Area	1.257E+5	0.511	1.257E+05
Intercept H	4278	0.017	4278
Intercept V	4506	0.018	4506
Perimeter	16069	0.065	16069
Count	85	3.459E-04	85
Area Fraction	0.511	-	0.511
Anisotropy	0.949	-	0.949
Area Fill	1.046	-	1.046
Mean Chord	29.374	-	29.374
Frame Area	2.458E+05	-	2.458E+05

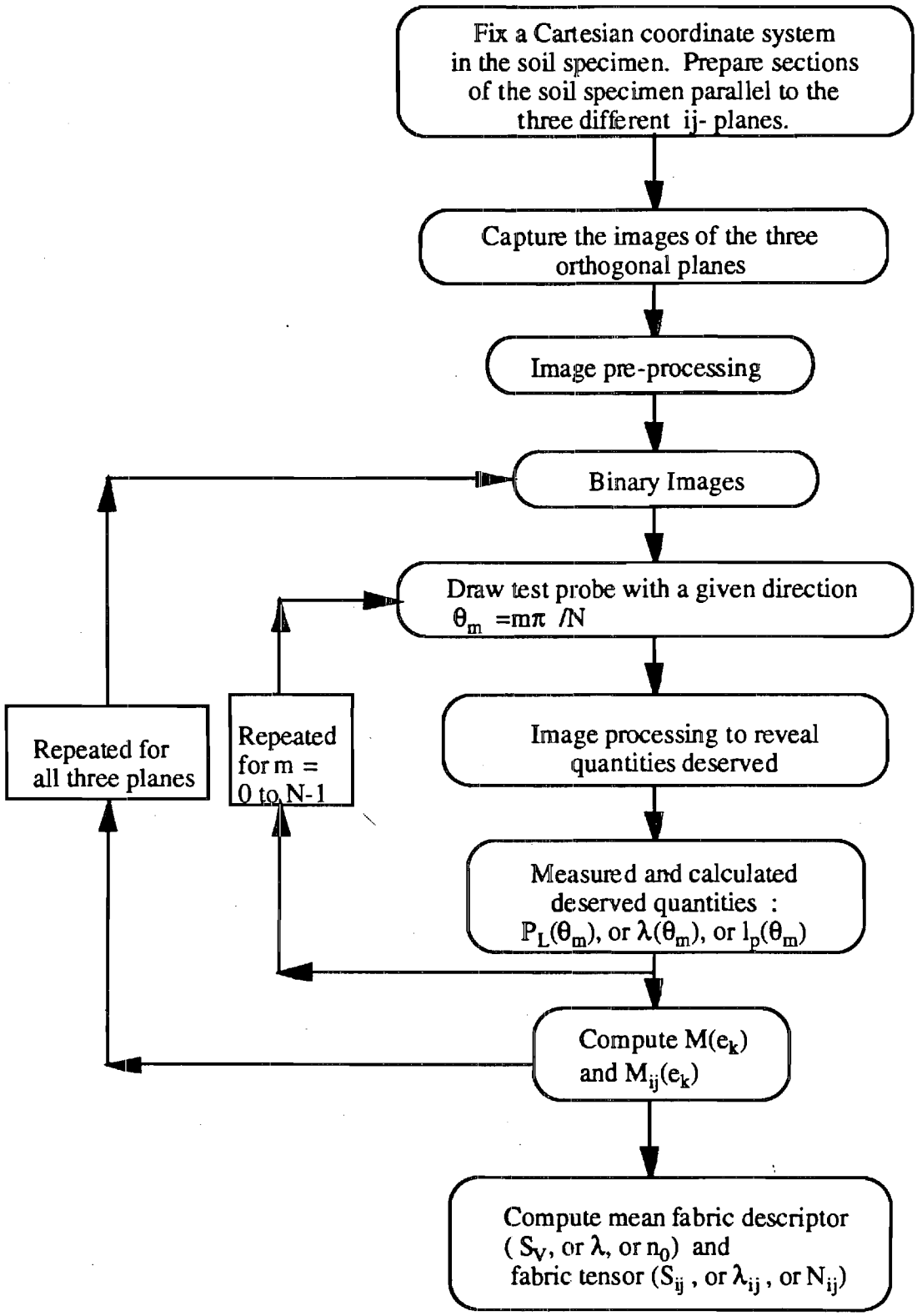

Figure 1 The general procedures to determine fabric tensors in an image analyzer

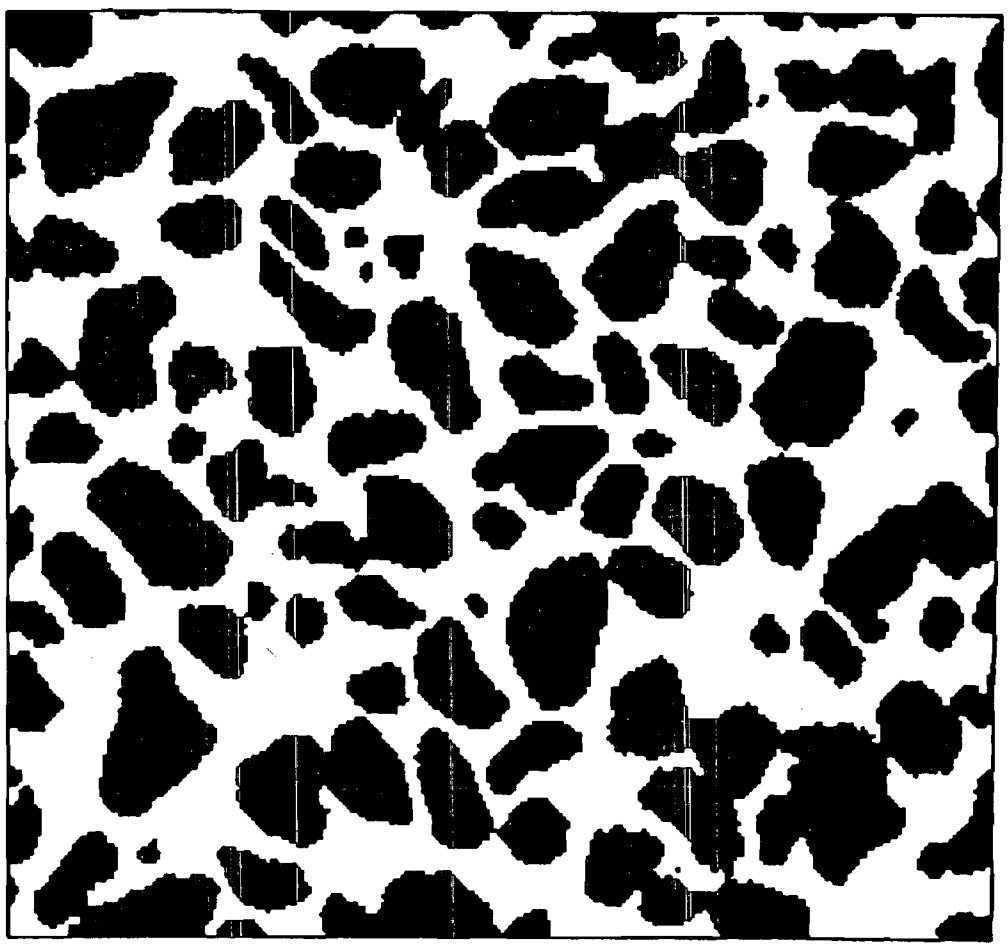

Figure 2 Example image (reproduced from part of Fig. 4(c) of Bhatia and Soliman, 1990)

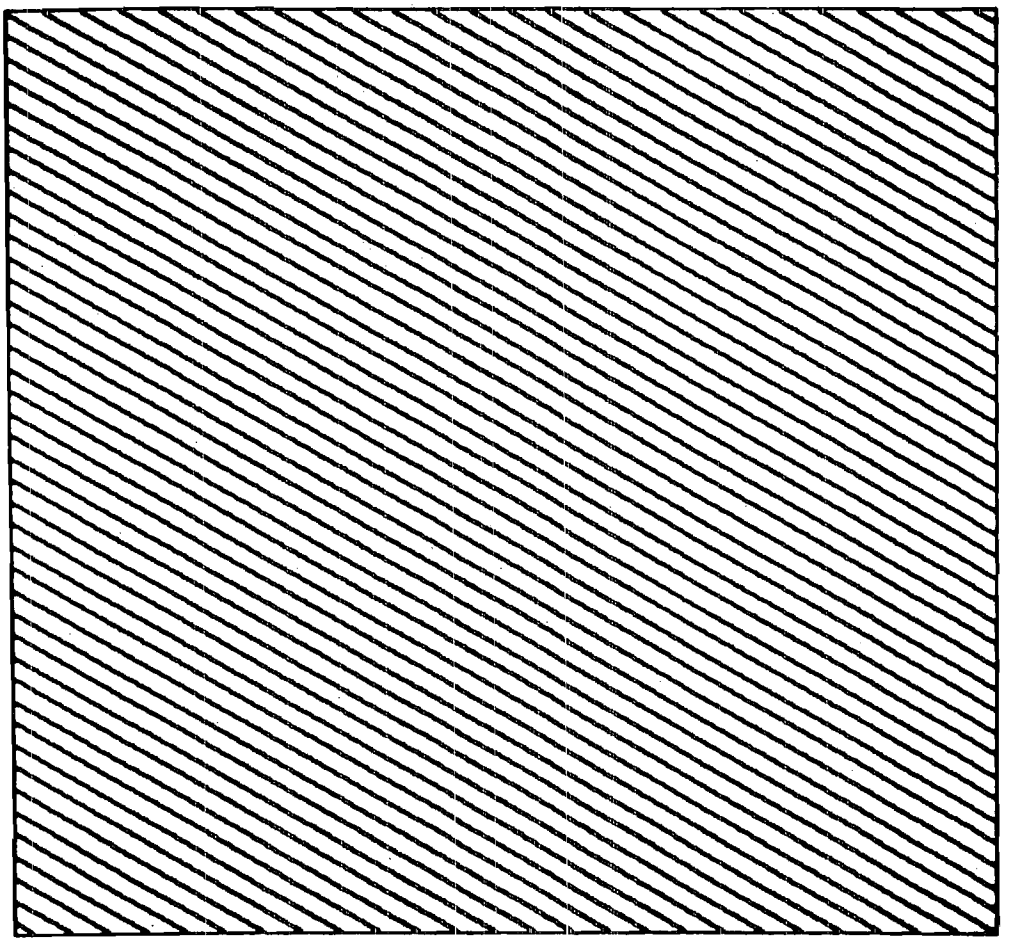

Figure 3 A grid of parallel test lines

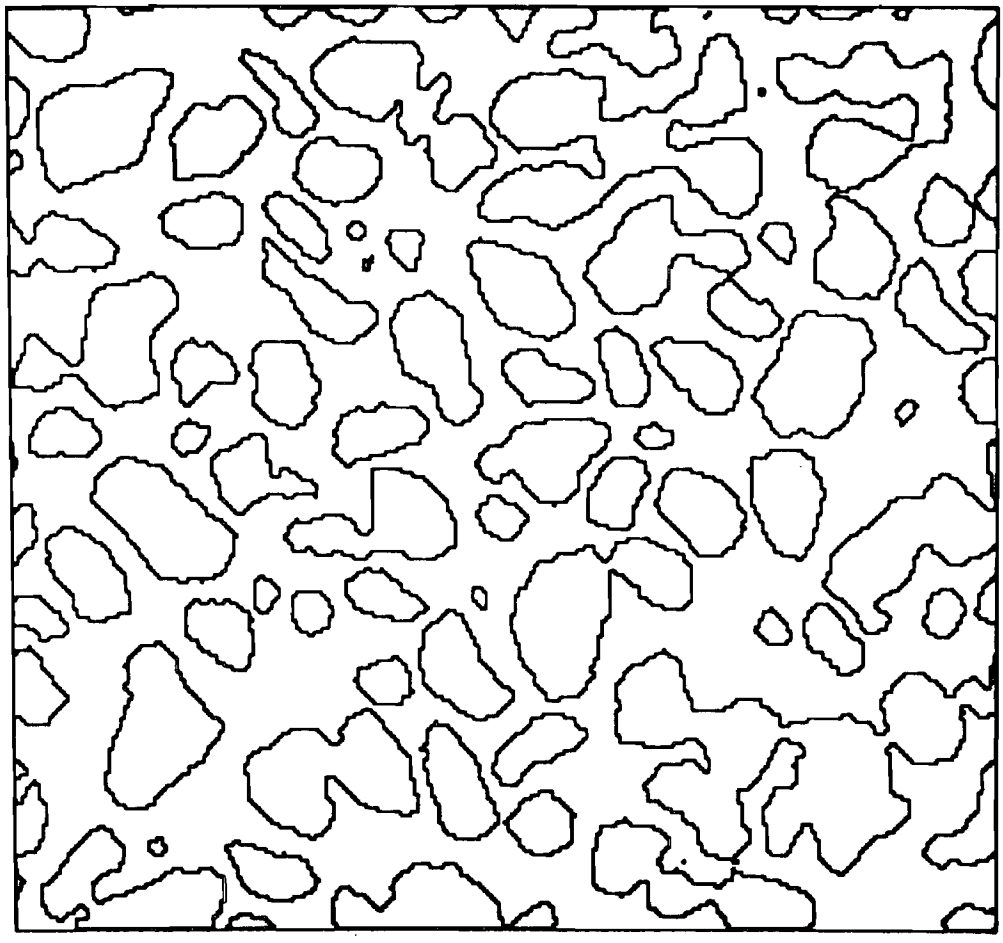

Figure 4 Outline of example image (Figure 2)

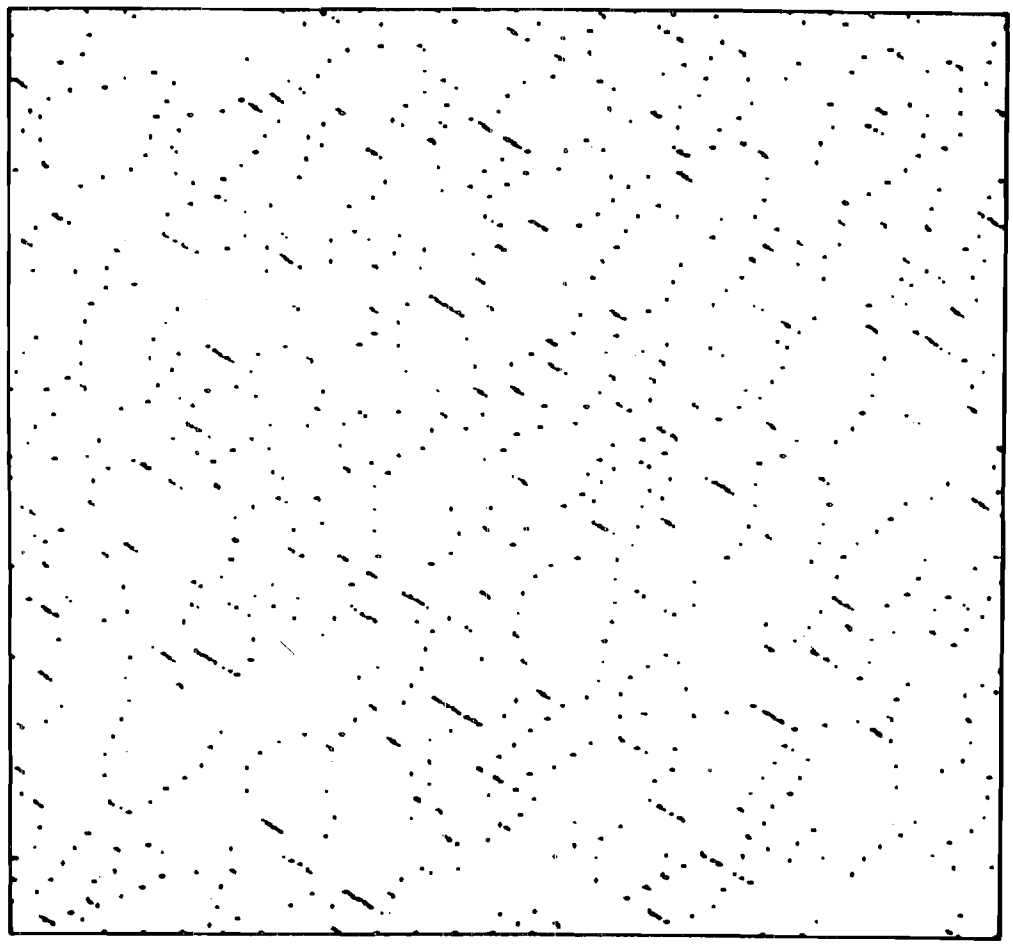

Figure 5 Intercepts of test lines and soil particles of the example image (Figure 2)

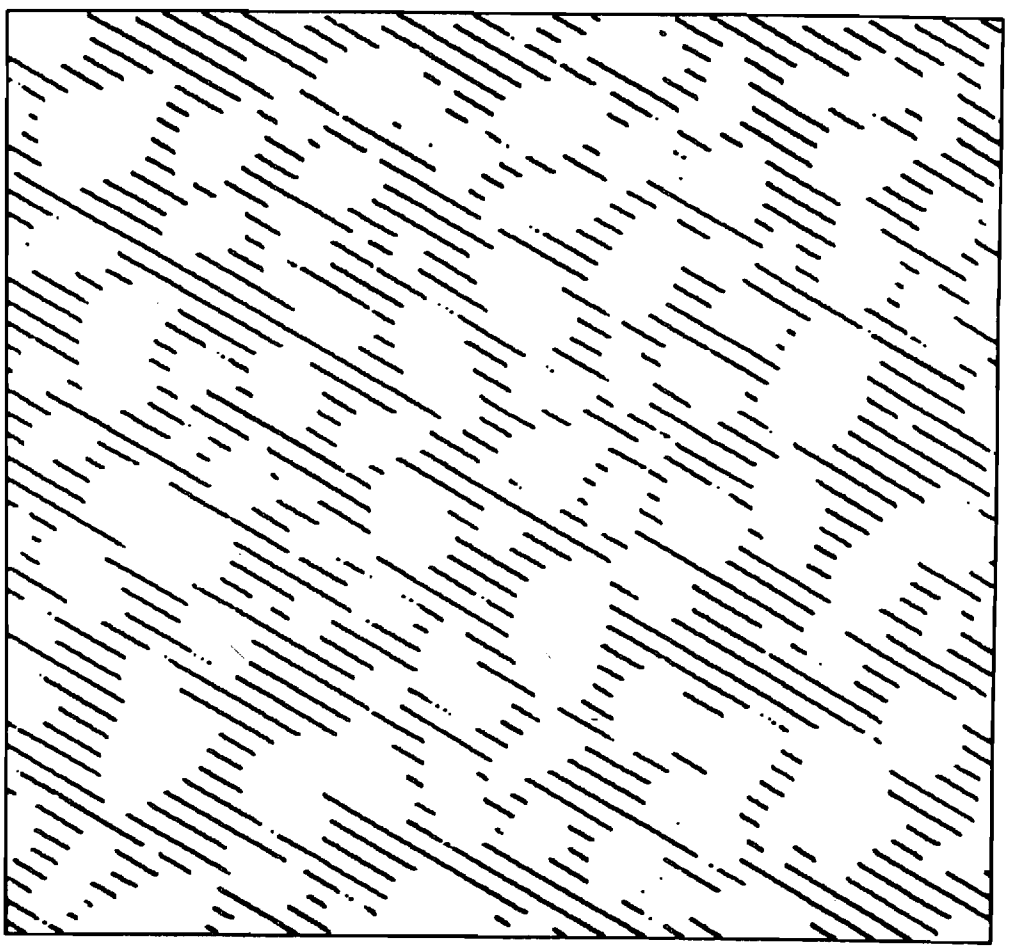

Figure 6 Free paths between particles of example image (Figure 2) in a given direction

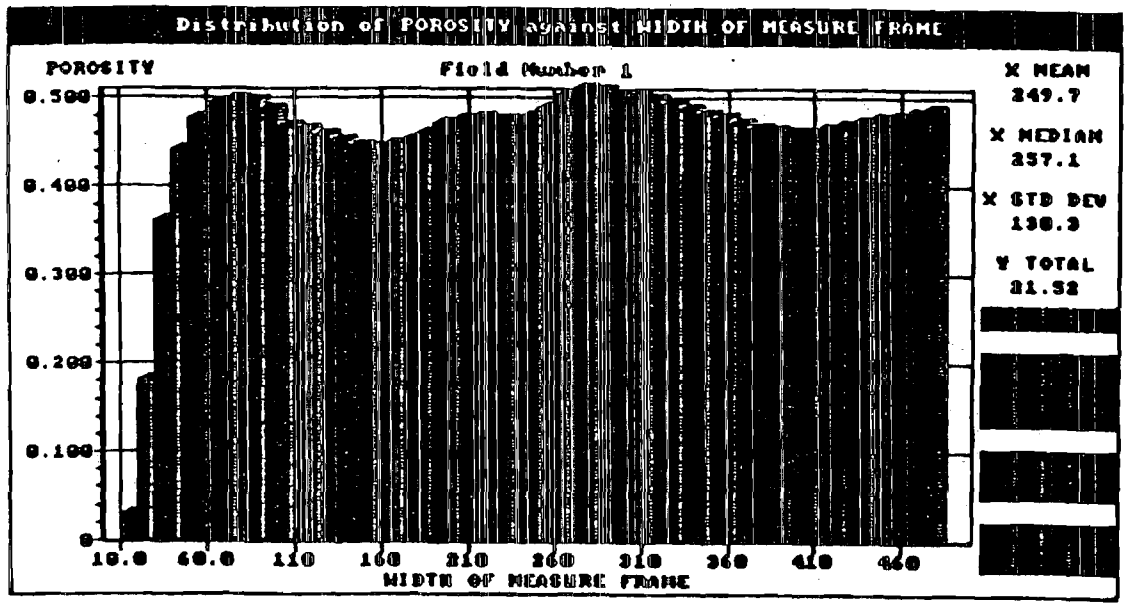

Figure 7 Measured porosities with different size of measure frame for example image (Figure2)

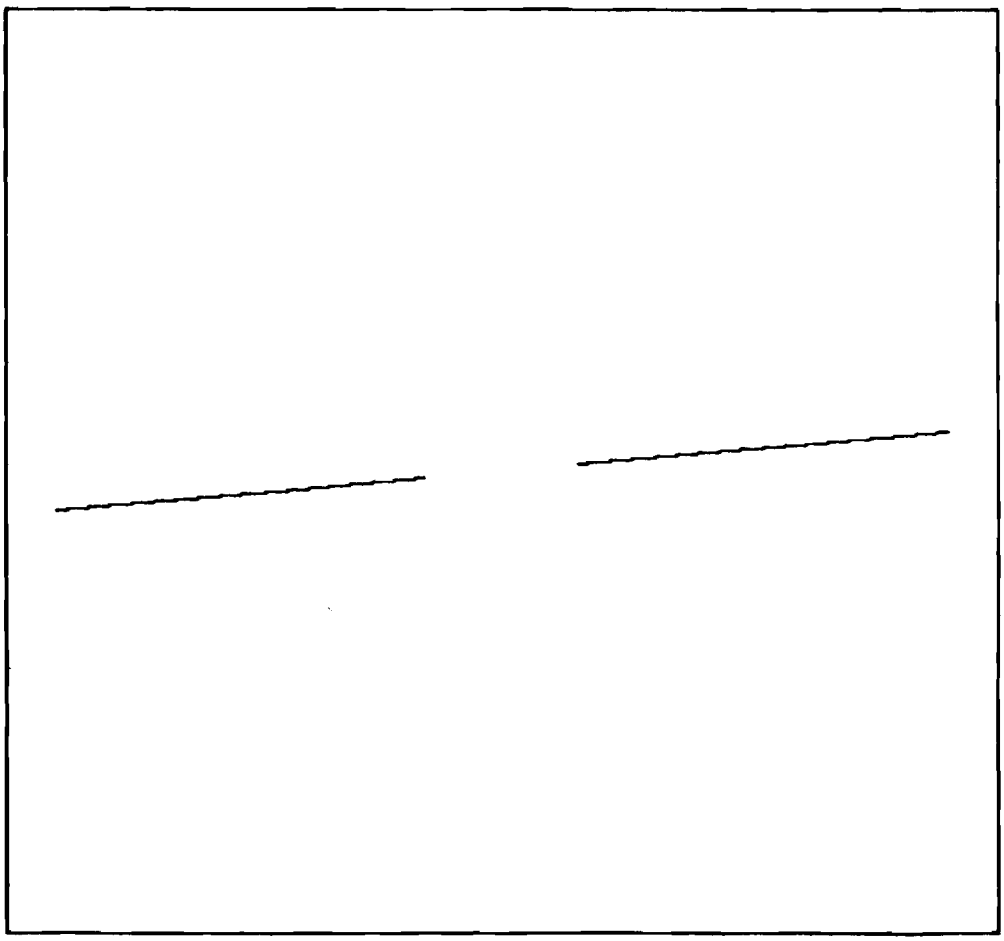

Figure 9 Test line used in a given direction for determining porosity tensor

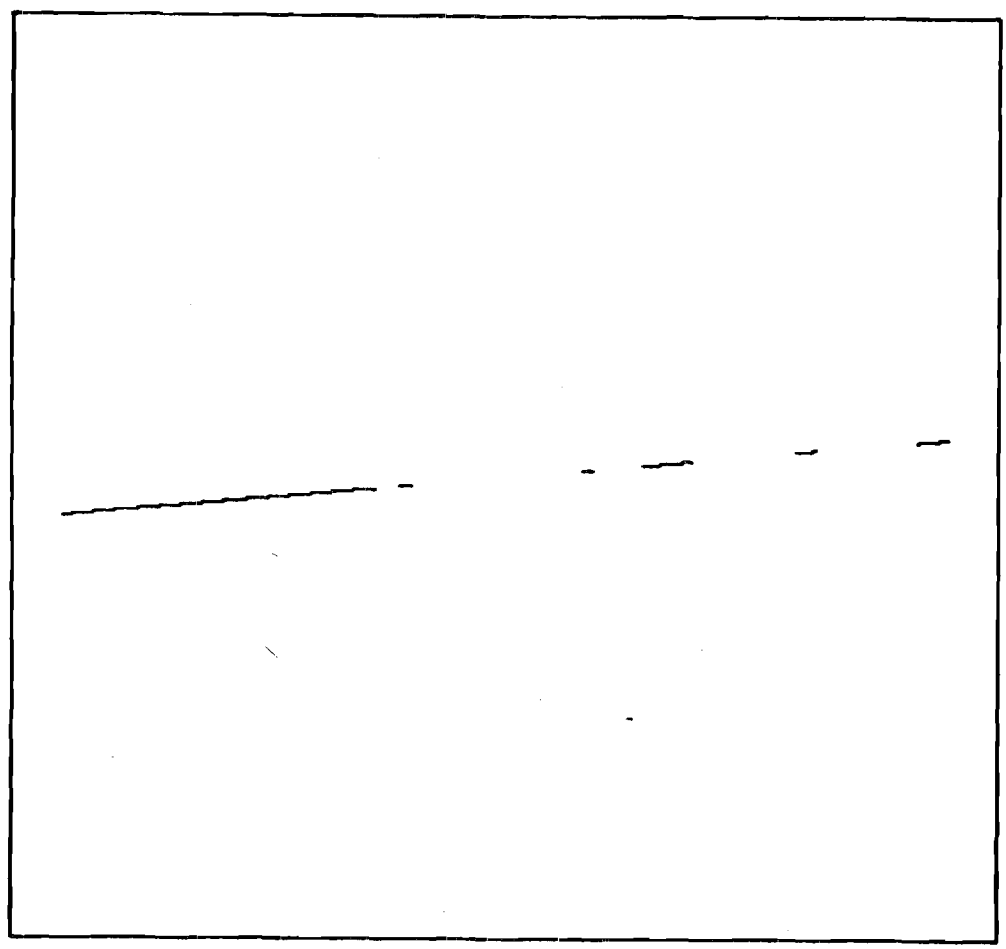

Figure 10 The portions of the test line occupied by void $l_p(\theta_m)$

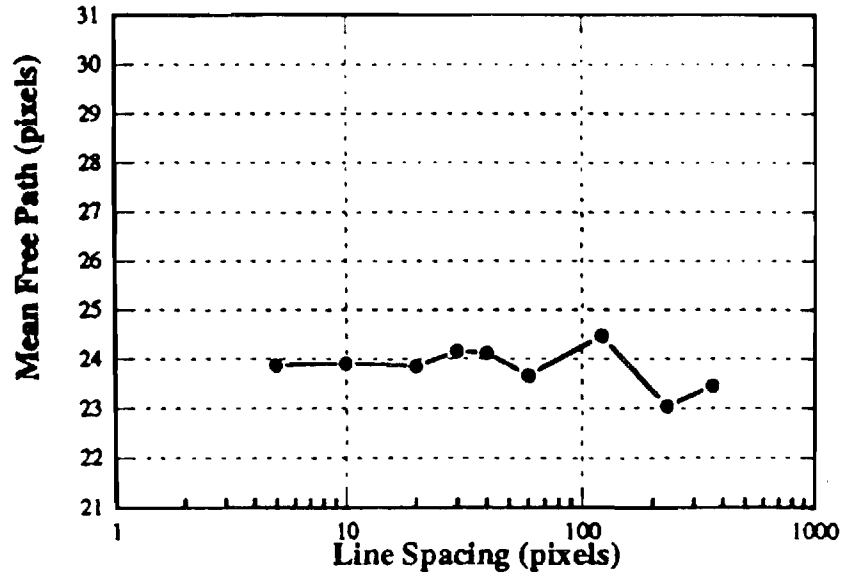

(a)

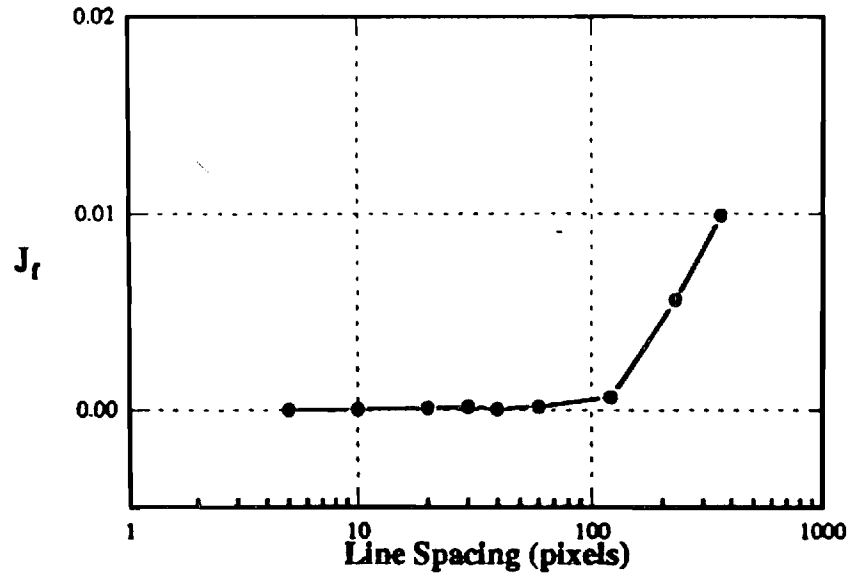

(b)

Figure 11 Effect of line spacing on the resulting mean free path and J_f for the example image of Figure 2

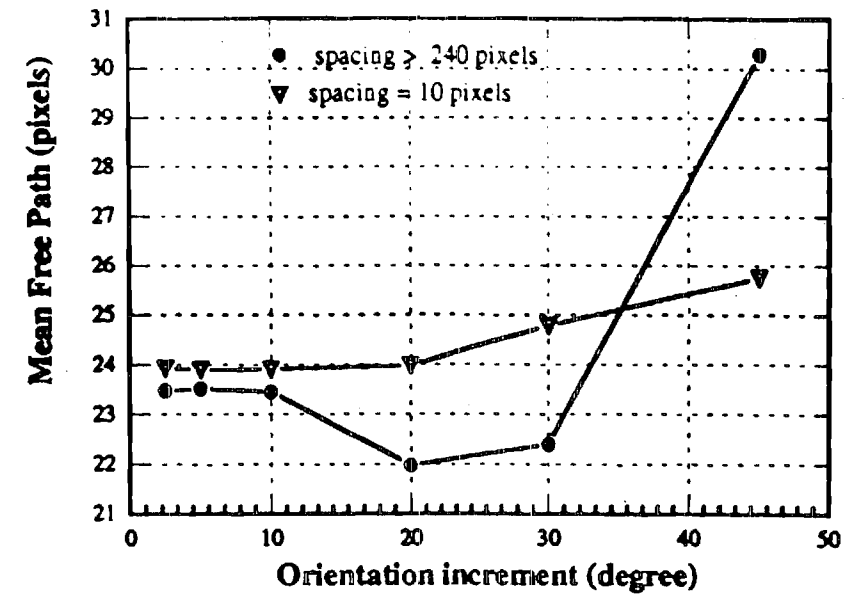

(a)

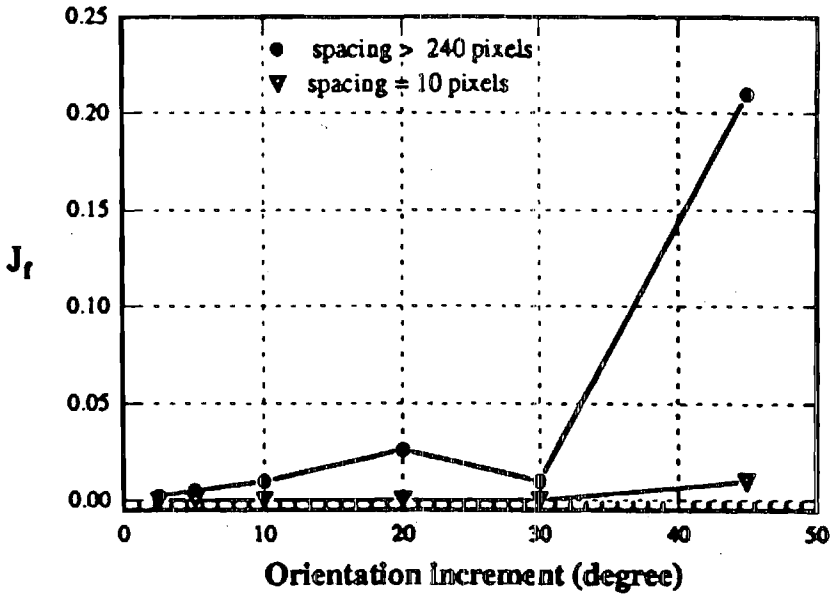

(b)

Figure 12 Effect of orientation increment for the resulting mean free path and J_f, for the case of line spacing > 240 pixels (a single test line) and line spacing =10 pixels, for example image of Figure 2

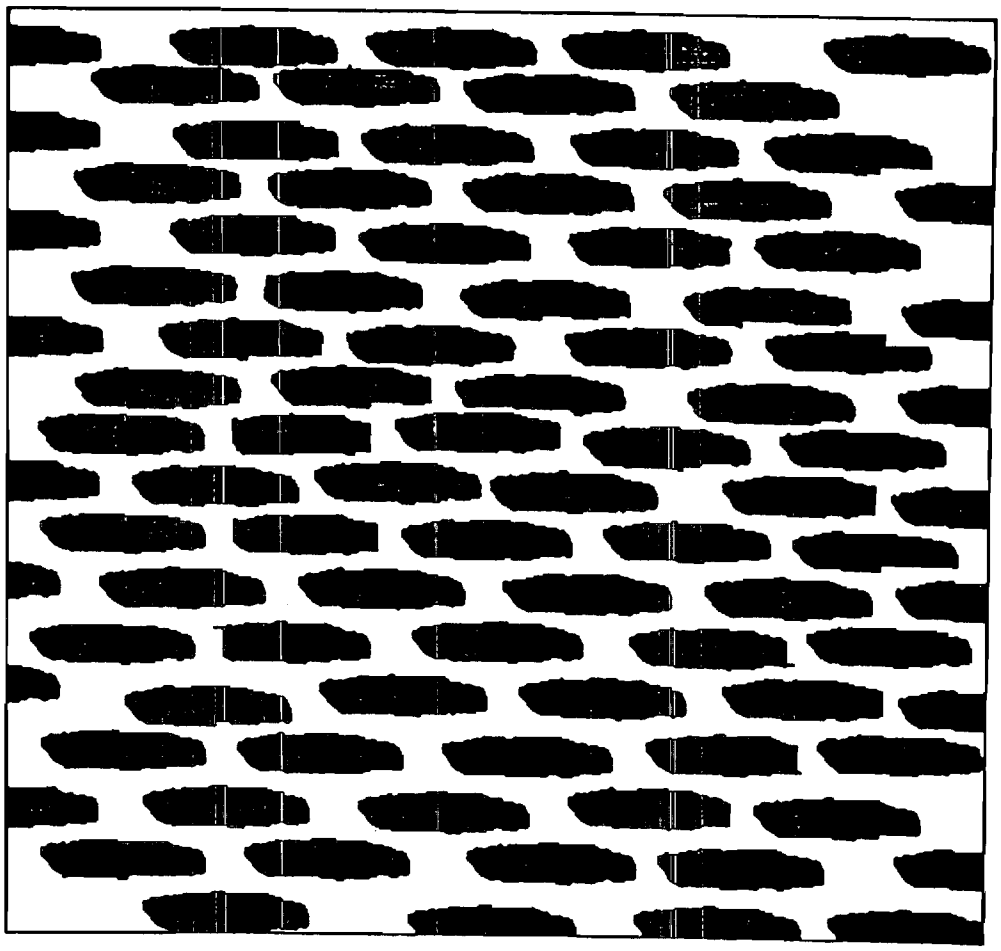

Figure 13 Anisotropic synthetic image

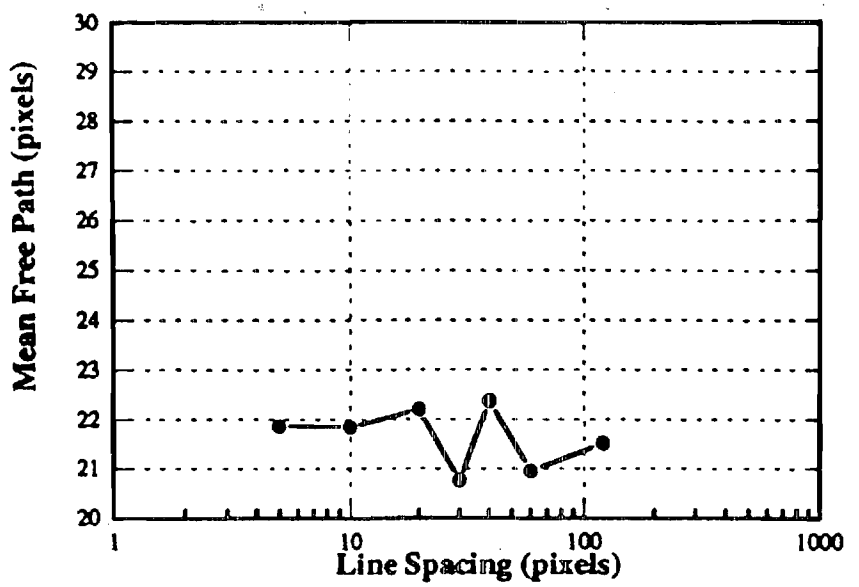

(a)

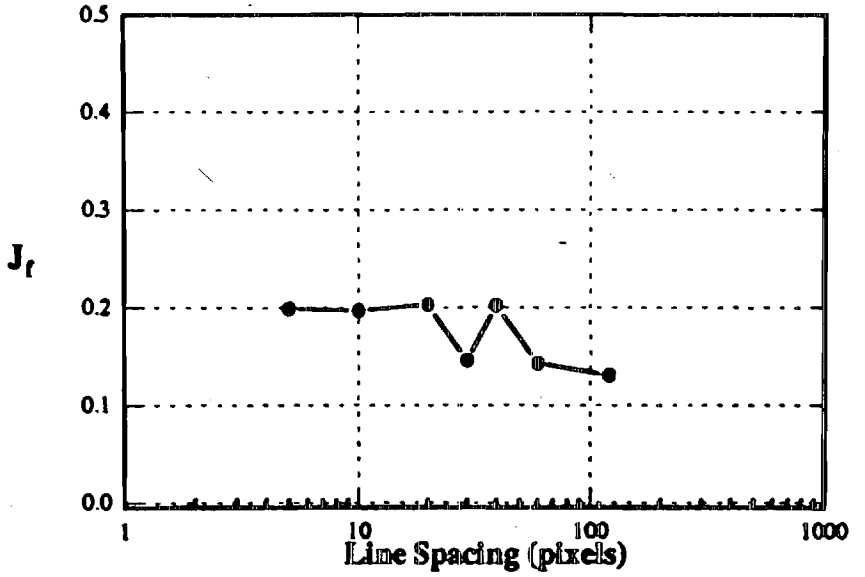

(b)

Figure 14 Effect of line spacing on the resulting mean free path and J_f for the anisotropic synthetic image of Figure 13

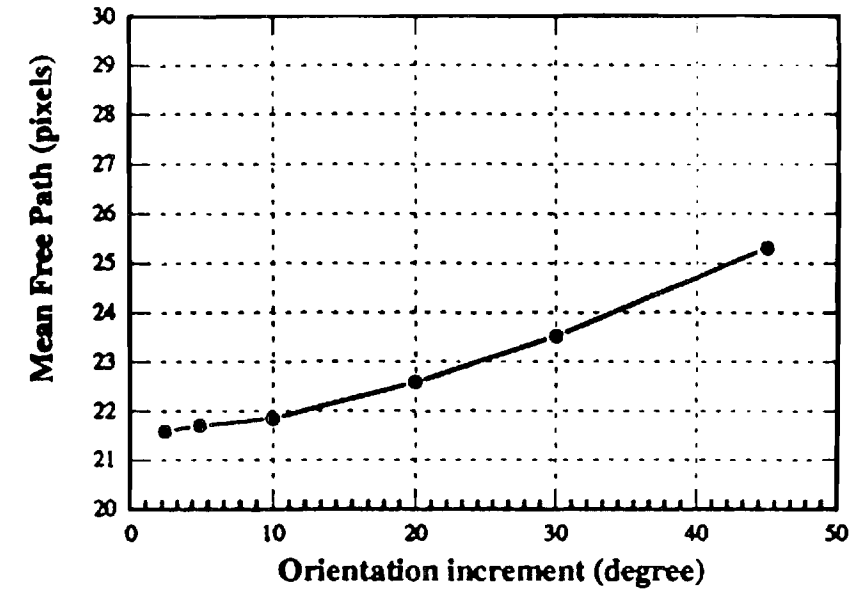

(a)

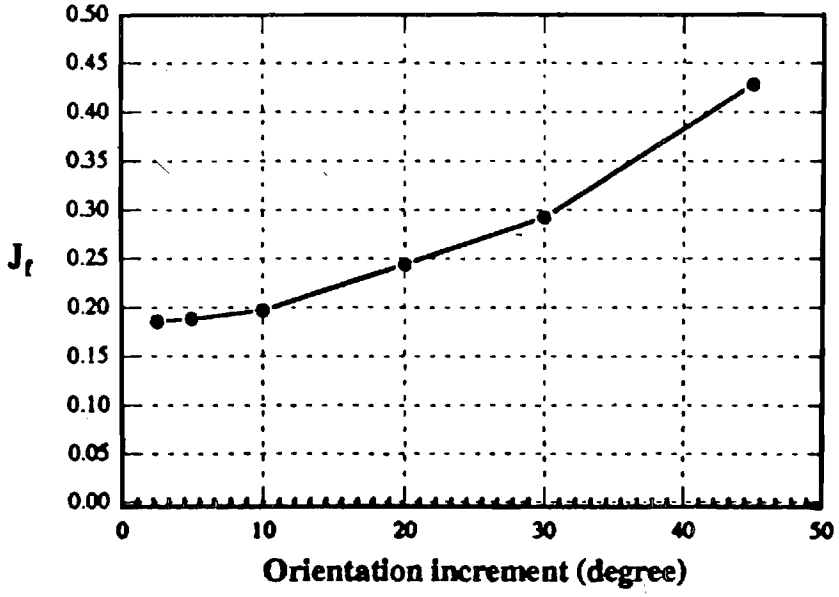

(b)

Figure 15 Effect of orientation increment on the resulting mean free path and J_f for the anisotropic synthetic image of Figure 13

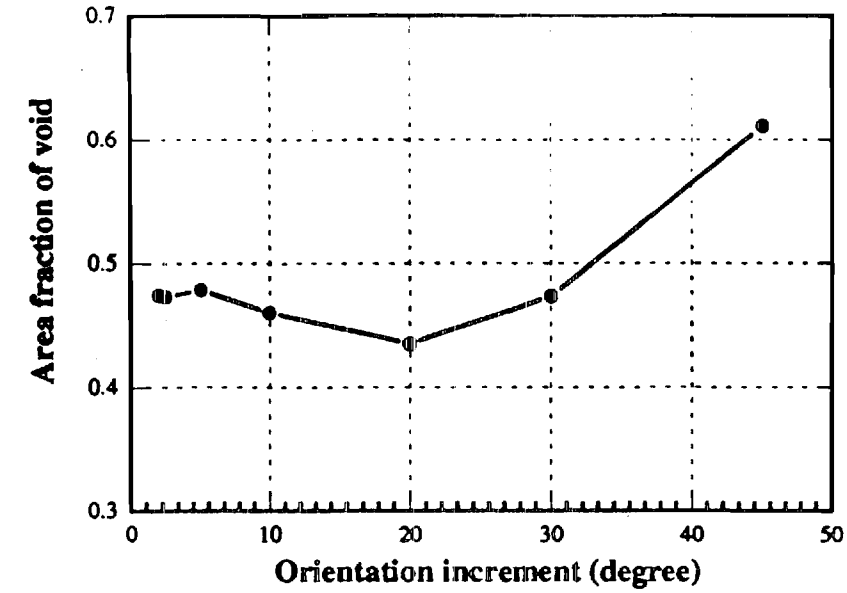

(a)

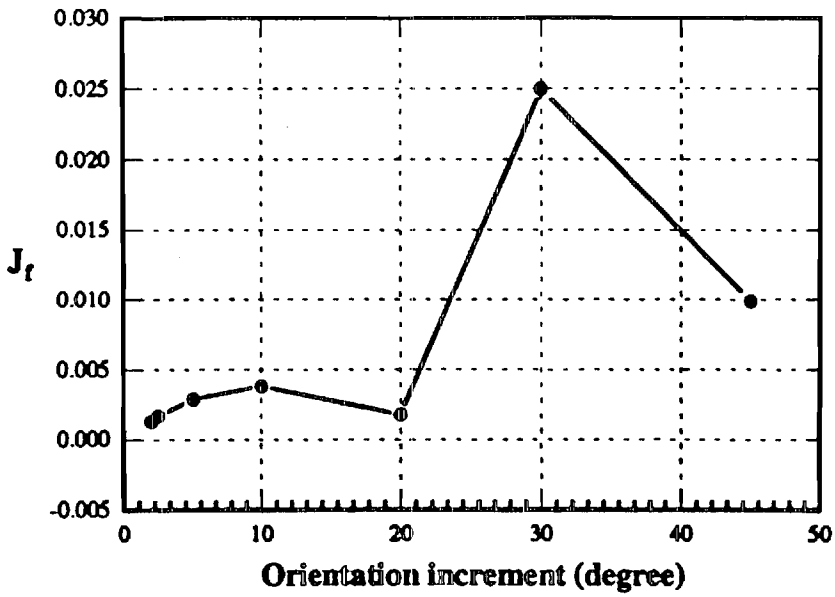

(b)

Figure 16 Effect of orientation increment on the resulting area fraction and J_f for the example image of Figure 2

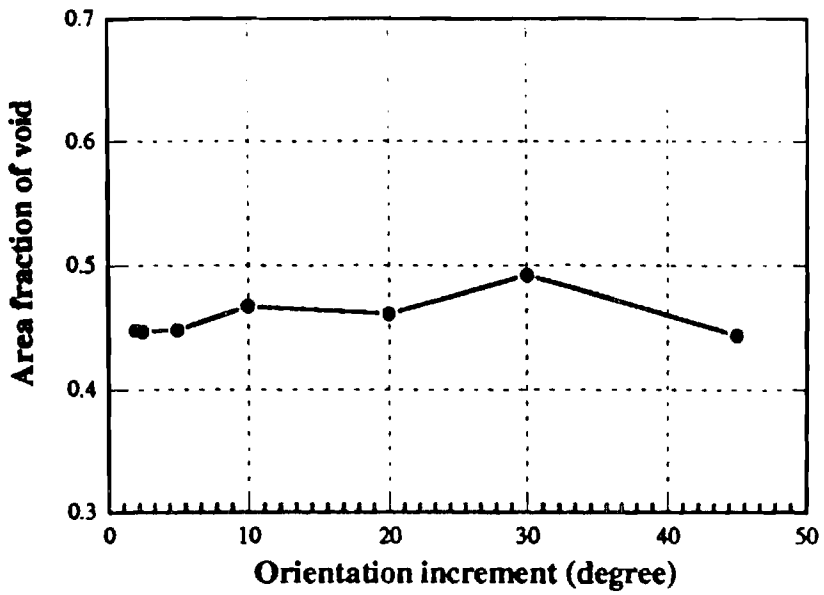
0.7
0.6
0.5
0.4
0.3
Area fraction of void
0
10
20
30
40
50
Orientation increment (degree)

(a)

E-20-X46
3

Georgia Institute of Technology
School of Civil and Environmental Engineering

Geosystems Engineering Program
Atlanta, Georgia 30332-0355 USA
TEL 404-894-2282
FAX 404-894-2281
http://geosystems.gatech.edu

April 30, 1997

Dr. Clifford J. Astill,
Program Director, Siting & Geotechnical Systems
Earthquake Hazard Mitigation Program
National Science Foundation
4201 Wilson Boulevard, Room 545
Arlington
VA 22230

Final Report: CMS-9304897, "Energy Principles for Monotonic and Cyclic Loading of Cohesionless Soils"

Dear Dr. Astill,

Please find attached the final report for the project CMS-9304897, "Energy Principles for Monotonic and Cyclic Loading of Cohesionless Soils". The work described in the report has been performed by 2 graduate research assistant at the Georgia Institute of Technology under the direction of Dr. J. David Frost and Dr. Jean-Lou Chameau. In addition, the work has been coordinated with the activities being undertaken by a graduate research assistant at Washington State University under the direction of Dr. Balasingham Muhunthan.

Please do not hesitate to contact the undersigned by phone at (404) 894-2280, fax at (404) 894-2281 or email at dfrost@ce.gatech.edu if you have any questions about the report. We sincerely appreciate the support we have received from the National Science Foundation for this project.;

Sincerely,

J. David Frost, Ph.D., P.E., P.Eng.
Associate Professor of Civil Engineering

OMB Number 345-0058

NATIONAL SCIENCE FOUNDATION
4201 Wilson Blvd.,
Arlington, VA 22230

BULK RATE
POSTAGE & FEES PAID
National Science Foundation
Permit No. G-69

PI/PD Name and Address

Jean-Lou A. Chameau
[redacted]
790 Atlantic Drive
Atlanta , GA [redacted]

0325

NATIONAL SCIENCE FOUNDATION
FINAL PROJECT REPORT

PART I - PROJECT IDENTIFICATION INFORMATION

1. Program Official/Org. Clifford J. Astill - CMS

2. Program Name EARTHQUAKE HAZARD MITIGATION PROGRAM

3. Award Dates (MM/YY) From: 08/93 To: 01/97

4. Institution and Address
[redacted]
Administration Building
Atlanta GA 30332

5. Award Number [illegible]

6. Project Title
Energy Principles for Monotonic and Cyclic Loading of [illegible]

** You are encouraged to submit your Final Project Report electronically through the NSF FastLane home page (www.fastlane.nsf.gov). **

This Packet Contains
NSF Form 98A
And 1 Return Envelope

F Grant Conditions (Article 17, GC-1, and Article 9, FDP-11) require submission of a Final Project port (NSF Form 98A) to the NSF program officer no later than 90 days alter the expiration of the ard. Final Project Reports for expired awards must be received before new awards can be made iF Grants Policy Manual Section 677).

w, or on a separate page attached to this form, provide a summary of the completed projects and technical information. Be to include your name and award number on each separate page. See below for more instructions.

PART II - SUMMARY OF COMPLETED PROJECT (for public use)

summary (about 200 words) must be self-contained and intelligible to a scientifically literate reader. Without restating the ect title, it should begin with a topic sentence stating the project's major thesis. The summary should include, if pertinent ie project being described, the following items:

ie primary objectives and scope of the project
ie techniques or approaches used only to the degree necessary for comprehension
ie findings and implications stated as concisely and informatively as possible

SEE ATTACHMENT

PART III - TECHNICAL INFORMATION (for program management use)

references to publications resulting from this award and briefly describe primary data, samples, physical collections, ntions, software, etc. created or gathered in the course of the research and, if appropriate, how they are being made available ie research community. Provide the NSF Invention Disclosure number for any invention.

SEE ATTACHMENT

tify to the best of my knowledge (1) the statements herein (excluding scientific hypotheses and scientific opinion) are true and complete, and he text and graphics in this report as well as any accompanying publications or other documents, unless otherwise indicated, are the original k of the signatories or of individuals working under their supervision. I understand that willfully making a false statement or concealing a erial fact in this report or any other communication submitted to NSF is a criminal offense (U.S. Code, Title 18, Section 1001).

	4/30/97
Principal Investigator/Project Director Signature	**Date**

IMPORTANT:
MAILING INSTRUCTIONS
Return this *entire* packet plus all attachments in the envelope attached to the back of this form. Please copy the information from Part I, Block I to the *Attention block* on the envelope.

PART IV -- FINAL PROJECT REPORT -- SUMMARY DATA ON PROJECT PERSONNEL

(To be submitted to cognizant Program Officer upon completion of project)

The data requested below are important for the development of a statistical profile on the personnel supported by Federal grants. The information on this part is solicited in resonse to Public Law 99-383 and 42 USC 1885C. All information provided will be treated as confidential and will be safeguarded in accordance with the provisions of the Privacy Act of 1974. You should submit a single copy of this part with each final project report. However, submission of the requested information is not mandatory and is not a precondition of future award(s). Check the "Decline to Provide Information" box below if you do not wish to provide the nformation.

Please enter the numbers of individuals supported under this grant.
Do not enter information for individuals working less than 40 hours in any calendar year.

	Senior Staff		Post-Doctorals		Graduate Students		Under-Graduates		Other Participants[1]	
	Male	Fem.	Male	Fem.	Male	Fem.	Male	Fem.	Male	Fem.
A. Total, U.S. Citizens										
B. Total, Permanent Residents										
U.S. Citizens or Permanent Residents[2]:										
American Indian or Alaskan Native										
Asian					2					
Black, Not of Hispanic Origin										
Hispanic										
Pacific Islander										
White, Not of Hispanic Origin	1									
C. Total, Other Non-U.S. Citizens										
Specify Country 1.										
2.										
3.										
D. Total, All participants (A + B + C)	1				2					
Disabled[3]										

☐ Decline to Provide Information: Check box if you do not wish to provide this information (you are still required to return this page along with Parts I-III).

[1] Category includes, for example, college and precollege teachers, conference and workshop participants.

[2] Use the category that best describes the ethnic/racial status lo all U.S. Citizens and Non-citizens with Permanent Residency. *(If more than one category applies, use the one category that most closely reflects the person's recognition in the community.)*

[3] A person having a physical or mental impairment that substantially limits one or more major life activities; who has a record of such impairment; or who is regarded as having such impairment. *(Disabled individuals also should be counted under the appropriate ethnic/racial group unless they are classified as "Other Non-U.S. Citizens.")*

AMERICAN INDIAN OR ALASKAN NATIVE: A person having origins in any of the original peoples of North America and who maintains cultural identification through tribal affiliation or community recognition.

ASIAN: A person having origins in any of the original peoples of East Asia, Southeast Asia or the Indian subcontinent. This area includes, for example, China, India, Indonesia, Japan, Korea and Vietnam.

BLACK, NOT OF HISPANIC ORIGIN: A person having origins in any of the black racial groups of Africa.

HISPANIC: A person of Mexican, Puerto Rican, Cuban, Central or South American or other Spanish culture or origin, regardless of race.

PACIFIC ISLANDER: A person having origins in any of the original peoples of Hawaii; the U.S. Pacific territories of Guam, American Samoa, and the Northern Marinas; the U.S. Trust Territory of Palau; the islands of Micronesia and Melanesia; or the Philippines.

WHITE, NOT OF HISPANIC ORIGIN: A person having origins in any of the original peoples of Europe, North Africa, or the Middle East.

Energy Principles for Monotonic and Cyclic Loading of Cohesionless Soils
Final Report: Project CMS-9304897

Introduction

Significant advances have been made in improving the understanding of the stress-strain behavior of saturated cohesionless soils. Numerous methods of testing and equipment have been developed over the past 30 years in an effort to simulate in situ conditions and characterize the soil's response to undrained static and cyclic loading. Castro (1969) performed extensive stress-controlled tests on a variety of specimens with different gradations, grain sizes and shapes of sands prepared by the moist-tamping method. The steady state line was found to be a unique function of void ratio for each material and thus a potentially useful reference line. However, conflicting evidence regarding this concept of uniqueness exists in the literature (Poulous, 1981; Poulos et al., 1985; Alarcon et al., 1988; Frost, 1989; Konrad, 1990a, 1990b; Vaid et al., 1990; DeGregorio, 1990).

The concept of structural collapse was introduced to explain the sudden increase in pore pressure associated with the initiation of strain softening under either monotonic or cyclic loading (Alarcon et al, 1988). The concept was used to explain why steady state conditions in drained shear are not necessarily the same as in undrained shear. The pore pressure response of sand in undrained shear depends not only on the potential volume changes, as determined in drained tests, but also on the tendency to collapse, i.e. tendency for a sudden change in particle arrangement (fabric). The degree to which a specimen collapses, and hence its steady state position in the state diagram, is dependent of the loading conditions and the initial fabric of the sand (Degregorio, 1990; Frost et al, 1991). Ibrahim and Kagawa (1991) showed the effects of the specimen preparation method on the fabric of sand and the change of sand fabric due to cyclic loading leading to liquefaction. With the help of microscopic measurement it was qualitatively observed that for a "randomly" arranged sand specimen prepared by dry pluviation, cyclic shear tends to line up the arrangement of sand particles, resulting in a less random arrangement of sand particles. In the case of "regularly " arranged sand specimen prepared by wet tamping methods, the opposite trend was observed.

Fabric Effect on the Behavior of Sand

Fabric refers to the arrangement of particles, particle groups, and pore spaces in a soil. Fabric is usually defined as the spatial arrangement of particles, which includes the orientation of each particle, the distribution of the contact normal, and the distribution of void ratios. The characteristics of the fabric depend on the sample preparation method.

Figure 1 compares results from tests performed on specimens at approximately the same void ratio but prepared using different techniques (Frost, 1989). The specimens exhibit significantly different behavior in terms of both peak strength and post-peak strain softening. It is also noted that the stress-strain curve for the specimen prepared using the dry tubing method exhibits larger local fluctuations when compared to the specimen prepared with the modified air pluviation method and this is believed to reflect the importance of fabric at a more local level even at shear strain levels approaching steady state. Figure 2 shows similar variations in stress-strain behavior and stress path for three specimens at almost the same void ratio but prepared by different methods (DeGregorio, 1990).

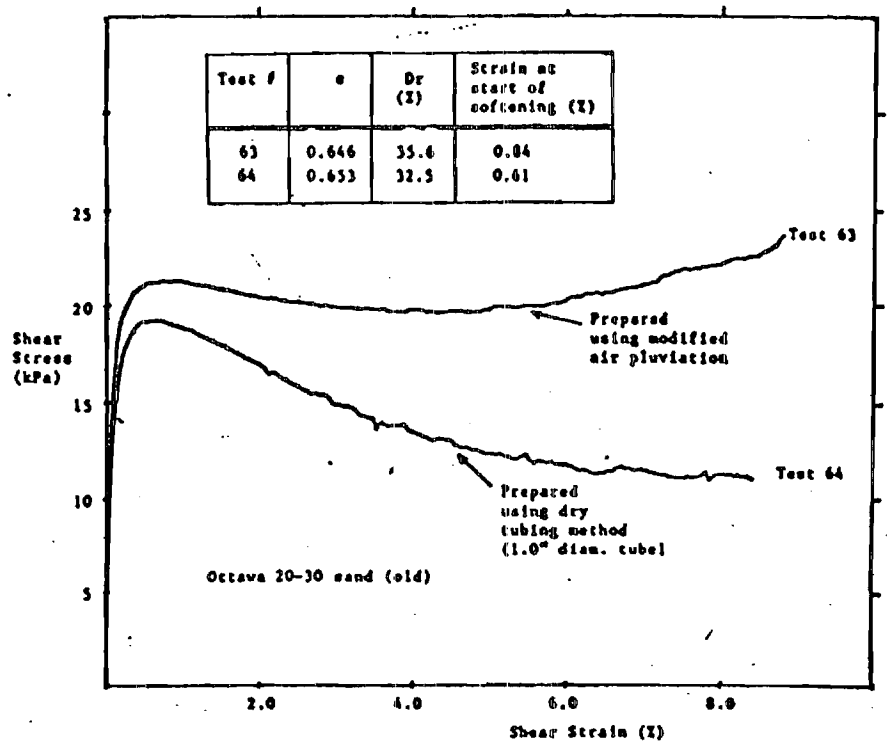

Figure 1. Effect of Method of Preparation on Stress-Strain Behavior (Frost, 1989)

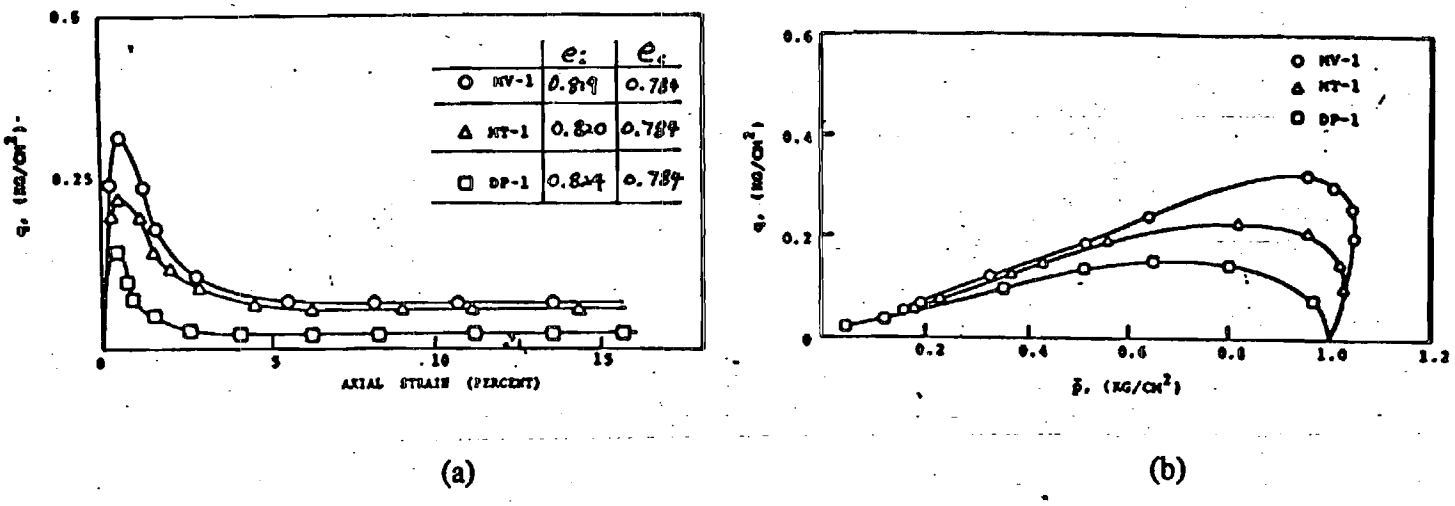

Figure 2. Effect of Method of Preparation on
(a) Stress -Strain Behavior (b) Effective Stress Path (DeGregorio, 1990)

Structural Collapse in Cyclic Tests

At a given void ratio, the monotonic stress path seemed to constitute a collapse boundary that determines the initiation of strain softening behavior under cyclic loading, provided that the stress paths are similar and the cyclic shear stress amplitude is larger than the steady state strength. The initiation of strain softening behavior is characterized by an increase in the rate of pore pressure generation. The manner in which the pore pressure generation rate increases for a given void ratio is related to the actual stress state at which the stress path during cyclic loading reaches the effective stress path from the monotonic test (point C, C' in Figure 3)

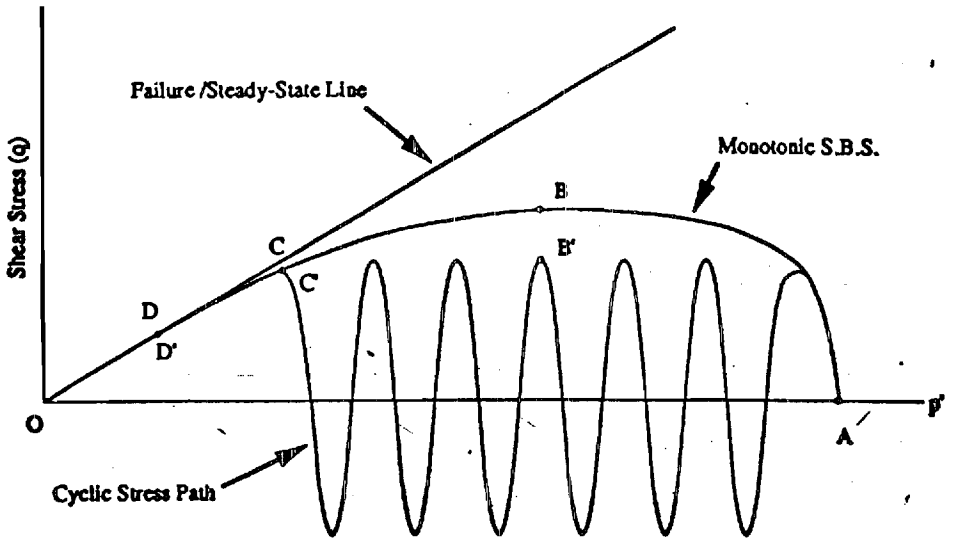

Figure 3 Schematic Stress Path for Monotonic and Cyclic (after Alarcon et al, 1988)

Fabric Quantification

The importance of fabric was noted earlier in the behavior of saturated sand under monotonic and cyclic loading. This research project has resulted in the development of image analysis based methods to quantify the fabric of specimens of granular materials. Techniques to examine local void ratio distributions, anisotropy (fabric tensor), and uniformity have been developed (Kuo, 1994 - Attachment #1). The method and results are presented in detail in a paper that has been submitted to Geotechnique for possible publication (Attachment #2).

The methodologies that have been developed, have been used to study the evolution of fabric in cohesionless soils under drained monotonic loading and relate this to the observed collapse behavior. Accordingly, the initial and post- consolidation fabric of specimens (point O and A in Figure 3) prepared by 2 different sample preparation methods have been quantified with the help of the new methodology. Further, changes in the fabric have been observed at points B, C, and D under monotonic loading. Points B is on the monotonic stress path at an effective stress

Attachment # 1

QUANTIFYING THE FABRIC OF GRANULAR MATERIALS - AN IMAGE ANALYSIS APPROACH

A Thesis
Presented to
The Academic Faculty

by

Chun-Yi Kuo

In Partial Fulfillment
of the Requirements for the Degree
Doctor of Philosophy in Civil and Environmental Engineering

Georgia Institute of Technology

August 1994

TABLE OF CONTENTS

SUMMARY

A soil mass is essentially composed of discrete soil particles, the mechanical behavior of which is influenced to a great extent by the arrangement of individual particles, particle groups, and pore spaces. This arrangement is usually termed "fabric". Previous work on fabric analysis brings recognition of the importance of fabric in the observed response of particulate media under monotonic and cyclic loading. However, most studies on soil fabric still yield results that are more qualitative than quantitative. The reason for this disappointing progress to date is clearly that the existing quantitative techniques were too laborious. This research explores a new, viable procedure of quantifying soil fabric with the aid of an image analysis system. New procedures which integrate aspects of image analysis, mathematical morphology and stereology have provided valuable insight into the fabric of soil.

The fabric of granular materials is quantified by employing image analysis techniques to examine its local void ratio distribution, its anisotropy (fabric tensor), and its uniformity. A new method using image processing and analysis techniques was developed to determine local void ratio distribution. This method eliminates the operator judgment and the manual work of earlier studies, and makes local void ratio distribution more viable as a parameter to quantify sand fabric. The definitions and measurement techniques for some stereology based fabric tensors: surface area tensor, mean free path tensor, and porosity tensor are introduced. Those measurement techniques are then implemented using an automated image analysis system. Computer algorithms are developed that allow determination of these fabric tensors easily using image analysis techniques. Experimental examinations of uniformity at a small scale are

Attachment # 2

December 10, 1996

Revised paper submitted for possible publication in Geotechnique

IMAGE ANALYSIS DETERIMINATIONS OF STEREOLOGY BASED FABRIC TENSORS

Chun-Yi Kuo[1],

J. David Frost[2]

and

Jean-Lou A. Chameau[3]

[1] NRC Postdoctoral Research Associate, Waterways Experiment Station, Vicksburg, MS 39180-6199, USA. [2]Associate Professor and [3]Professor, School of Civil & Environmental Engineering, The Georgia Institute of Technology, Atlanta, Georgia 30332, USA.

Note: Contact author : Dr. Chun-Yi Kuo

Airfields and Pavements Division

Geotechnical Laboratory

Waterways Experiment Station

Vicksburg, MS 39180-6199

USA

Abstract

Fabric tensors which characterize the distribution of directional data from microscopic observations are considered to be a useful measure of anisotropy for granular materials. This paper describes several stereology based fabric tensors such as surface area tensor (S_{ij}), mean free path tensor (λ_{ij}) and porosity tensor (N_{ij}) whose formulations in three dimensions can be obtained with observations on three mutually perpendicular planes. The measurement techniques and the implementation of these measurement techniques using image analysis are described. The implementation of these techniques is illustrated using typical images. The sensitivity, generality, practical implications and limitations of the techniques are also discussed.

Introduction

There is increasing evidence that the mechanical behavior of granular materials depends to a great extent on the relative arrangement of voids and particles or "fabric". Several attempts have been made to develop fabric tensors which describe the packing of granular materials (e.g. Oda et al., 1985; Cowin, 1985; Tobita, 1989; Muhunthan, 1991). Fabric tensors which characterize the distribution of directional data are measures of the anisotropy of the microstructure and are thus considered to be useful measures of fabric in addition to porosity for granular materials. Moreover, they can be used explicitly in a constitutive model thus allowing the discrete granular medium to be described in a continuum sense (e.g., Tobita, 1989; Muhunthan, 1991; Oda and Ohnishi, 1992).

The spatial distribution of various micromechanical quantities such as contact normals, the orientation of long axis of particles and the shape of associated voids have been used to define the fabric tensor. However, it is almost impossible to identify contact normals or the particle orientation for each particle in three dimensions. In practice, two dimensional equivalent tensors that can be determined by measuring contact normal distribution (or particle orientation) from vertical and horizontal sections are introduced.

Then, the two dimensional equivalent tensors ($\vec{F}_{ij}$) are extended to one three dimensional fabric tensor (F_{ij}) under assumptions of (1) axial symmetry and (2) the principal values of $\vec{F}_1$ and $\vec{F}_2$ in two dimensions (2-D) are proportional to the principal values F_1 and F_2 in three dimensions (3-D) (Oda and Nakayama, 1989). Furthermore, the determinations of contact normal, or branch, or void polygon rely on the contact of particles in 2-D sections. However, particles which contact in 3-D are unlikely to contact in a 2-D section since the probability of intercepting the contacts in a 2-D section is generally very small.

This paper describes different fabric measures for granular materials in which fabric tensors are formulated in three dimensions based on the principle of stereology. Stereological methods are tools for obtaining 3-D quantitative information based mainly on observations made on 2-D sections. Hilliard (1967) has provided a mathematical framework for the quantitative description of anisotropic structures. He dealt with the orientation distribution of lines in a plane, of surfaces in space, and of lines in space and related them to the number of intersections per unit length of test line, P_L, and the number of interactions per unit area of test plane, P_A. If intersections are counted for each different orientation of the probe line or plane, then the "structure anisotropy", i.e. the distribution of the curves or surfaces can be determined. Hilliard's method was further formulated into a Cartesian tensor by Kanatani (1984a, 1984b, 1985a). Kanatani described distribution densities of directional data in terms of what he called fabric tensors. He first generalized Hilliard's method for different types of problems into a single mathematical framework called the Buffon transform. Then, he derived its inverse transform in term of Cartesian tensor equations which made it possible to determine the fabric tensors directly from the results of intersection counting.

Muhunthan (1991) outlined an experimental technique for determining the components of a void tensor from microscopic observations which makes use of classical stereology principles and the analysis by Kanatani (1984a, 1984b, 1985a). However, Muhunthan's scheme has been shown to introduce bias into the results of analysis. A

revised methodology (Kuo and Frost, 1993) was subsequently proposed by considering the concept of Representative Element Circle, REC, to minimize the bias.

This paper introduces several stereology based fabric tensors such as surface area tensors (S_{ij}), mean free path tensor (λ_{ij}), and porosity tensor (N_{ij}). The measurement techniques presented can be very efficient when they are implemented using an automated image analysis system as illustrated.

Stereological Method

A brief summary of the stereological method is presented herein. Detailed information of the theoretical developments can be found elsewhere (Kanatani 1984a, 1984b, 1985a). Examples of using this approach for geotechnical engineering purpose can also be found (Kanatani, 1985b; Muhunthan, 1991). The stereological approach offers a unified tensorial formulation for fabric tensors in which the structure of materials can be modeled via two measures : a scalar measure giving the mean value of a fabric descriptor and tensors giving its directional distribution in space. A symmetric distribution density f(n) is expressed in the form

$$f(n) = \frac{C}{4\pi}\left[1 + D_{ij}n_i n_j + D_{ijkl}n_i n_j n_k n_l + \ldots.\right] \qquad (1)$$

where $C = \int f(n)dn$ and the fabric tensor $D_{i_1 \ldots i_n}$ are the nth "fabric tensor" of the distribution.

Suppose high order fluctuations of the distribution density f(n) can be neglected, and f(n) is approximated by

$$f(n) = \frac{C}{4\pi}\left[1 + D_{ij}n_i n_j\right], \qquad (2)$$

which is to approximate distribution density f(n) with a ellipse in 2-D or a ellipsoid in 3-D.

It has been shown that the mean value C and fabric tensor D_{ij} can be obtained from two integrations, M(l) and $M_{ij}(l)$ of the observed quantity N(m) on three perpendicular planes given as:

$$M(l) = \int_{C(l)} N(m)dm \tag{3}$$

$$M_{ij}(l) = \int_{C(l)} m_i m_j N(m)dm \tag{4}$$

where C(l) is a unit circle encircling l perpendicularly, $\int_{C(l)} ds$ the line integral along C(l) normalized to 2π.

Experimental observations are based on three perpendicular planes with basis vectors $e_1=(1,0,0)$, $e_2=(0,1,0)$, $e_3=(0,0,1)$. For each plane, measurements are repeated for test probe oriented in several directions $\theta_m = m\,\pi/N$, m=0,1,2,...,N-1.

$M(e_k)$ and $M_{ij}(e_k)$ could be computed from:

$$M(e_k) \approx 2\pi \sum_{m=0}^{N-1} N_m^{(k)} / N \tag{5}$$

$$M_{ij}(e_k) = \pi \sum_{m=0}^{N-1} N_m^{(k)} \sin(2\pi m / N) / N \tag{6}$$

where i,j,k is a permutation of 1,2,3

Stereological Based Fabric Tensors and Their Determinations Using Image Analysis

Based on the analysis of Kanatani, stereology based fabric tensors such as surface area tensors (S_{ij}), mean free path tensor (λ_{ij}), or porosity tensor (N_{ij}) are proposed. This

section discuss the definitions of those stereology based fabric tensors and their determinations using imaging techniques.

The work reported herein was performed using a Cambridge Instruments Quantimet Q570 Image analysis system (Leica Cambridge Ltd., 1991) although any system of similar capabilities could be used to program the algorithms described herein. The techniques discussed herein rely on two types of measurements made on binary images:

1. Field Measurements - one total value per parameter for each field;

2. Feature Measurements - one individual value per parameter for each isolated object (feature) in the field. Basic parameters such as area, perimeter, and are measured and allow a complete quantitative description of the image contents.

The general procedure for implementing the measurements with an image analyzer is summarized in Figure 1. In the figure, the "Image pre-processing" stage is the stage to enhance the image to be analyzed and is case specific depending on the specimen illumination and capture conditions. Details used for studies of the type described herein are provided by Kuo and Frost (1995).

Starting with a good binary image (Figure 2), the procedure for image analysis implementation is summarized below:

Surface Area Tensor :

The orientation distribution function of $S_v(\phi,\theta)$ which is defined as the fraction of surface area per unit volume having a unit normal vector in the range ϕ to $(\phi + d\phi)$ and θ to $(\theta + d\theta)$ can be used as a quantitative descriptor of anisotropy. The total surface area density, S_v, is given by simply integrating this function over a unit sphere.

Let $$S_v(n) = \frac{S_v}{4\pi}\left[1 + S_{ij}n_i n_j\right] \quad (7)$$

where $$S_v = \int S_v(n)dn \quad (8)$$

and S_{ij} is called the surface area tensor.

Based on Kanatani's (1984a, 1984b, 1985a) analysis, S_V and S_{ij} can be obtained by observing $P_L(\theta_m)$, the number of intersections with the surface per unit length of test line at direction m.

The test probe for determining the number of intercepts per unit length in a given direction θ_m ,$P_L(\theta_m)$, is a set of parallel test lines (see Figure 3). To identify the intercepts of test lines and soil particles, the image processing operation "outline" is first used to identify the outlines of particles in the image (Figure 4). The intercepts (shown as Figure 5) are simply obtained by using a logical "and" operation on the images from Figure 3 and 4. The intercept count $P(\theta_m)$ then can be obtained by counting the number of intercepts in Figure 5.

The total length of test lines is obtained from the coordinates of the two end pixels of each test line. For a test line with two end pixels (x_0,y_0) and (x_1,y_1), the length of this test line in unit of pixel is calculated as :

$$L = ((x_1 - x_0)^2 + (y_1 - y_0)^2)^{0.5} + 1 \quad (9)$$

The number of intercepts per unit length $P_L(\theta_m)$ is simply the ratio of the intercept count $P(\theta_m)$ to the total length of all parallel test lines $TL(\theta_m)$ on a given direction m. When all the directions of $P_L(\theta_m)$ has been determined, it is ready to

are computed

compute $M(e_k)$ and $M_{ij}(e_k)$ and then determine the mean descriptor and fabric tensor (S_v and S_{ij}) are determined.

Mean Free Path Tensor:

The mean free path, λ, between particles is a spatial parameter of importance in a particulate system. Mean free path, λ, is essentially a mean edge-to-edge distance. It represents the uninterrupted interparticle distance through the matrix averaged between all possible pairs of particles and gives the true three-dimensional distance between particles. The directional variation of linearly measured mean free path $\lambda(\phi,\theta)$ also gives a quantitative description of anisotropy.

The orientation distribution $\lambda(n)$ is described by the mean free path, λ, and the mean free path tensor, λ_{ij}.

as
$$\lambda(n) = \frac{C}{4\pi}\left[1 + \lambda_{ij} n_i n_j\right] = \lambda\left[1 + \lambda_{ij} n_i n_j\right] \qquad (10)$$

The test probe for determining mean free path tensor (λ_{ij}) is also a set of parallel test lines in a given direction θ_m (Figure 3). To determine the mean free path tensor (λ_{ij}), the free paths between particles (Figure 6) can be obtained by applying the logical operation "and" to the test lines (Figure 3) and the inverse of the example image (Figure 2).

To calculate the mean free path at a given direction $\lambda(\theta_m)$, the number and the total length of free paths are needed. The number of free paths is obtained from feature number by applying "feature measurement" to Figure 6. The total length of free paths could be obtained from the "pixel number (area)" by applying "field measurement" to

Figure 6. Since the width of all test lines (free paths) is 1 pixel, the number of total pixels of free paths is the total length of free paths if all lines are "straight".

However, except for horizontal and vertical directions, lines have a saw-tooth appearance in a digitized image (see Figure 3). For a given direction (θ_m), the factor $k(\theta_m)$, which is the ratio of pixels number to the true length of lines on a digital image, is equal or greater than 1 and should be accounted for. This factor $k(\theta_m)$ at any specific direction θ_m can be obtained by applying "field measurement" to the test lines at the direction (Figure 3) to obtain the total number of pixels of test lines and by calculating the true length of test lines $TL(\theta_m)$ as previously described. Knowing the factor $k(\theta_m)$, the total length of free paths is then equal to the total pixel numbers of free paths divided by $k(\theta_m)$. When all the directions of $\lambda(\theta_m)$ has been determined, it is ready to compute $\hat{M}(e_k)$ and $M_{ij}(e_k)$ and then calculate the mean free path, λ and mean free path tensor, λ_{ij} readily calculated.

Porosity Tensor :

The orientation distribution function of $N(\phi,\theta)$ which is defined as the porosity, the ratio of void volume to the total volume, of the volume element in the orientation range ϕ to $(\phi + d\phi)$ and θ to $(\theta + d\theta)$ can also be used for quantitative description of anisotropy. This function is described by the porosity of the specimen n_0 and the porosity tensor, N_{ij}, as

$$N(n) = n_0 \left[1 + N_{ij} n_i n_j\right] \tag{11}$$

The linear fraction of void $I_p(\phi,\theta)$ is used as an estimator of volume fraction of void (porosity), $N(\phi,\theta)$, and the test probe is a test line within the region between two representative element circles (RECs) in a given direction θ_m (Kuo and Frost, 1993).

Before the test line can be drawn, the regions of RECs need to be determined. A program was written to measure the porosities of an image with different sizes of square measure frame. For the image of Figure 2, the measured porosities with different size of measure frame are shown in Figure 7 and which show that the measured porosities become stable after the width of measure frame is larger than about 50 pixels. Based on this information, the radius of the inner REC(r_1) and the outer REC(r_2) can be selected as 40 pixels and 230 pixels (see Figure 8, $r_1 \geq \frac{\sqrt{2}}{2} w_1$ and $r_2 \leq 0.5 \cdot w_2$). Note that this value is related to the size of the particles in the image and thus should be computed for each experimental configuration. This issue is discussed further later in this paper. The test line within the region between the two RECs in a given direction θ_m is shown in Figure 9.

To determine the porosity tensor (N_{ij}), the portions of test line occupied by voids $l_p(\theta_m)$ (Figure 10) can easily be obtained by applying a logical operator to the test probe and the inversion of the example image. The fraction of the test line occupied by voids $l_p(\theta_m)$ can be determined by the ratio of the number of pixels measured when "Field Measurement" is applied to the test line (Figure 9) and the portions of the test line occupied by voids (Figure 10). When all the distribution of $l_p(\theta_m)$ has been computed, it is ready to compute $M(e_k)$ and $M_{ij}(e_k)$ and then the mean descriptor and fabric tensor, n_0 and N_{ij}, can be determined. can be computed

Similarly, if only a single plane section is available, two dimensional tensors: length tensor (l_{ij}), mean free path tensor (λ_{ij}), and area fraction tensor (A_{ij}) can also be obtained by measuring the distributions of intercept density $P_L(\theta_m)$, mean free path $\lambda(\theta_m)$, and linear fraction $l_p(\theta_m)$ respectively.

The imaging implementation of measurement techniques for determining stereology based fabric tensors described above was programmed using the Q570 image

analysis system built-in Basic like Macro-language- QBASIC, and the codes can be found in Kuo and Frost (1995).

Illustration of the Techniques

Applications to Two Dimensional Tensors

For the binary image shown in Figure 2, the resulting mean fabric descriptors and fabric tensors using the measurement techniques described above are

$$L_A = 0.067 / \text{pixel}, \qquad L_{ij} = \begin{bmatrix} -0.0092 & -0.0075 \\ -0.0075 & 0.0092 \end{bmatrix} \tag{12}$$

and

$$\lambda = 23.905 \text{ pixel}, \qquad \lambda_{ij} = \begin{bmatrix} -0.0054 & 0.0032 \\ 0.0032 & 0.0054 \end{bmatrix} \tag{13}$$

and

$$A_A^{\vee} = 0.478, \qquad A_{ij} = \begin{bmatrix} 0.0316 & 0.0440 \\ 0.0440 & -0.0316 \end{bmatrix} \tag{14}$$

The results of "field measurement" of the binary image (Figure 2) show that the area fraction of voids is 0.489. It is evident that the proposed measurement technique gives a very good approximation of the area fraction of void which is 0.478 measured using the stereology based method versus the value of 0.489 obtained directly from the field measurement. Similarly, the total length per unit area, L_A, can be obtained from the results of field measurement as perimeter/ frame area which is 0.065/pixel. The proposed stereological measurement technique estimates the value of L_A as 0.067/ pixel which again agrees closely with the value obtained from the field measurement.

The results of "field measurement" offer an independent check to the proposed measurement techniques. The good agreement between the results of the proposed

measurement techniques and the "field measurements" supports the correctness of the measurement techniques and their implementation.

Applications to Three Dimensional Tensors

For images from three orthogonal planes (Figures 11-13), the surface area density and surface area tensor are given as:

$$S_v = 0.1545 / \text{pixel} \qquad S_{ij} = \begin{bmatrix} 0.3430 & 0.0180 & 0.0331 \\ 0.0180 & -0.1654 & 0.0164 \\ 0.0331 & 0.0164 & -0.1776 \end{bmatrix} \tag{15}$$

The mean free path and mean free path tensor are given as:

$$\lambda = 8.88 \text{ pixels} \qquad \lambda_{ij} = \begin{bmatrix} -0.1314 & -0.0120 & 0.0111 \\ -0.0120 & 0.1110 & -0.0062 \\ 0.0111 & -0.0062 & 0.0205 \end{bmatrix} \tag{16}$$

and the porosity and porosity tensor are given as:

$$n_0 = 0.362, \qquad N_{ij} = \begin{bmatrix} 0.0087 & 0.0494 & -0.0591 \\ 0.0494 & 0.0392 & 0.0479 \\ -0.0591 & 0.0479 & -0.0479 \end{bmatrix} \tag{17}$$

The calibration factor for images shown in Figures 11 to 13 is 0.025 mm/pixel. Thus the surface area density S_v is 6.18/mm, and the mean free path λ is 0.222 mm, and the porosity n_0 is 0.362. The estimated porosity 0.362 agrees well with the global specimen porosity of 0.366.

Theoretically, there are interrelationships between surface area density S_V, mean free path λ, and porosity n_0. It can be shown that (Underwood, 1970):

$$\lambda = \frac{4 \cdot n_0}{S_v} \tag{18}$$

For n_0 of 0.362, S_V of 6.18/mm, λ is calculated as 0.234 mm from equation 18 which agrees well with 0.222 mm obtained with the proposed procedure.

Discussion

Surface area density S_V, mean free path λ, and porosity n_0 are physical properties of materials which possess real physical meaning. It has been shown in this paper that S_V, λ, and n_0 and their corresponding fabric tensors could be obtained from distribution of measurable quantities : intercept density $P_L(\theta_m)$, mean free path $\lambda(\theta_m)$, and linear fraction $l_p(\theta_m)$ respectively. S_V, λ, and n_0 and their corresponding fabric tensors are important structural parameters in practice. The behavior of soils are closely related to these parameters. For example, by knowing surface area and porosity, permeability can be estimated from the Kozeny - Carman relation. Berryman and Blair (1987) have utilized the Kozeny - Carman relation to estimate the permeability of porous materials where porosity and specific surface area are provided from image analysis measurements.

As shown in equation 18, there are interrelationships between surface area density, S_V, mean free path, λ, and porosity, n_0, so only two independent parameters exist among these three parameters. Similarly, there are some interrelationships between surface area tensor, mean free path tensor and porosity tensor. Among these three tensors, any two are expected to be independent. Thus, to fully quantify the anisotropy of the material, at least two such fabric tensors may be needed.

The eigenvalues of fabric tensor indicate the degree of anisotropy, and the corresponding principal axes show the principal directions of this distribution function. Muhanthan (1991) proposed the use of the second invariant J_2 of fabric tensor ψ_{ij} as a fabric parameter, J_f.

$$\text{where } J_f = J_2 = \frac{1}{6}\left[(\psi_{11}-\psi_{22})^2+(\psi_{22}-\psi_{33})^2+(\psi_{33}-\psi_{11})^2\right]+\psi_{12}^2+\psi_{23}^2+\psi_{31}^2 \quad (19)$$

~~In following section, the sensitivity, generality, practical implications and limitations of the techniques are discussed.~~

Sensitivity Study

For the illustrations described above, the test set (Figure 3) had interline spacing of 10 pixels and was rotated for every 10 degrees of orientation. It is of interest to evaluate the sensitivity of the proposed methods to different line spacing and orientation increments. Detailed analyses have been conducted (Kuo and Frost, 1995) and show that this setting will be adequate for most soil images in practice, although this factor should be routinely verified.

The effect of the increment of orientation on the measured area fraction and area fraction tensor (or porosity and porosity tensor for 3-D) was also examined. Current measurements are based on a 5 degree increment for the orientation. Kuo and Frost (1995) show that the increment of orientation should be less than or equal to 10 degrees to obtain a reasonable estimate of area fraction and associated fabric tensor.

The analyses show that the current default values for the line spacing and orientation increment are adequate. However, the appropriate setting of line spacing and orientation increment is case dependent. Since the determinations of mean fabric descriptor and its associated tensor can be efficiently performed with an image analysis

system (less than 3 minutes with current spacing and orientation values), it is recommended that these defaults be routinely verified.

Generality of Methodology

The formulations of fabric tensors introduced in the paper are based on the principle of stereology. The attraction of these proposed stereology based fabric tensors is that there are no assumptions on the shape or size of particles and voids. Thus, the methods developed here can generally be applied to any materials of interest. Even though the illustrations of the methods are made on sandy materials, the methods can be applied to clayey soils or cracks in rocks, for example.

Practical Implications and Limitations

In general, in order to formulate the fabric tensor in three dimensions, three orthogonal planes are needed. However, if axial symmetry is assumed, only one horizontal and one vertical plane are required. It is reported that the axial symmetry characteristic is common in artificially deposited sands. However, this characteristic disappears in many undisturbed natural sands. This will be likely due to the depositional environment where water (or air) flow at the time of sedimentation may have an effect on the particle orientation.

In obtaining the surface area density and surface area tensor or mean free path and mean free path tensor from three orthogonal planes, it is crucial to know the magnification and keep the same magnification for each plane observed. For porosity and porosity tensor, since the quantities examined are dimensionless, the magnification can be unknown. The magnifications of the three planes observed can also be slightly different. Of course, keeping the same magnification is preferable.

The measurements of distribution of porosity versus frame width provides guidelines for selecting a suitable sample size for analyzing porosity and porosity tensors.

It is desired that the radius of inner REC(r_1) is smaller than 1/3 of the radius of the outer REC(r_2) such that over 90% of the area inside the outer REC is analyzed. For the maximum image size of many analyzers (512 pixels x 512 pixels), it is desirable to have the radius of the outer REC(r_2) as large as possible (230 or 240 pixels). Thus, the radius of the inner REC(r_1) should be kept smaller than 80 pixels if possible. If the distribution of porosity does not stabilize at frame widths of up to 110 pixels, it is likely that the sample size may be too small. Decreasing the magnification and observing larger sample sizes will allow the porosity distribution to become stable within a frame width of 110 pixels. Figure 14 shows an image of insufficient sample size that is not suitable for analysis of porosity and porosity tensor at the current magnification.

Conclusion

On the basis of Kanatani's analysis, stereology based fabric tensors such as a surface area tensors (S_{ij}),a mean free path tensor (λ_{ij}), and a porosity tensor (N_{ij}) can be determined experimentally from microscopic observations. Those measurement techniques were implemented using an automated image analysis system. Computer algorithms were developed to permit the determination of mean fabric descriptors and their associated tensors efficiently, using image analysis techniques. Furthermore, the attraction of these proposed stereology based fabric tensors is that there are no assumptions on the shape or size of particles and voids. Thus, the methods described here can generally apply to other materials.

Acknowledgments

The work reported in this paper was supported by National Science Foundation Grant No.'s MSS-9011232, MSS-9007581 and BCS-9304897. This support is gratefully acknowledged.

References

Berryman, J. G., and Blair, S. C., (1987). Kozeny-Carman Relations and Image Processing Methods for Estimating Darcy's Constant. Journal of Applied Physics, Vol. 62, No.6, pp. 2221-2228.

Cowin, S. C. (1985). The Relationship Between the Elasticity Tensor and the Fabric Tensor. Mechanics of Materials. Vol. 4, pp. 137-147.

Hilliard, J. E. (1967). Determination of Structure Anisotropy. Stereology. Edited by H. Elias. Proc. Second International Congress for Stereology, New York : Springer-Verlag, pp. 219-227.

Kanatani, K. (1984a). Distribution of Directional data and Fabric Tensors. Int. J. Engng. Sci., Vol. 22, No. 2, pp. 149-164.

Kanatani, K. (1984b). Stereological determination of Structural Anisotropy. Int. J. Engng. Sci., Vol. 22, No. 5, pp. 531-546.

Kanatani, K. (1985a). Procedures for Stereological Estimation of Structural Anisotropy. Int. J. Engng. Sci., Vol. 23, No. 5, pp. 587-598.

Kanatani, K. (1985b). Measurement of Crack Distribution in a Rock Mass From Observation of Its Surfaces. Soils and Foundations, Vol. 25, No.1, pp. 77-83.

Kuo, C.-Y., and Frost, J. D. (1993). A Revised Methodology to Minimize Bias in Determining the Porosity and Void Tensor of Particulate Media. Digital Image Processing : Techniques and Applications in Civil Engineering. Frost & Wright (Editors), pp. 186-194.

Kuo, C.-Y. and Frost, J. D. (1995). Quantifying the Fabric of Granular Materials - An Image Analysis Approach. Research Report No. GIT-CEE/GEO-95-1. School of Civil and Environmental Engineering, Georgia Institute of Technology. 251 pp.

Leica Cambridge Ltd. (1991). Quantimet 570 - QUIC Menu System Operators Manual.

Muhunthan, B. (1991). Micromechanics of Steady State, Collapse and Stress-Strain Modeling of Soils. Ph.D. dissertation. Purdue University, IN., 222 pp.

Oda, M., and Nakayama, H. (1989). Yield Function for Soil with Anisotropic Fabric. Journal of Engineering Mechanics, ASCE. Vol. 115, No. 1, pp. 89-104.

Oda, M., Nemat-Nasser, S., and Konish, J., (1985). Stress-Induced Anisotropy in Granular Masses. Soils and Foundations, vol. 25, No. 3, pp. 85-97.

Oda, M., and Ohnishi, A. (1992). Plasticity Theory for Granular Soils with Induced Anisotropy. Advances in Micromechanics of Granular Materials. H. H. Shen et al. (Editors). pp. 193-202.

Tobita, Y. (1989). Fabric Tensors in Constitutive Equations for Granular Materials. Soils and Foundations. Vol. 29, No. 4, pp. 91-104.

Underwood, E. E. (1970). Quantitative Stereology. Addison-Wesley Publishing Company. 274 pp.

LIST OF FIGURES

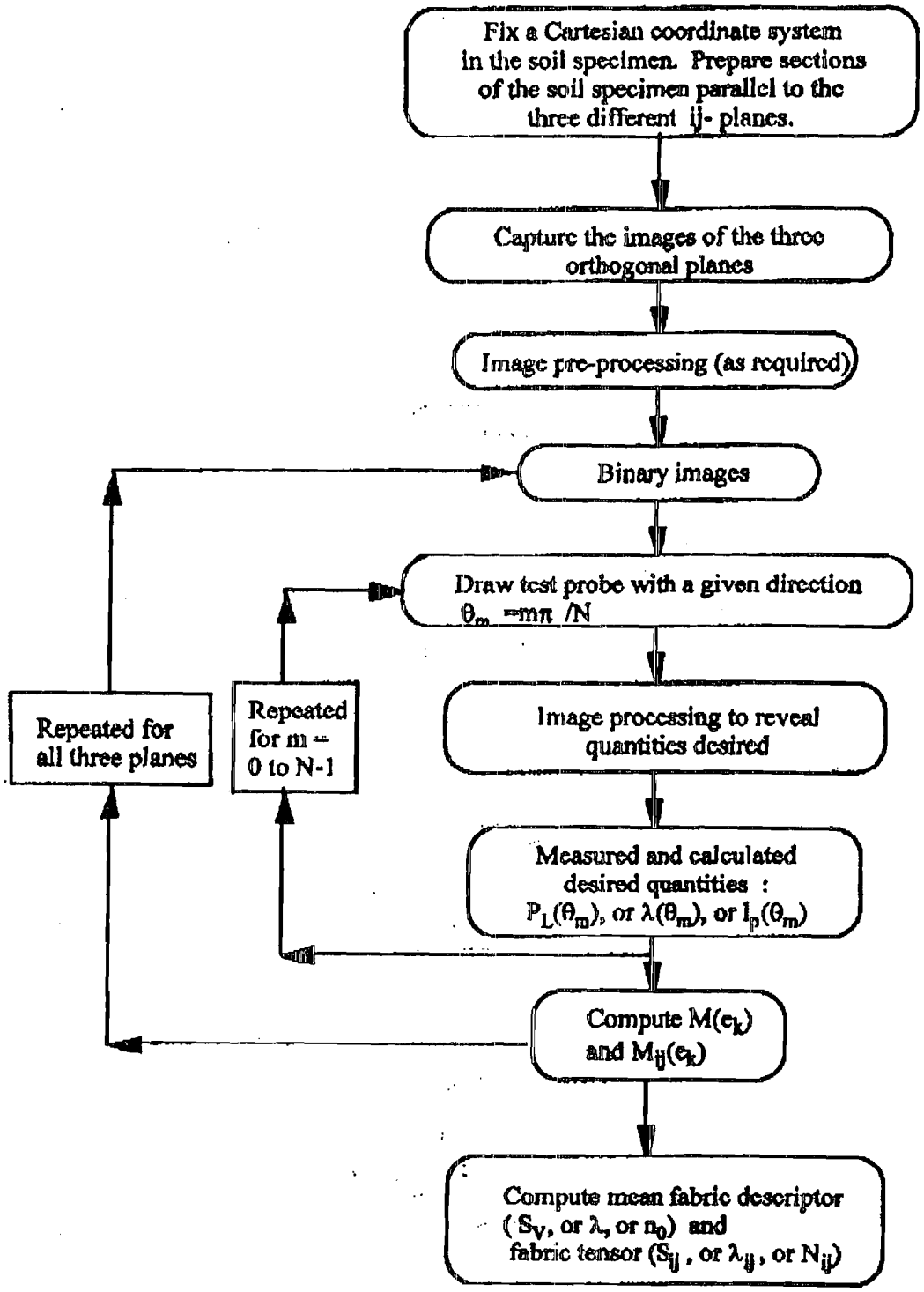
Fix a Cartesian coordinate system in the soil specimen. Prepare sections of the soil specimen parallel to the three different ij- planes.
Capture the images of the three orthogonal planes
Image pre-processing (as required)
Binary images
Draw test probe with a given direction $\theta_m = m\pi / N$
Image processing to reveal quantities desired
Measured and calculated desired quantities : $P_L(\theta_m)$, or $\lambda(\theta_m)$, or $I_p(\theta_m)$
Compute $M(e_k)$ and $M_{ij}(e_k)$
Compute mean fabric descriptor (S_V, or λ, or n_0) and fabric tensor (S_{ij} , or λ_{ij} , or N_{ij})
Repeated for all three planes
Repeated for m = 0 to N-1

Figure 1

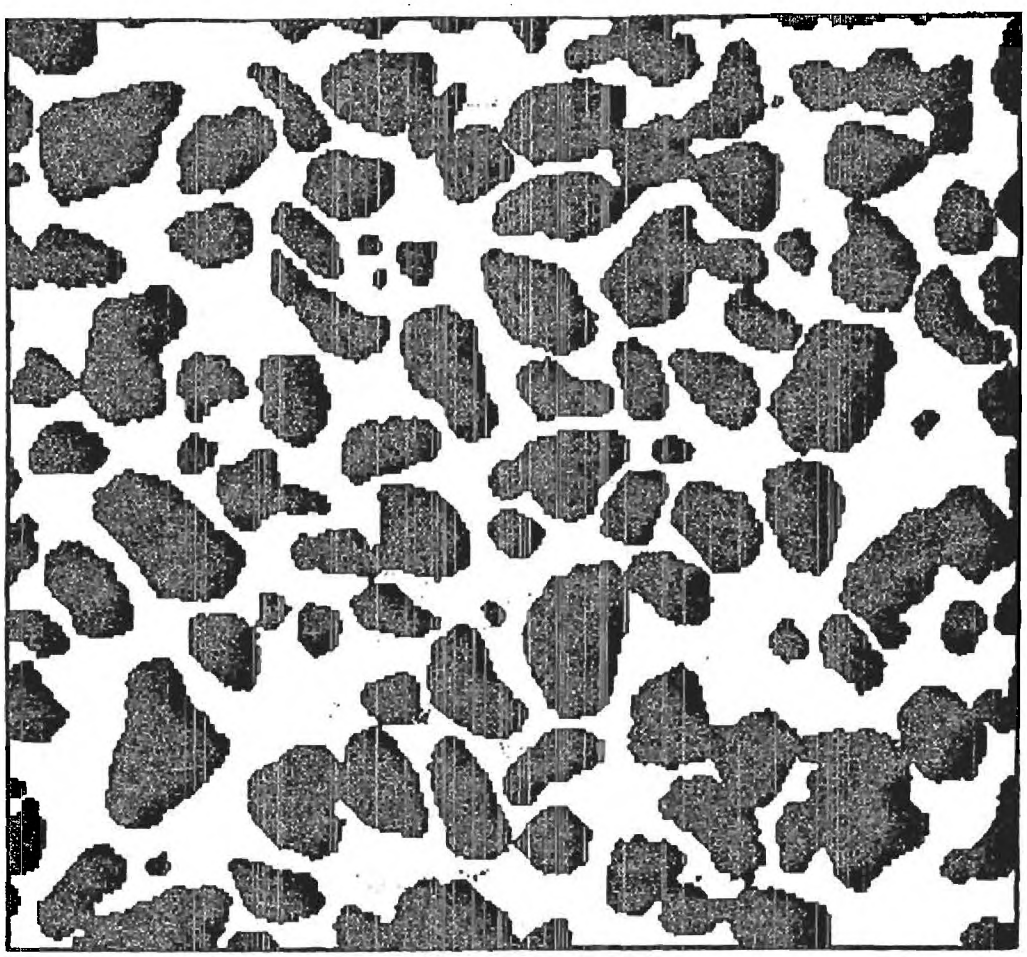

Figure 2

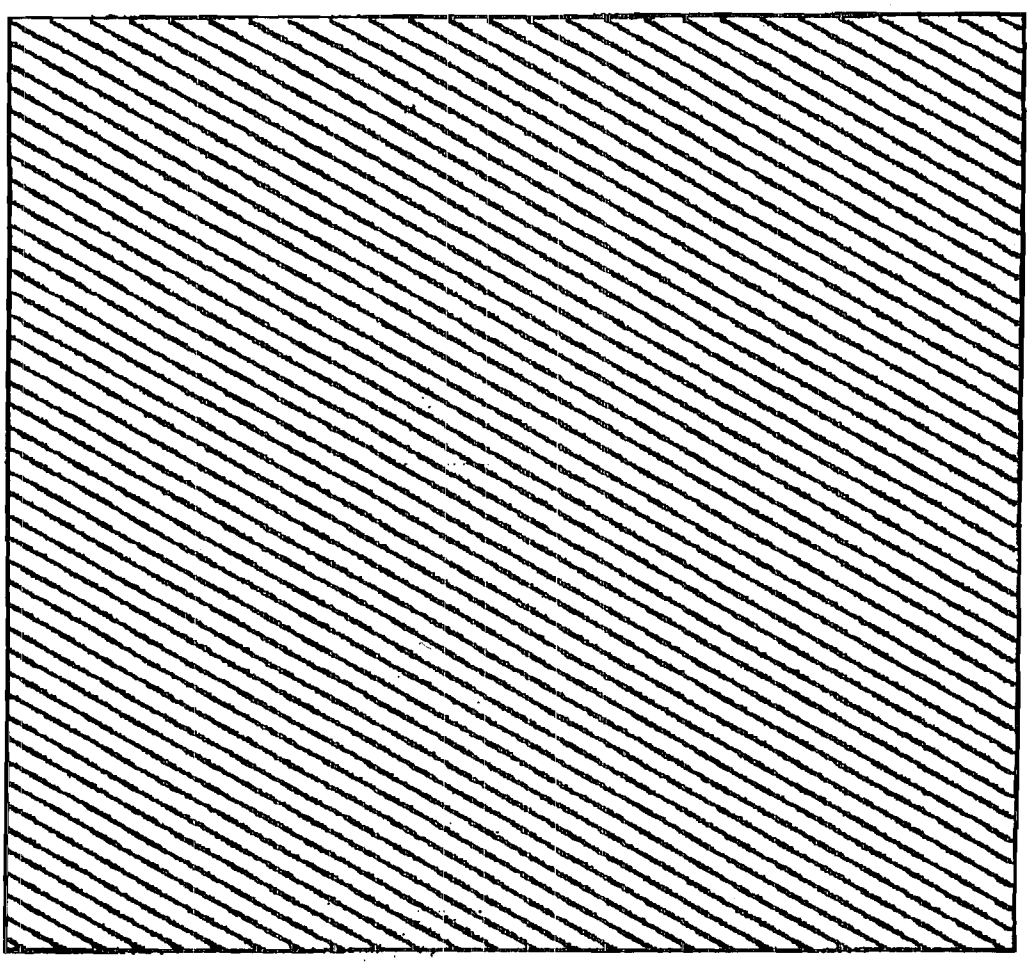

Figure 3

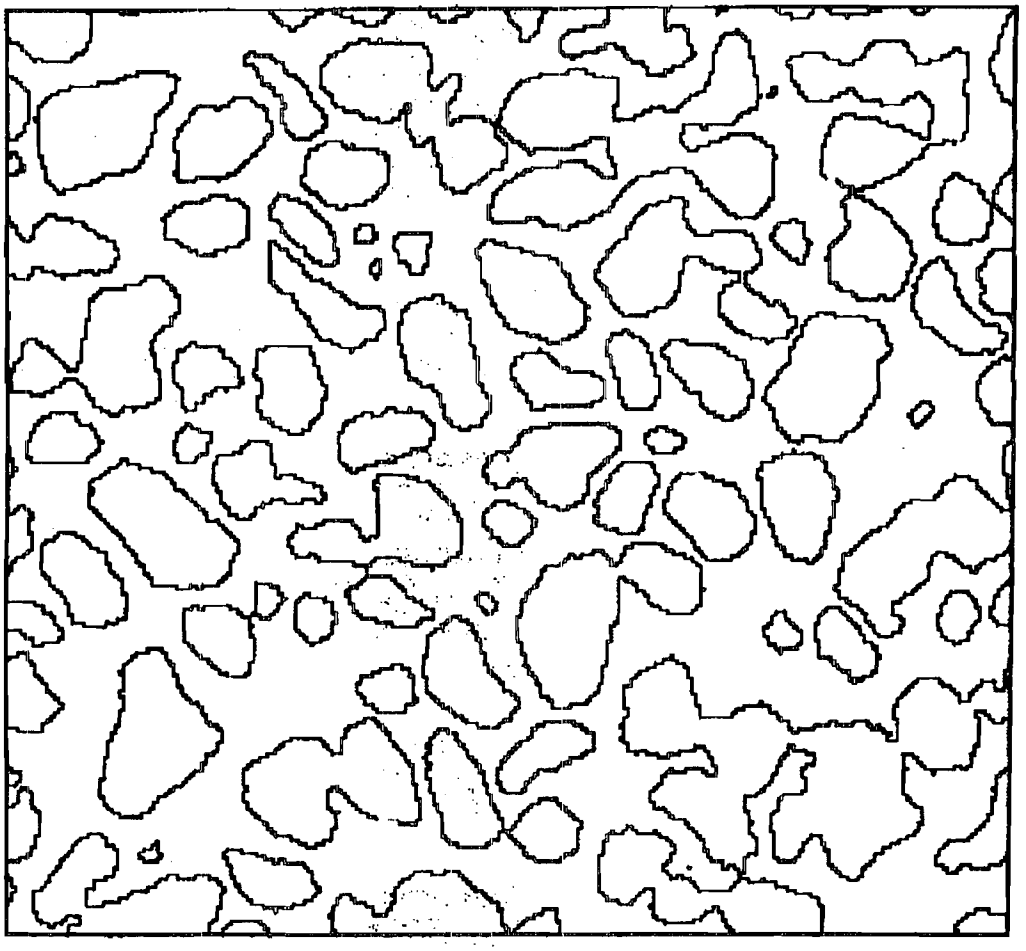

Figure 4

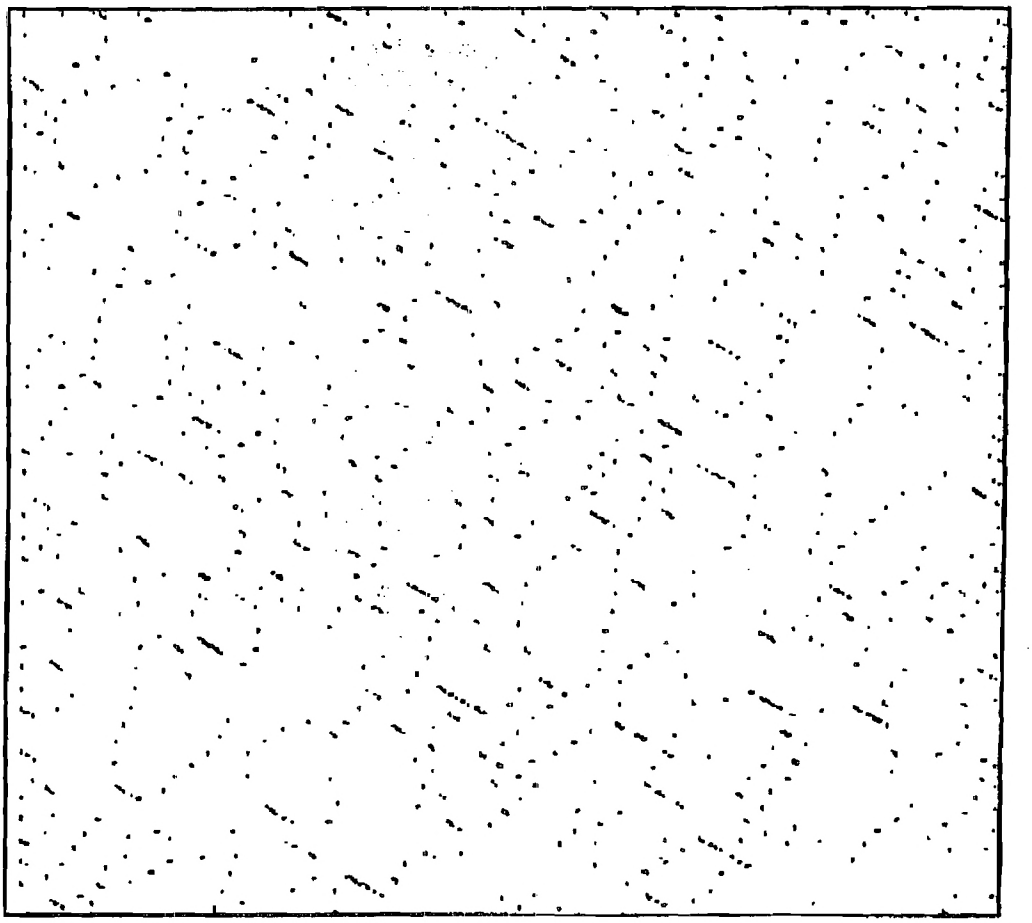

Figure 5

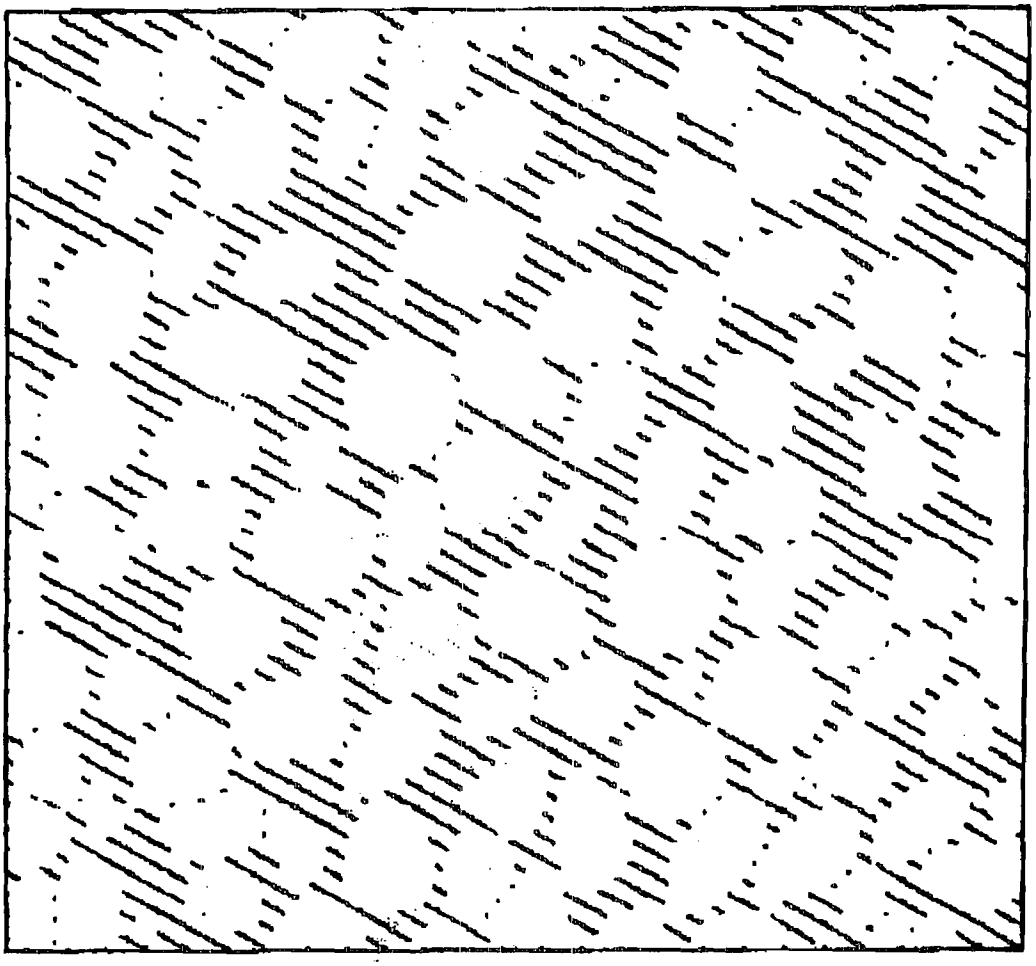

Figure 6

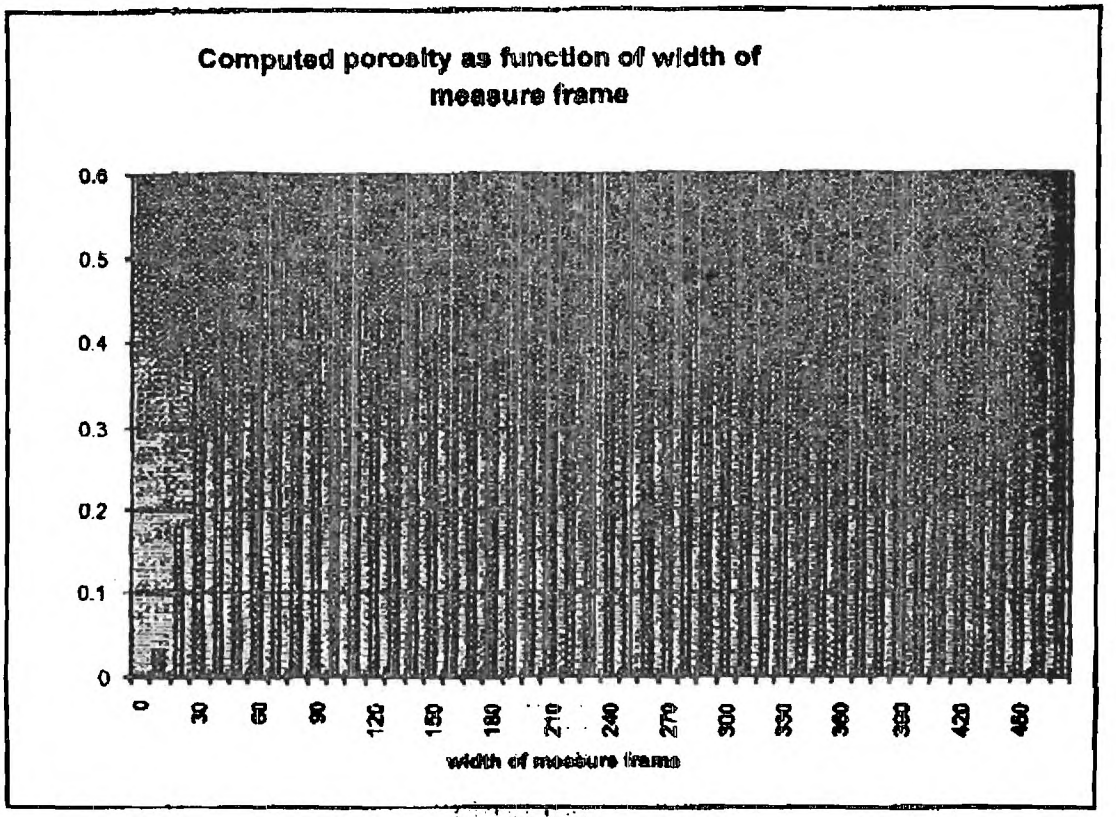
Computed porosity as function of width of measure frame
0.6
0.5
0.4
0.3
0.2
0.1
0
0
30
60
90
120
150
180
210
240
270
300
330
360
390
420
450
width of measure frame

Figure 7

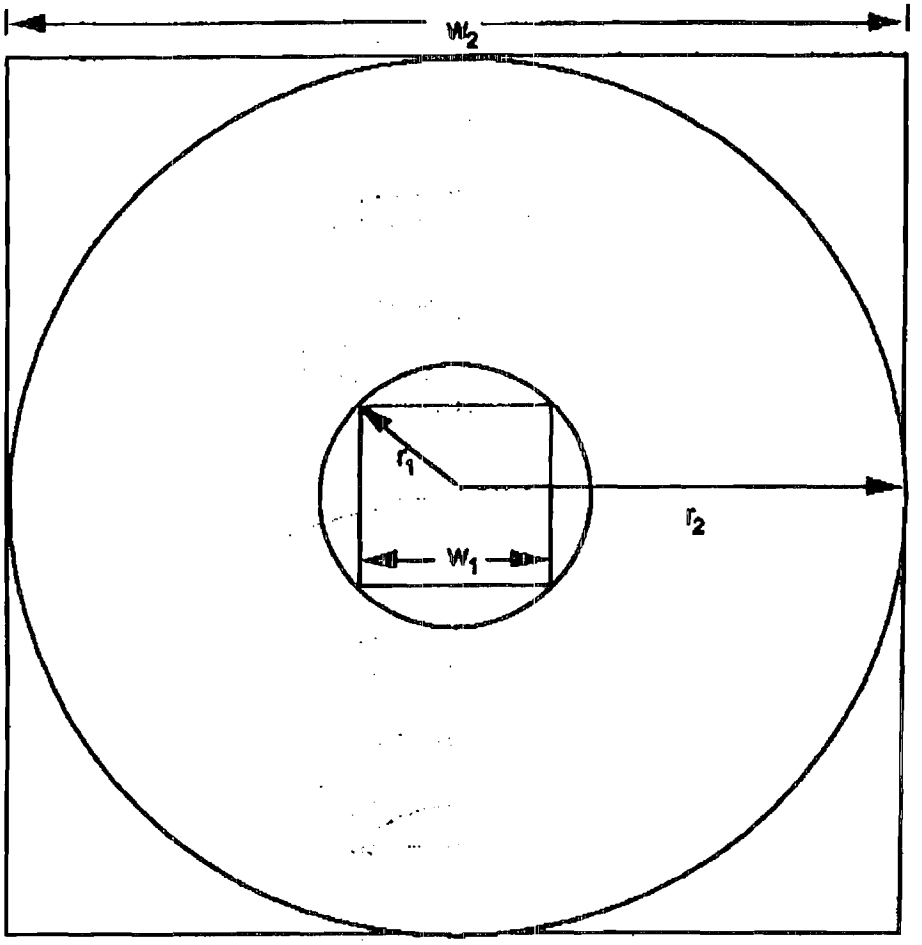

Figure 8

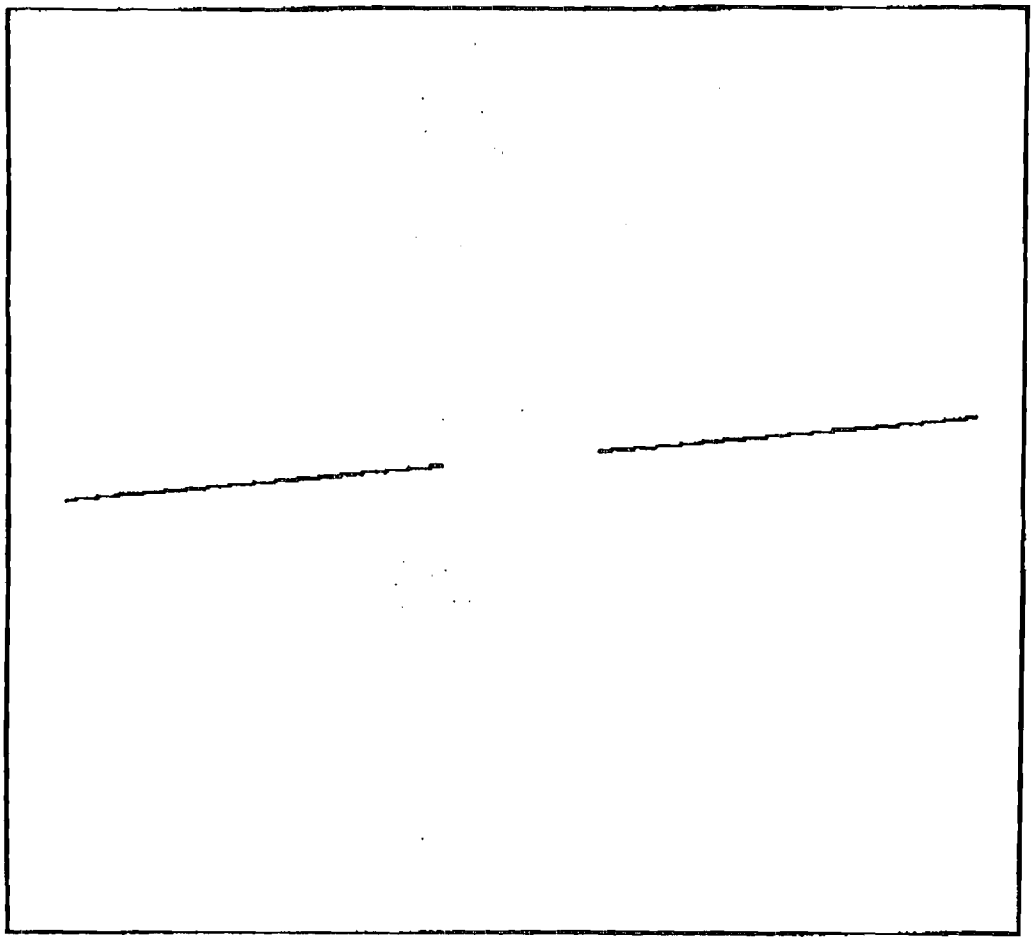

Figure 9

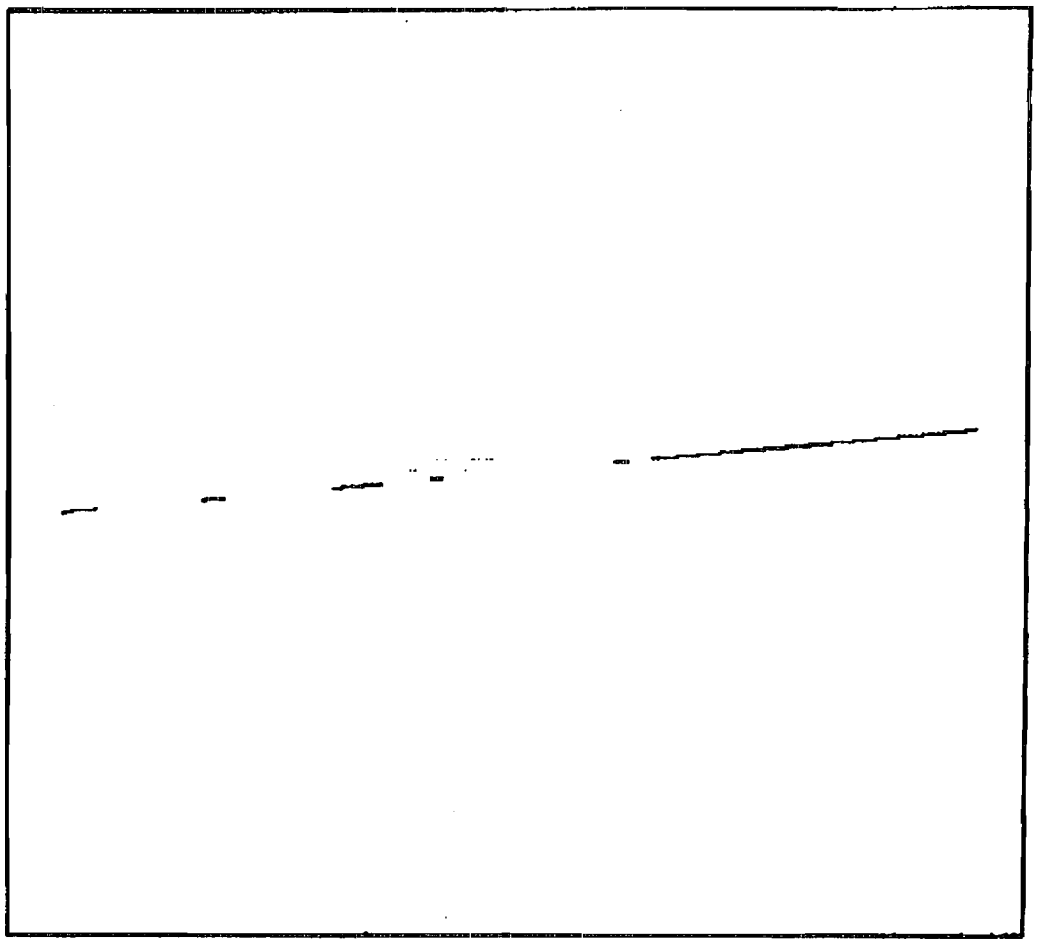

Figure 10

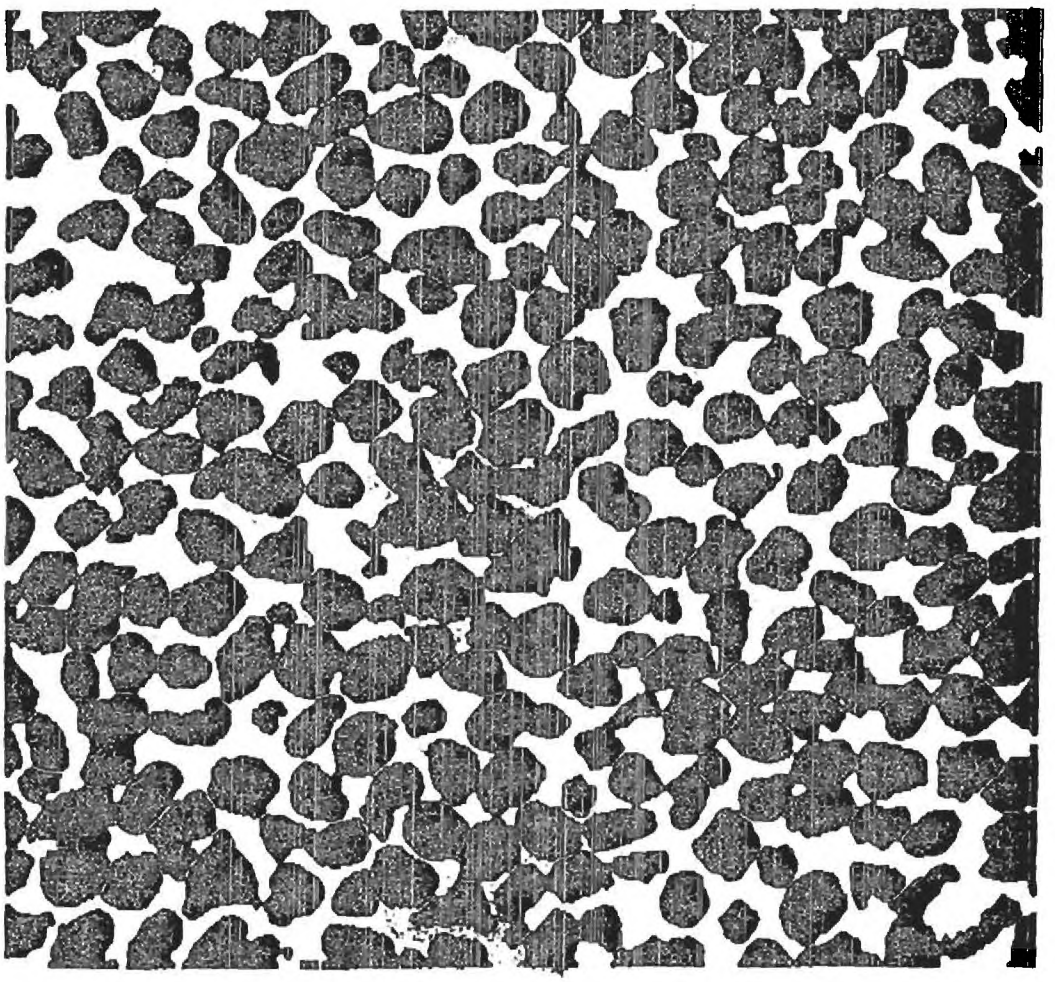

Figure 11

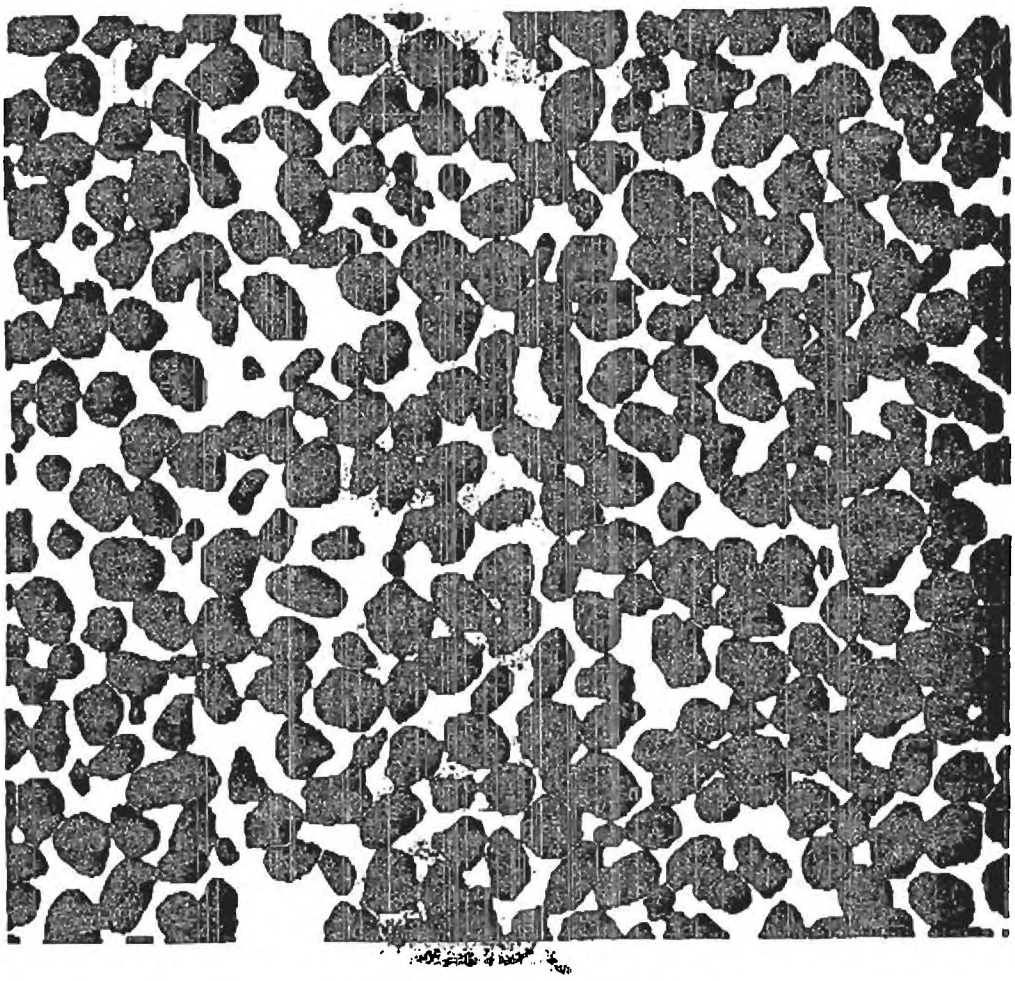

Figure 12

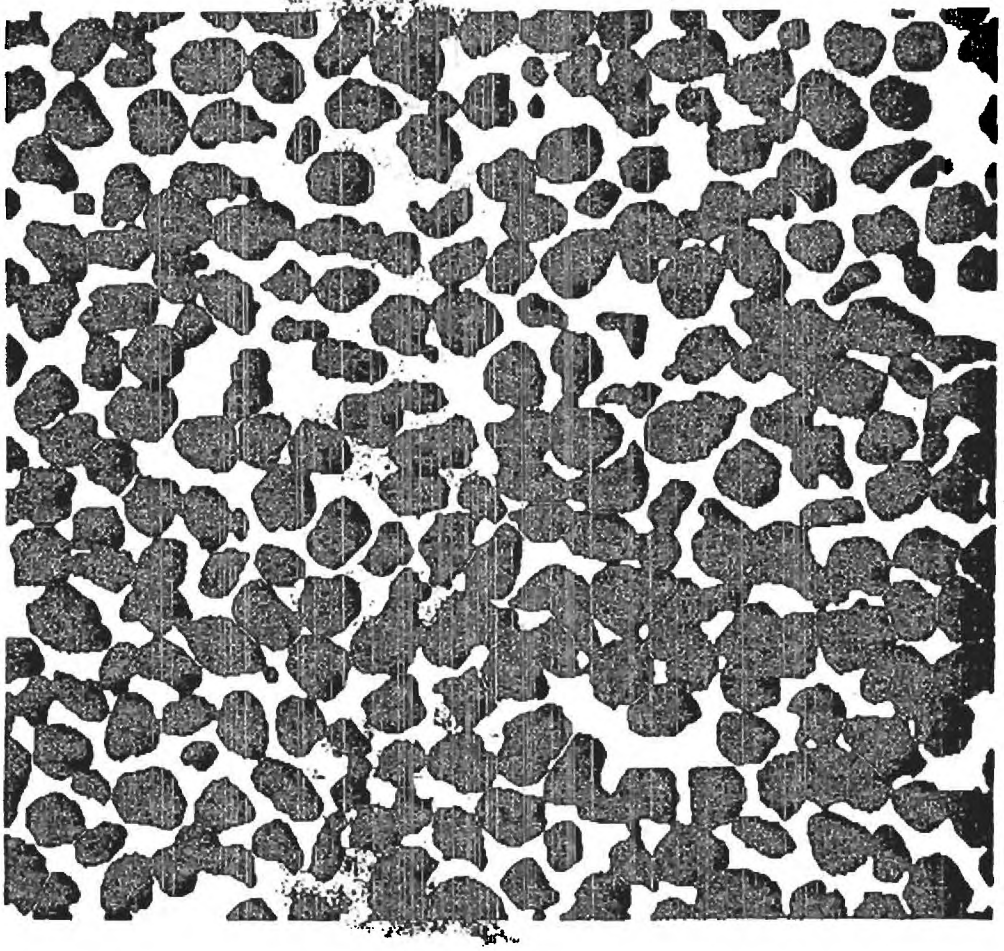

Figure 13

Attachment # 3

Post-Liquefaction Strength - The Role of Soil Structure

J. David Frost and Alaa K. Ashmawy,
Associate Professor and Post-Doctoral Research Fellow, respectively
School of Civil and Environmental Engineering
The Georgia Institute of Technology
Atlanta, GA 30332, USA

Introduction

Understanding of the behavior of granular soils under earthquake loading has advanced significantly since the mid 1960's as a result of contributions by many researchers around the world. These contributions have involved: (a) the development of practical procedures based on field tests or empirical relationships to permit evaluation of the potential for actual soil deposits to liquefy; (b) extensive studies of the behavior of model soil deposits under simulated conditions such as in centrifuges; (c) the development of a range of innovative laboratory testing systems to apply dynamic loading over a broad range of strains to cylindrical specimens; and (d) sophisticated numerical models to analyze the behavior of virtual soil masses using computer simulations. Obviously, the preceding list is in no way exhaustive but rather of value to illustrate the breadth of approaches which have been used by researchers to gain insight into the behavior of soils under earthquake loading. Despite the accomplishments and contributions of the many researchers that have performed these studies, there still remain some significant "gaps" in our knowledge and hence our framework of understanding. Without doubt, one such "gap" is a clear understanding of the role of soil structure. Equally importantly, not only is it critical in our understanding of the behavior of real undisturbed soil deposits, but it is central to our interpretation of the results of studies using any of the approaches listed above to investigate the behavior of granular soils under earthquake loading. Using results from recent and ongoing digital image analysis based research at Georgia Tech, this paper attempts to provide new insight into the role of soil structure in post-liquefaction strength.

Definition of Post-Liquefaction Strength

Prior to discussing a number of issues related to the role of structure in the strength of granular soils, it is first appropriate to review what is meant by the term post-liquefaction strength in the context of the various investigation approaches listed above .

Investigation Approach	Correct Definition of Post-Liquefaction Strength	Strength Actually Interpreted or Used
Field studies and empirical correlations	Strength after all earthquake induced pore pressure in soil deposit has dissipated	Tests typically performed after earthquake and thus reflect true post-liquefaction strength
Centrifuge model studies	Strength after all simulated earthquake pore pressure in model soil has dissipated	Studies tend to model behavior during event rather than provide post-liquefaction strength values
Laboratory specimen tests	Strength after all laboratory loading induced pore pressure in specimen has dissipated	Steady state or critical state strength values and not post-liquefaction strengths evaluated
Computer models	Strength after all computer simulated loading induced pore pressure in computer model soil has dissipated	Constitutive soil models calibrated with steady state or critical state strength values and not post-liquefaction strengths

Table 1 Definitions of Post-Liquefaction Strength

Two Load Sequence Laboratory Tests

A review of the strength values interpreted or used in the various investigation approaches summarized in Table 1 shows that there are some significant deficiencies in how we have historically evaluated post-liquefaction soil strength conditions. In the case of investigations which use tests on laboratory specimens, it is not possible to determine post-liquefaction strengths from a test with a single loading sequence only, although this is commonly done. In reality, we should perform a two load sequence test where after the first undrained loading phase in which we liquefy the specimen, we reconsolidate the specimen by allowing drainage to take place, and then reload the specimen under undrained conditions. The strength determined during this second undrained load phase is the post-liquefaction strength. The results of such a two load sequence test are summarized below.

Figure 1 shows the results of a quasi-static undrained torsional shear test performed on a specimen of Ottawa 20-30 sand that was isotropically consolidated to a mean effective confining stress of 100 kPa and a void ratio of 0.682 (Dr = 24%). The maximum shear modulus was determined from a resonant column test to be 82.4 MPa. The specimen was first subjected to a cyclic shear stress of about 14 kPa. Strain softening was initiated at a shear strain of about 0.3% after the application of 9 cycles as shown in the figure at which stage the rate of pore pressure development increased. A steady state condition was reached at a shear strain of about 5% and the test was terminated at a shear strain of 13%. The shear stress was then removed from the specimen and the drainage lines were opened to allow it to reconsolidate isotropically to a mean effective confining stress of about 100 kPa. The void ratio at this stage had decreased to 0.641 (Dr = 41%) and the maximum shear modulus was determined to be 77.5 MPa. It is noted that for this new combination of confining stress and void ratio, a maximum shear modulus of about 90 MPa would have been expected based on extensive tests on reconstituted specimens prior to the application of large strains. This reduction in maximum shear modulus is attributed to a change in the grain structure during the initial loading and strain softening phase, thus while the specimen is denser following reconsolidation, it has a structure which is less stiff in the direction of the applied torsional vibration loading.

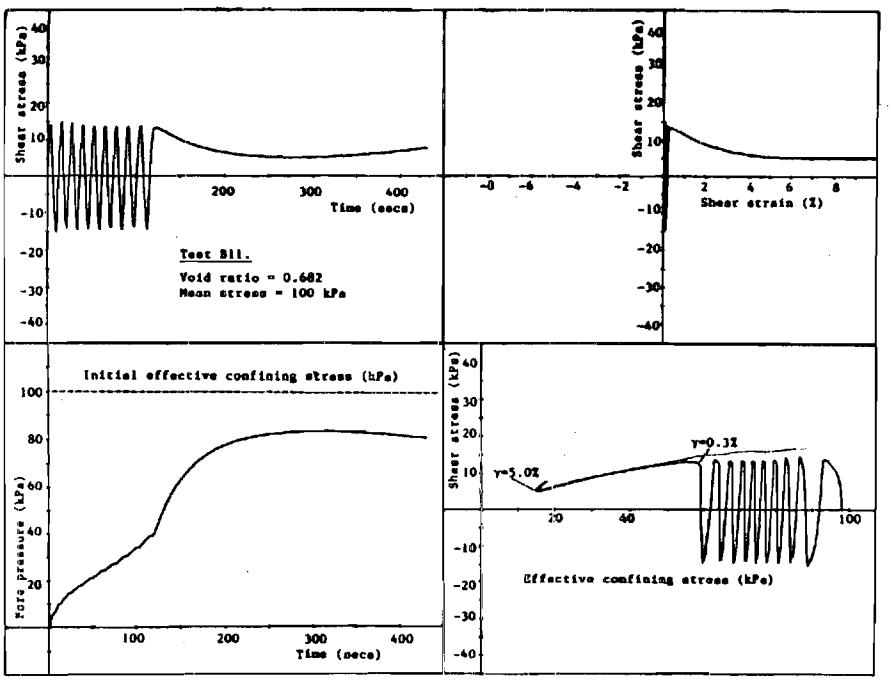

Figure 1 Cyclic Torsional Shear Test Results during Initial Load Sequence

At this stage, it was intended to subject the specimen to a second load sequence of cyclic shear stress of about 14 kPa as in the initial load sequence however, during the first load cycle, strain softening accompanied by the development of large pore pressure was observed (Figure 2) with the specimen reaching steady state at a shear strain of about 3.5%. Several aspects of the results shown in Figures 1 and 2 are of interest. The peak shear strength for the reconsolidated specimen was attained at a shear strain of about 0.7%, compared to 0.3% during initial loading. The application of large shear strains during the initial loading resulted in a particle arrangement which while denser was more conducive to pore pressure build-up during subsequent undrained loading. During the initial loading, the specimen reached a steady state of deformation at a shear strain of 5% at which stage the specimen was able to sustain a shear stress of 5.2 kPa at a mean normal effective stress of 15 kPa. Following reconsolidation, the denser specimen reached steady state at a shear strain of about 3.5% and was able to sustain a shear stress of only 2.6 kPa at a mean normal effective stress of 12 kPa. This difference is clearly of interest in that it has been suggested that the steady state condition is only a function of the initial void ratio for undrained tests. The results of the tests presented above appear to substantiate the argument that the structure may also be reflected in the behavior at steady state. Further they clearly demonstrate the difference between post-liquefaction strength and steady state strength and lend credence to the argument that post-liquefaction strength determination in the laboratory requires a two load sequence test, one to first liquefy the specimen and the second to determine the post-liquefaction strength.

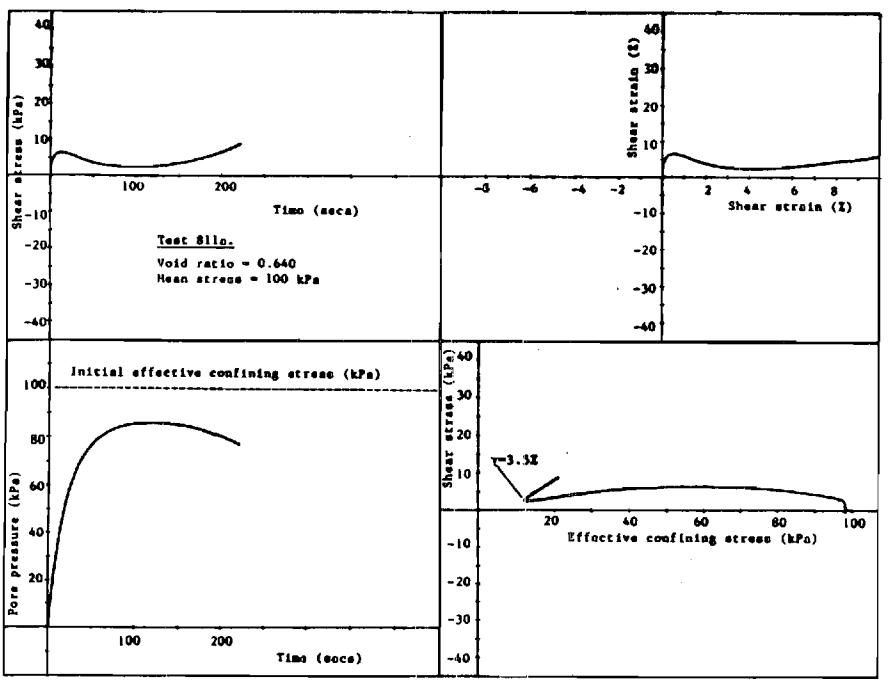

Figure 2 Cyclic Torsional Shear Test Results during Second Load Sequence

Quantitative Measurements of Structure

There is compelling indirect experimental and analytical evidence that soil structure is a critical parameter in the behavior of granular soils under earthquake loading. Ongoing research at Georgia Tech is using digital image processing and analysis to provide quantitative measures of the structure of granular soils. One parameter which is currently being used is Oda's local void ratio distribution. Figure 3 shows the distributions of local void ratio for measurements on two specimens of standard Ottawa sand with the same global void ratios but reconstituted using different methods of preparation (moist tamping and air pluviation). While the distributions appear

similar, there are quantifiable and important differences between them as shown in Figure 4. For example, the specimen prepared using air pluviation has a less skewed distribution with more of the voids having values near the mode size. Ongoing measurements are quantifying the evolving local void ratio distribution at different strain levels during monotonic and cyclic loading.

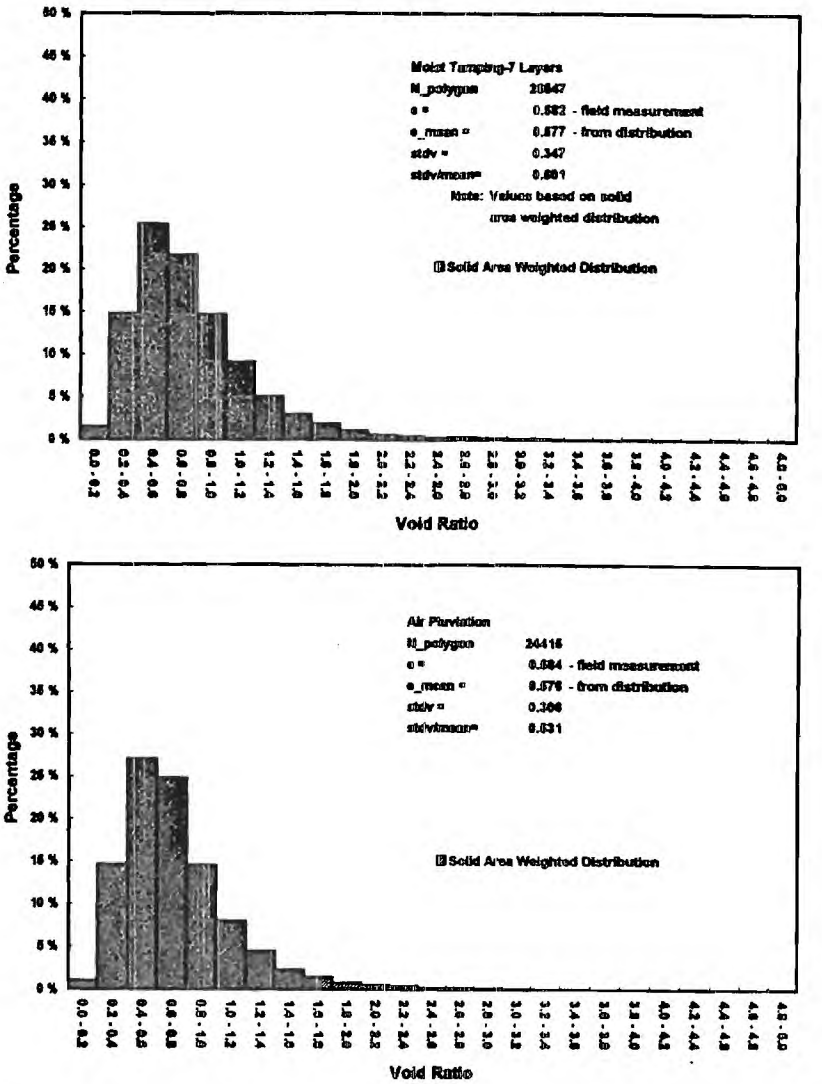

Figure 3 Distributions of Local Void Ratio for Different Preparation Methods

One of the important consequences of data such as shown in Figures 3 and 4 is that the manner in which global void ratio is used may not be sufficiently precise for many future applications, including those to study parameters such as post-liquefaction strength. For example, when referring to tests on saturated specimens, the terms "constant volume", "constant void ratio" and "undrained" are used interchangeably however while this is true in a global sense based on measurements of the mass and volume of the specimen, it may be appropriate to add an additional parameter to our terminology to more correctly describe the soil behavior. One approach to this is illustrated schematically in Figure 5 which shows the undrained behavior of isotropically consolidated specimens at different initial global void ratios. Using q-p'-e space, each test would in fact lie on a single plane parallel to the q-p' axes however, at any stress state within a given constant e plane, the distribution of local void ratio could vary not only as a function of the initial structure but also as a function of the stress path and hence state. This is illustrated in the figure by superimposing the local void ratio distribution plots perpendicular to the lines of constant void ratio to reflect the fact that while the global void ratio and hence the mean of the local void ratio distribution is constant, the distribution of the local void ratio about the mean is changing.

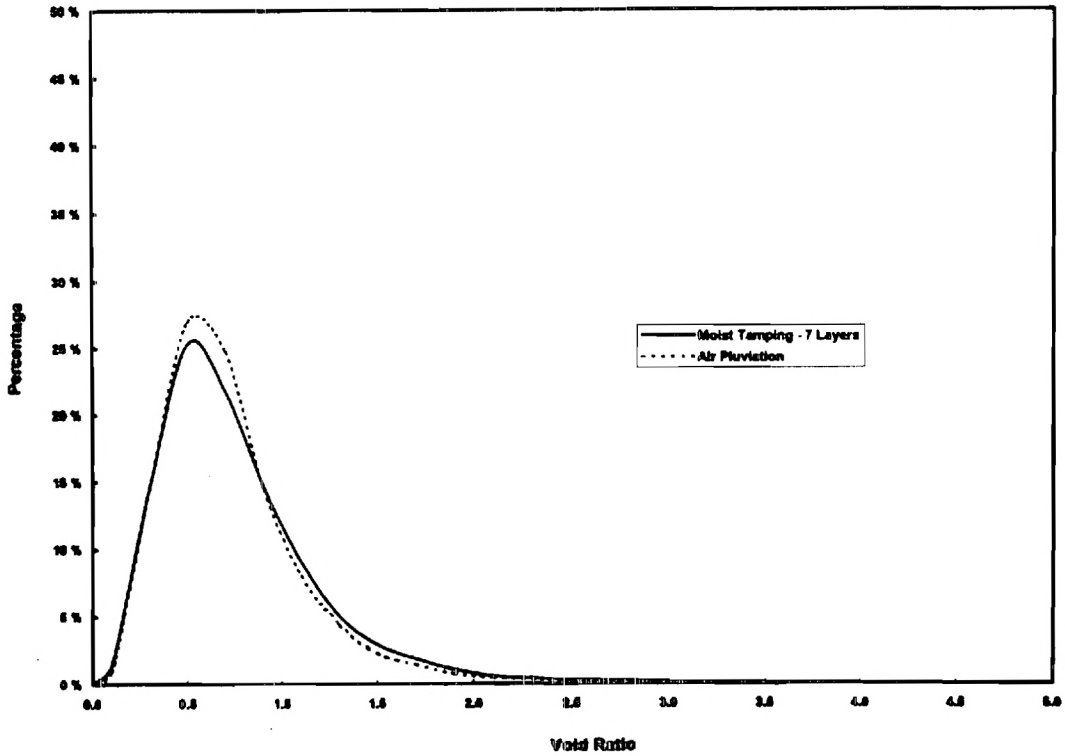

Figure 4 Comparison of Local Void Ratio Distributions

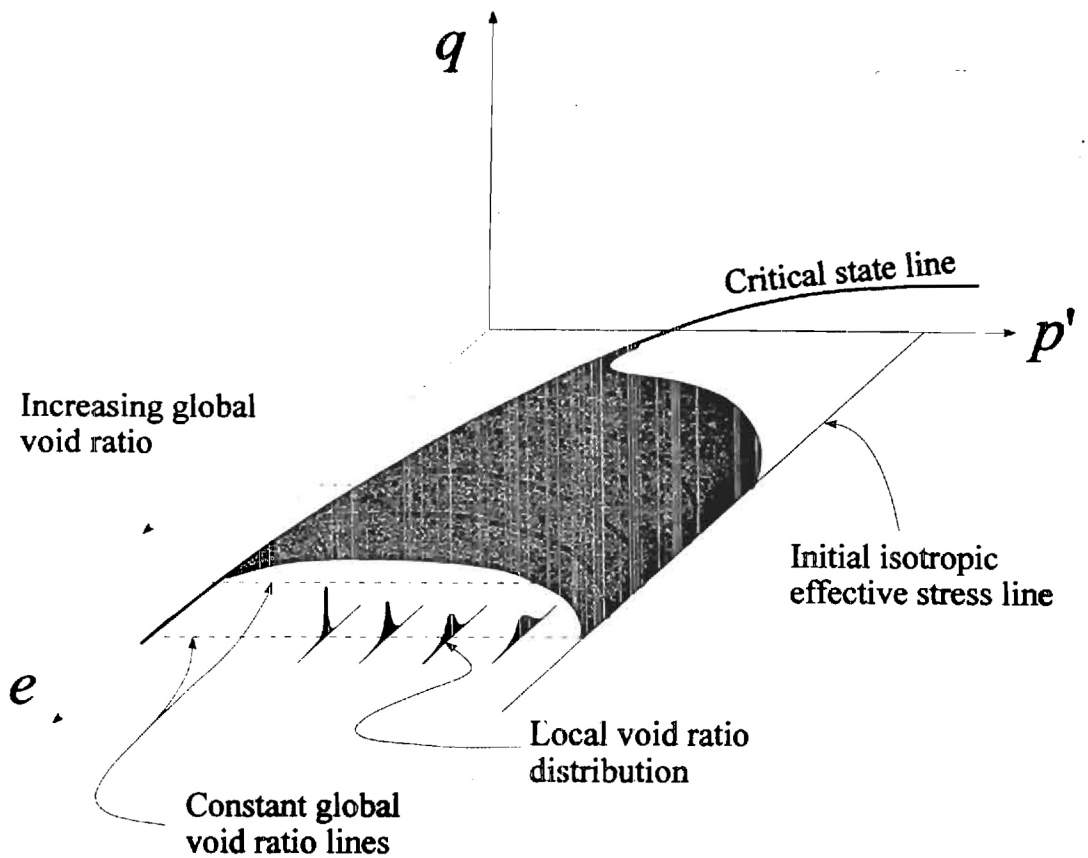

Figure 5 Illustration of the Distinction Between Global and Local Void Ratios

Attachment # 4

Quantification of Sand Structure and Its Evolution During Shearing Using Image Analysis

Chapter 1 Introduction

Chapter 2 Literature Review
- Reconstituted Soil Specimen Preparation Methods
- Soil Specimen Preservation
- Image Analysis of Soil Structure
- Statistics Modeling of Granular Material Packing

Chapter 3 Experimental Techniques and Developments
- Air Pluviation System
- Moist Tamping System

Chapter 4 Soil Specimen Preservation by Epoxy Impregnation
- Criteria of Epoxy Used for Soil Specimen Preservation
- Epoxy Impregnation System
- Effect of Initial Void Ratio on Final Void Ratio of Soil Specimen during Epoxy Impregnation and Curing
- Effect of Preparation Method on Final Void Ratio of Soil Specimen after Epoxy Impregnation and Curing

Chapter 5 Coupon Surface Preparation for Quantitative Image Analysis
- Introduction
- Microscope Illumination
- Coupon Surface Preparation
  - Sectioning
  - Planar Grinding
  - Sample Integrity
  - Polishing
- Image Accuracy and Calibration

Chapter 6 Study of Structure of Laboratory Reconstituted Soil Specimen
- Soil Properties
- Test Program
- Local Void Ratio Distribution
- Spatial Void Ratio Distribution
- Evolution of Local and Spatial Void Ratio Distribution during Drained Triaxial Compression Testing
- Statistical Modeling

Chapter 7 Study of Structure of Natural Soil
- Soil Specimen Tested - Canlex Fraser Delta Sand
- Image Analysis Results

Chapter 8 Conclusions and Recommendations

SUMMARY

Quantification of sand structure using image analysis is a noble and promising technique in soil mechanics research. It can provide vital information of sand structure, such as local void ratio distribution and fabric tensors (sand particle orientations), which directly affect the behavior of sands. However, accurate quantitative measurement of image requires high quality specimens, specimen coupon surfaces and accurate images.

A methodology was developed to preserve the structure of soils. Factors affecting the quality of the preserved specimens were investigated. As demonstrated in this research, both laboratory reconstituted soil specimen and natural soil specimens can be effectively preserved using this methodology.

A procedure was developed to prepare specimen coupon surfaces for image analysis. The effects of illumination and polishing on captured images were studied and discussed. The importance of image quality and accuracy in image quantification was emphasized. Procedures to calibrate an image were developed.

Specimens of laboratory reconstituted sand (ASTM Graded Sand), prepared by both moist tamping and air pluviation to different void ratios, were preserved by the developed epoxy impregnation procedure. Image analysis were then performed on the images captured from prepared specimen coupons' surface to quantify sand structure. Local void ratio distribution and spatial void ratio distribution of these specimens were calculated. Statistical parameters, the mean and the standard deviation, of local void ratio

distributions were found to be a function of the specimen preparation methods and specimens' densities. The characteristics of these two parameters with respect to moist tamping and air pluviation of ASTM graded sand were identified.

Spatial variation of void ratios was also studied. It was evident that, specimens prepared by air pluviation were not as uniform as expected. In specimens prepared by moist tamping, large variation of void ratios across the boundaries of moist tamped layers was also observed and quantified.

The effect of specimen preparation methods on the orientation of sand particles was studied via the anisotropy of the sand. The sand particles in moist tamped specimens were found to be more randomly oriented. It was also found that, air pluviation produced specimens with sand particles more horizontally oriented.

The evolution of sand structure along a stress path was studied via a series of specimens preserved at different states of triaxial shearing. According to the local and spatial void ratio distributions of the specimens, it was evident that, the dilation of sand particles initiated in the central region of a specimen during barreling failure. From this region, the dilation of sand particles expanded in all directions. Nevertheless, while the central region has reached critical state other regions, especially at both ends of a specimen, still maintained much lower void ratios. It was also found that, while sand particles dilated and approached critical state, void ratios became more uniform.

The shear band developed in a catastrophic failure was studied. From the spatial void ratio distributions, it was evident that sand particles had reached the critical state in the local regions along the shear band.

The anisotropy of sand particles during and after failure was studied. It was observed that, a strong particle alignment does not necessarily translate to high void ratio. It was therefore suggested, the major realignment of particles was a consequence of soil mass movement.

From this study, it was clearly evident that, the state of a soil can be more correctly identified by localized behavior of the soil, instead of the global measurement of a specimen. To quantify these localized soil behaviors, new technology is required. The methodology developed in this research proved itself as viable and practical. The study of natural sand (CANLEX Delta Fraser Sand) also demonstrated that, this methodology can effectively quantify the in-situ structure of the soil.

It was concluded that, statistical parameters, such as the mean and the standard deviation of the local void ratio distribution, should be introduced into existing mechanical models to better describe the behavior of soils.

J11 Void Ratio Distribution
Moist Tamping 7 layers
Void Ratio e_f = 0.577 (D_r=76%)

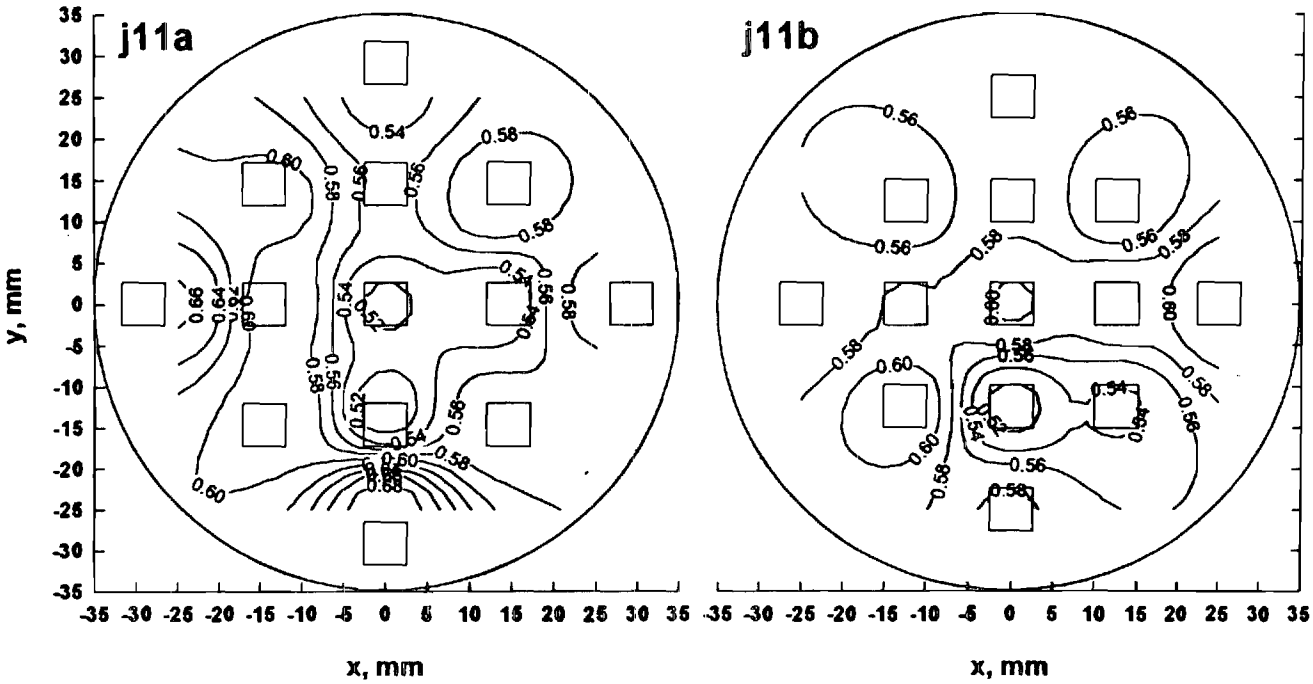

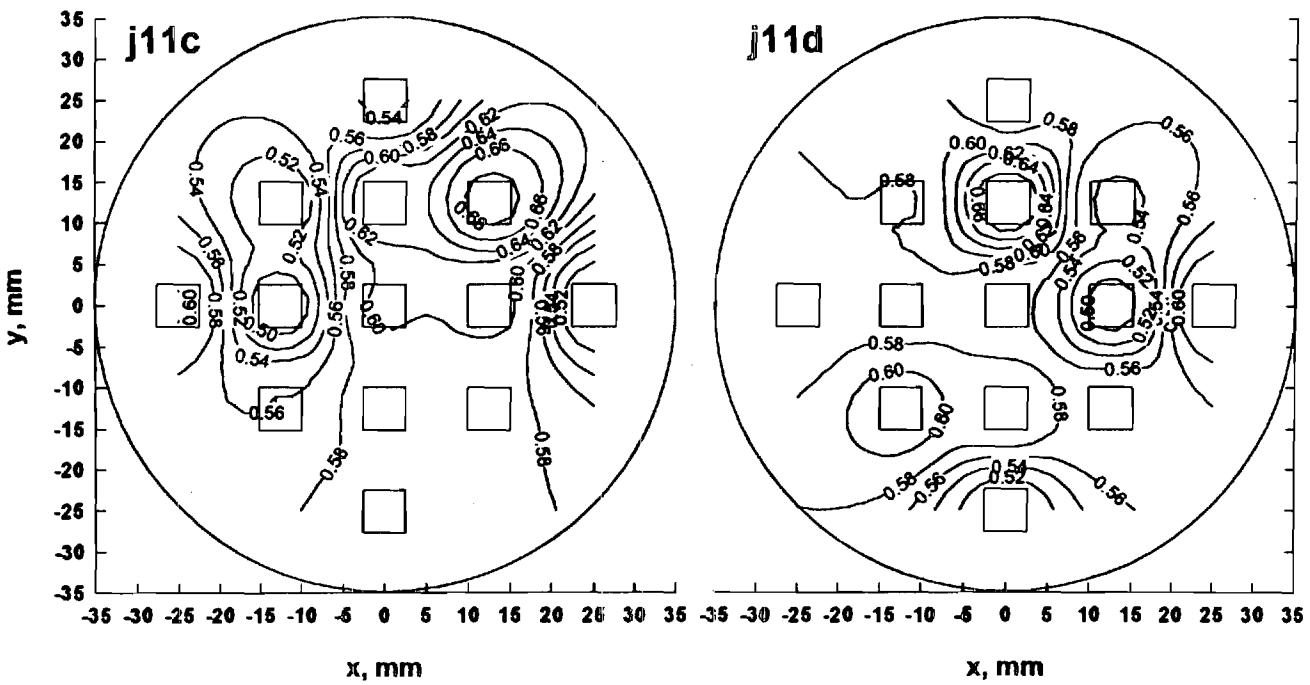

J11 Void Ratio Distribution
Moist Tamping 7 layers
Void Ratio e_f = 0.577 (D_r=76%)

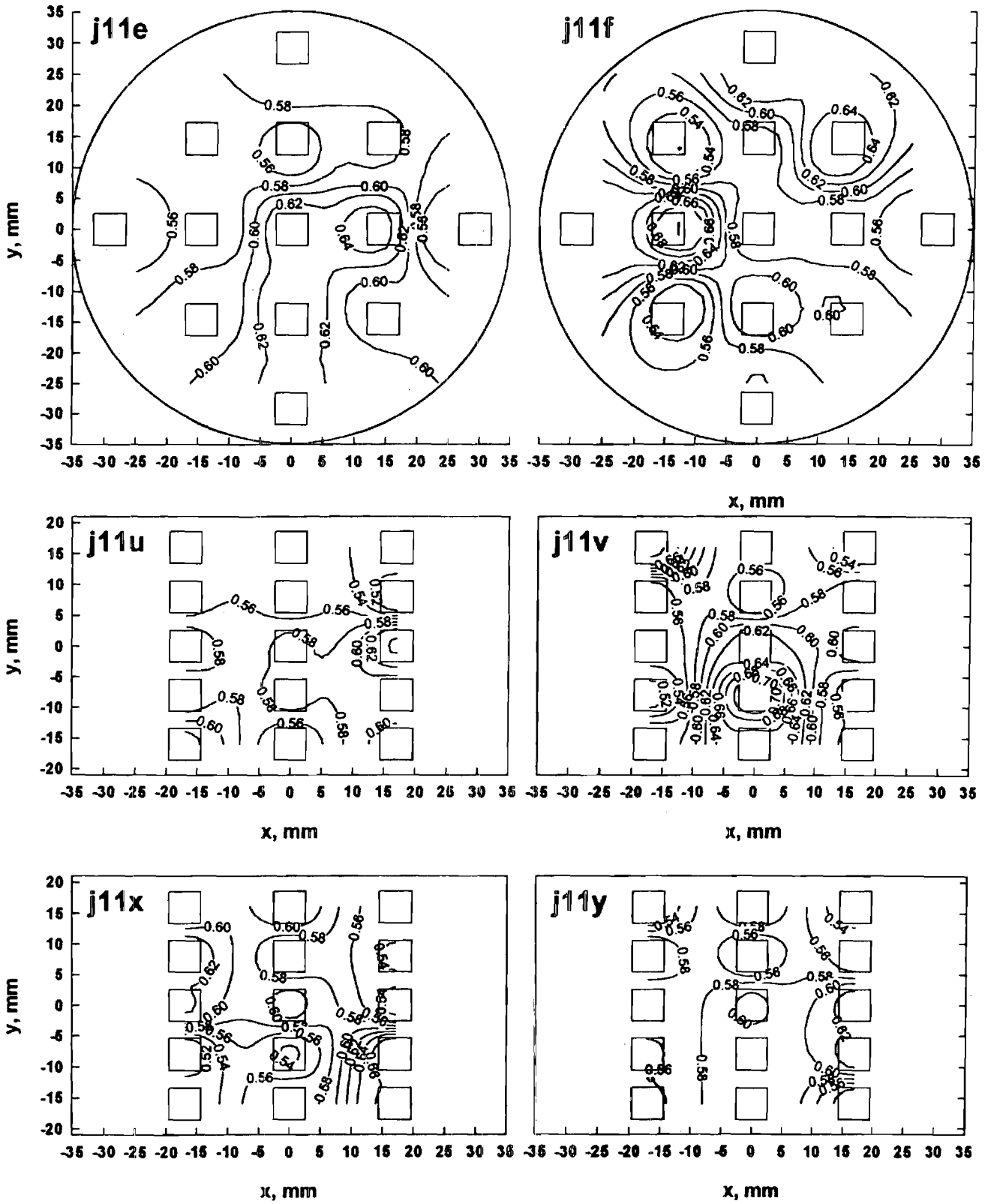

J13 Void Ratio Distribution
Moist Tamping 7 layers
Void Ratio e_f = 0.657 (D_r=51%)

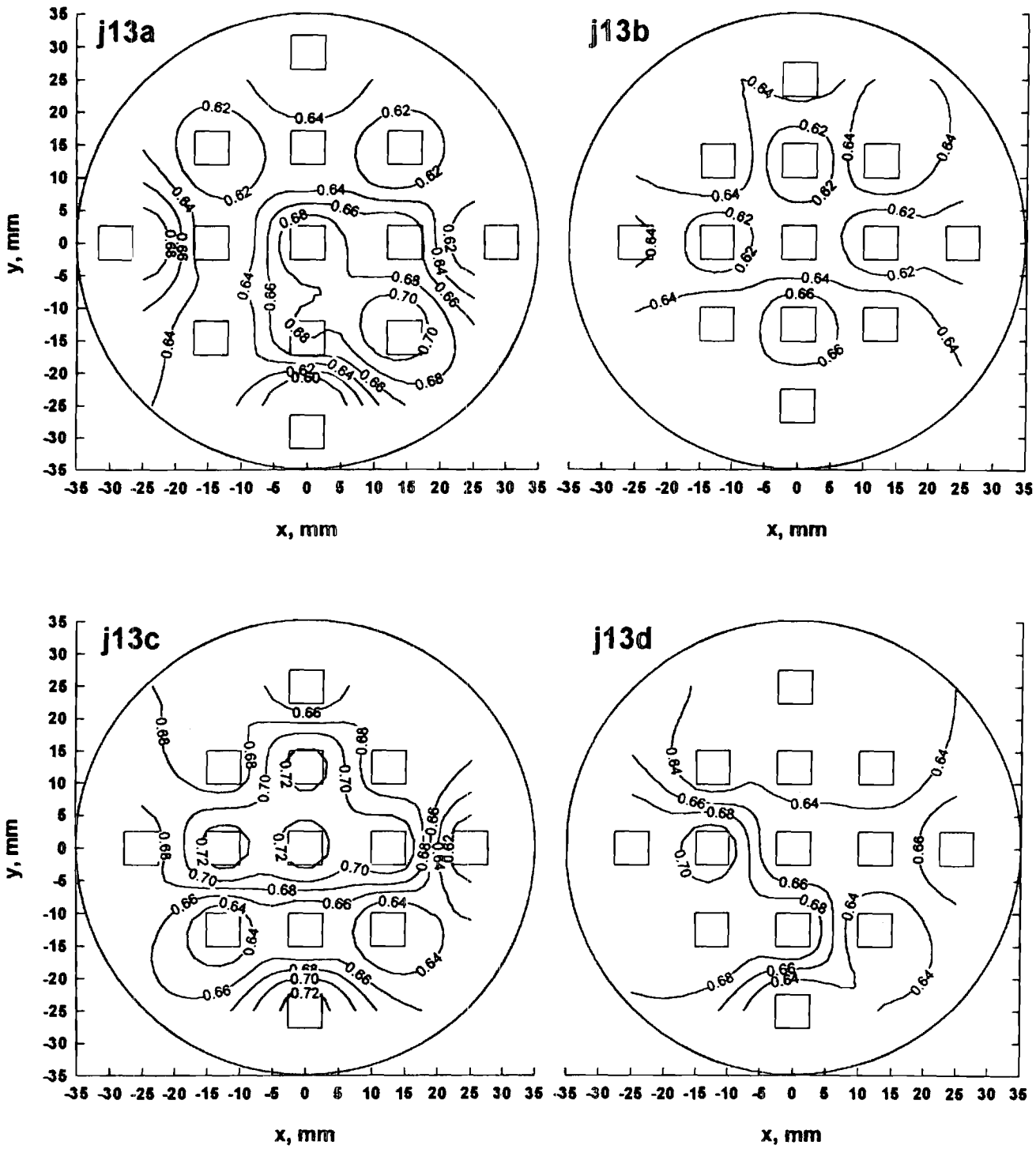

J13 Void Ratio Distribution
Moist Tamping 7 layers
Void Ratio e_f = 0.657 (D_r=51%)

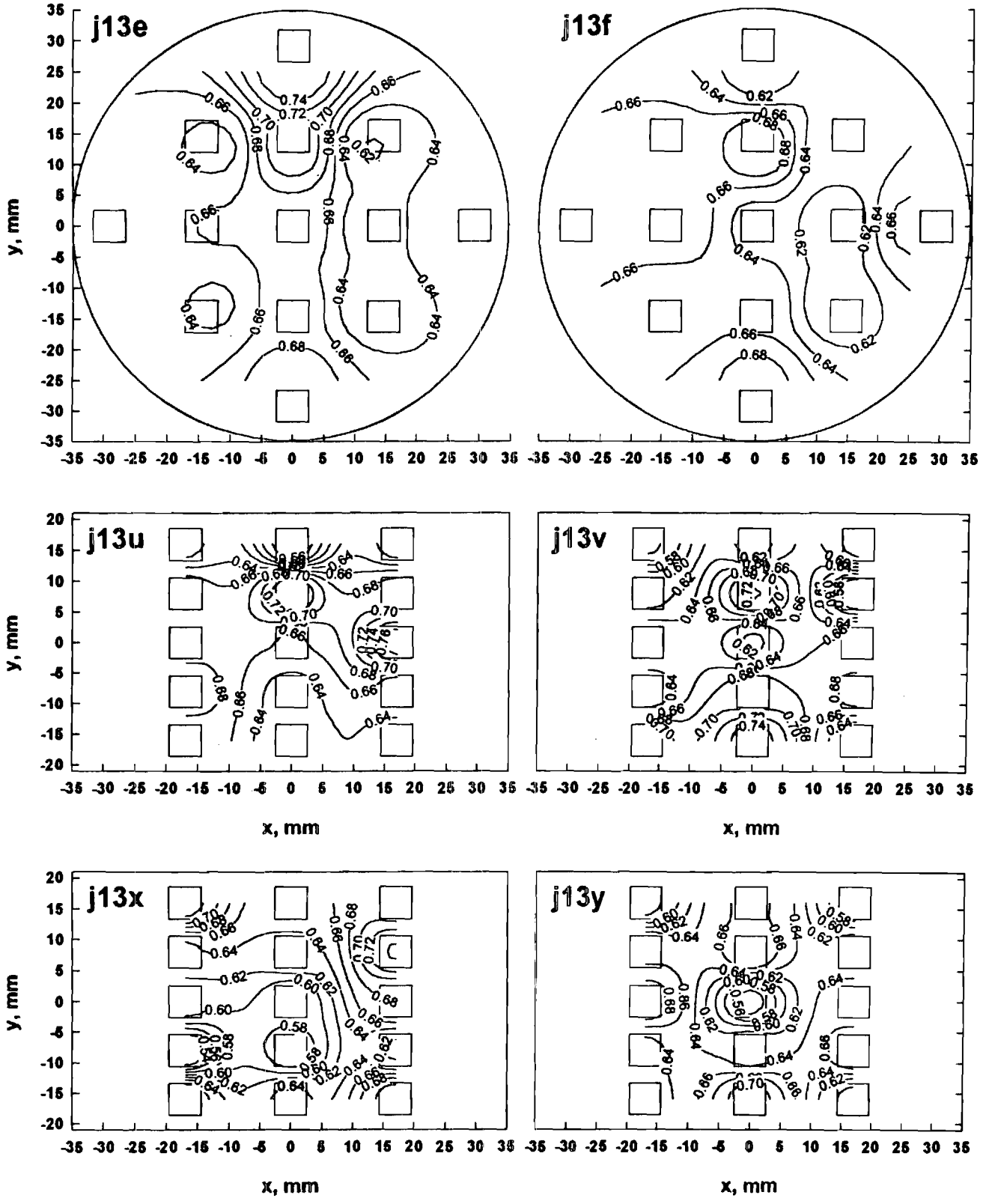

Local Void Ratio Distribution

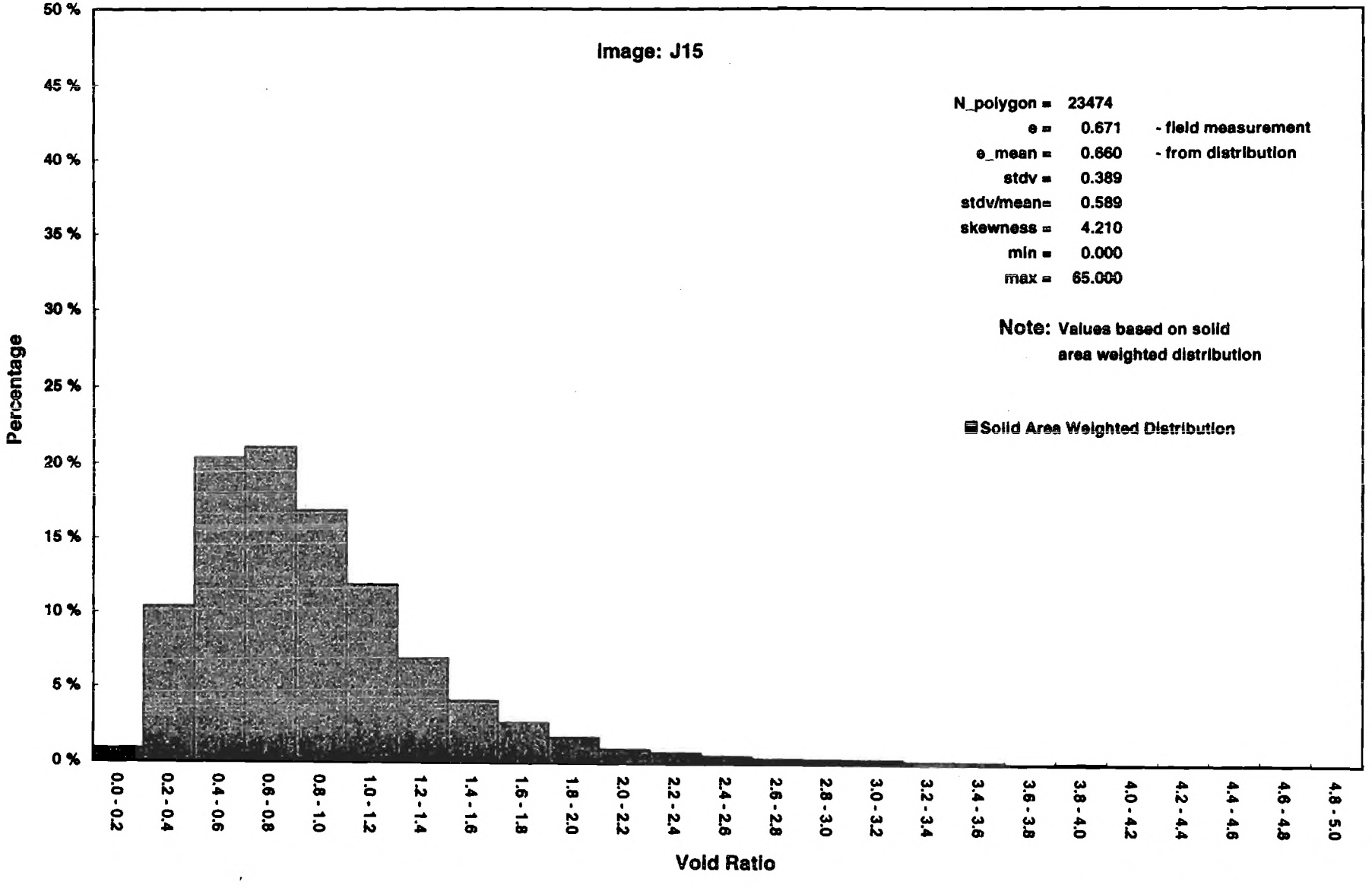

Local Void Ratio Distribution

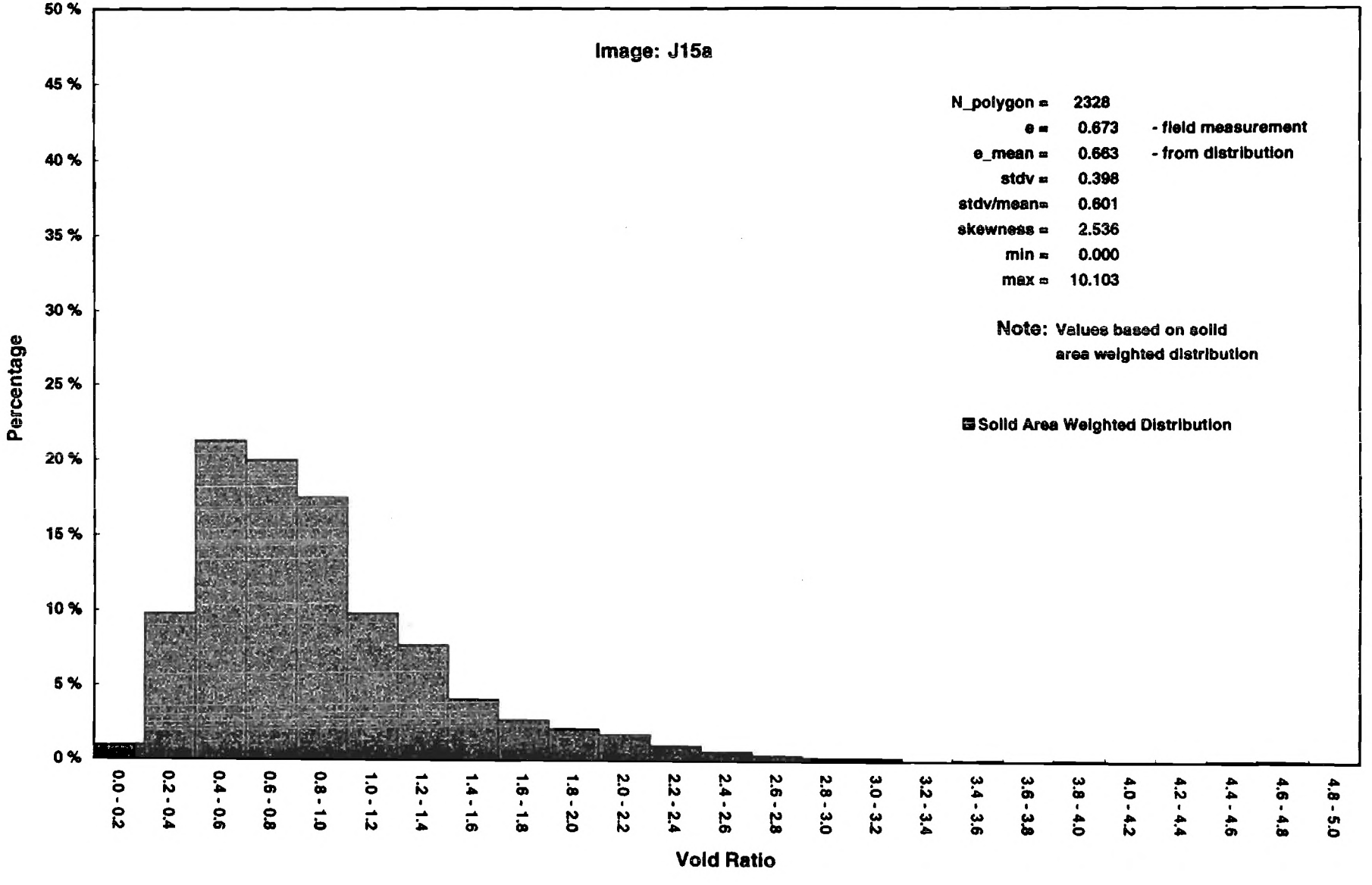

Deh-Jeng Jang

Local Void Ratio Distribution

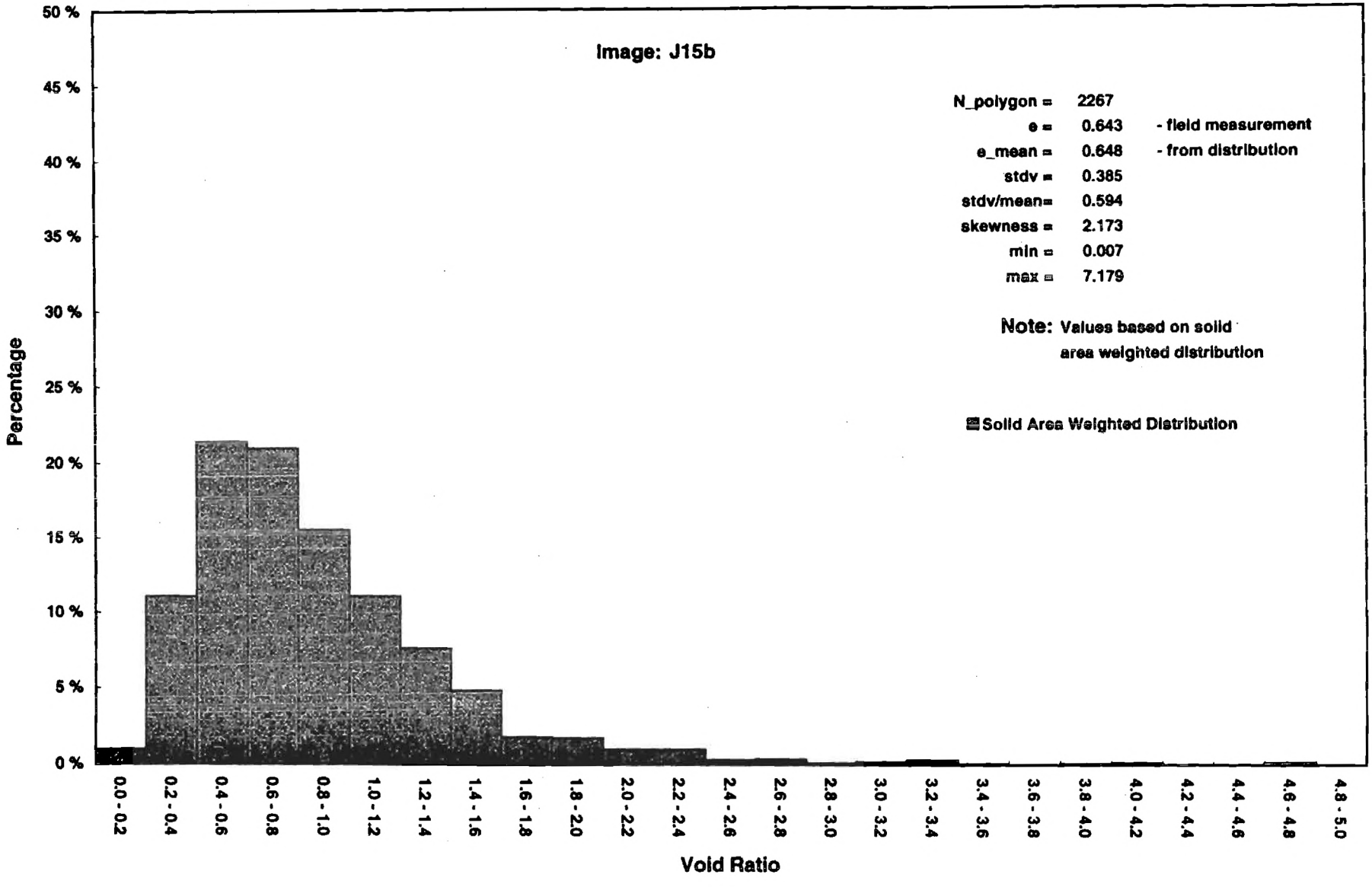

Local Void Ratio Distribution

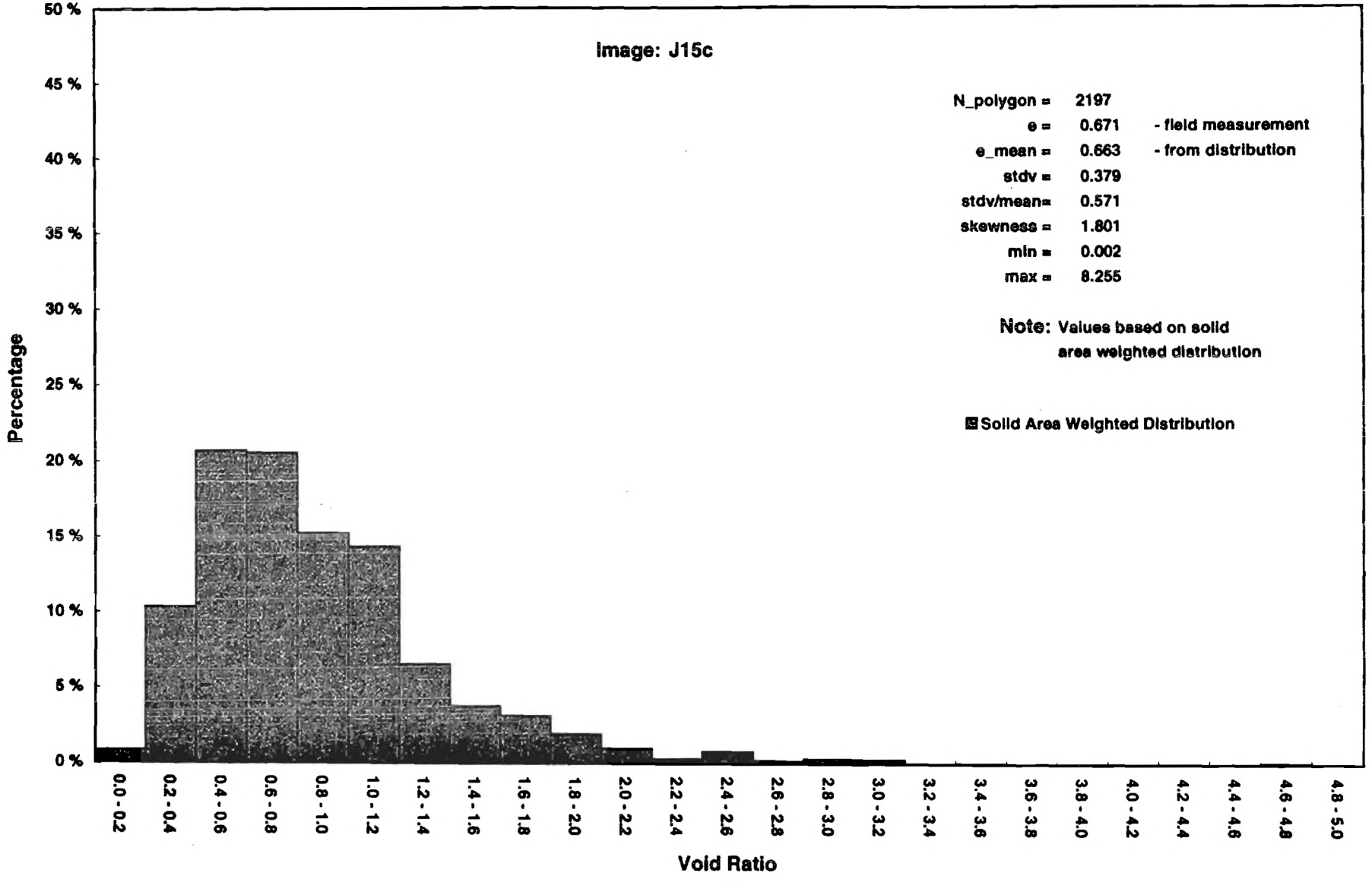

Local Void Ratio Distribution

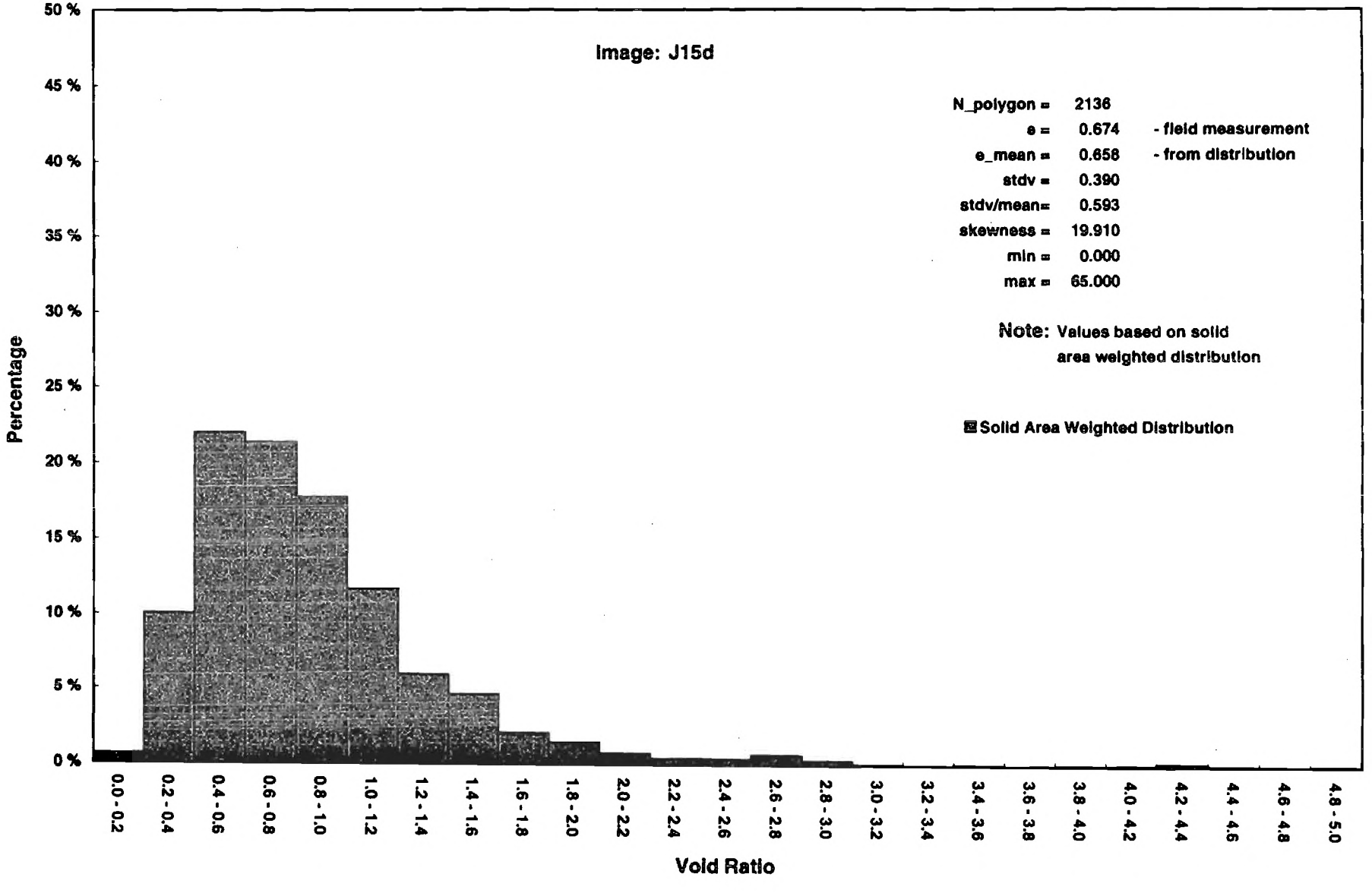

Local Void Ratio Distribution

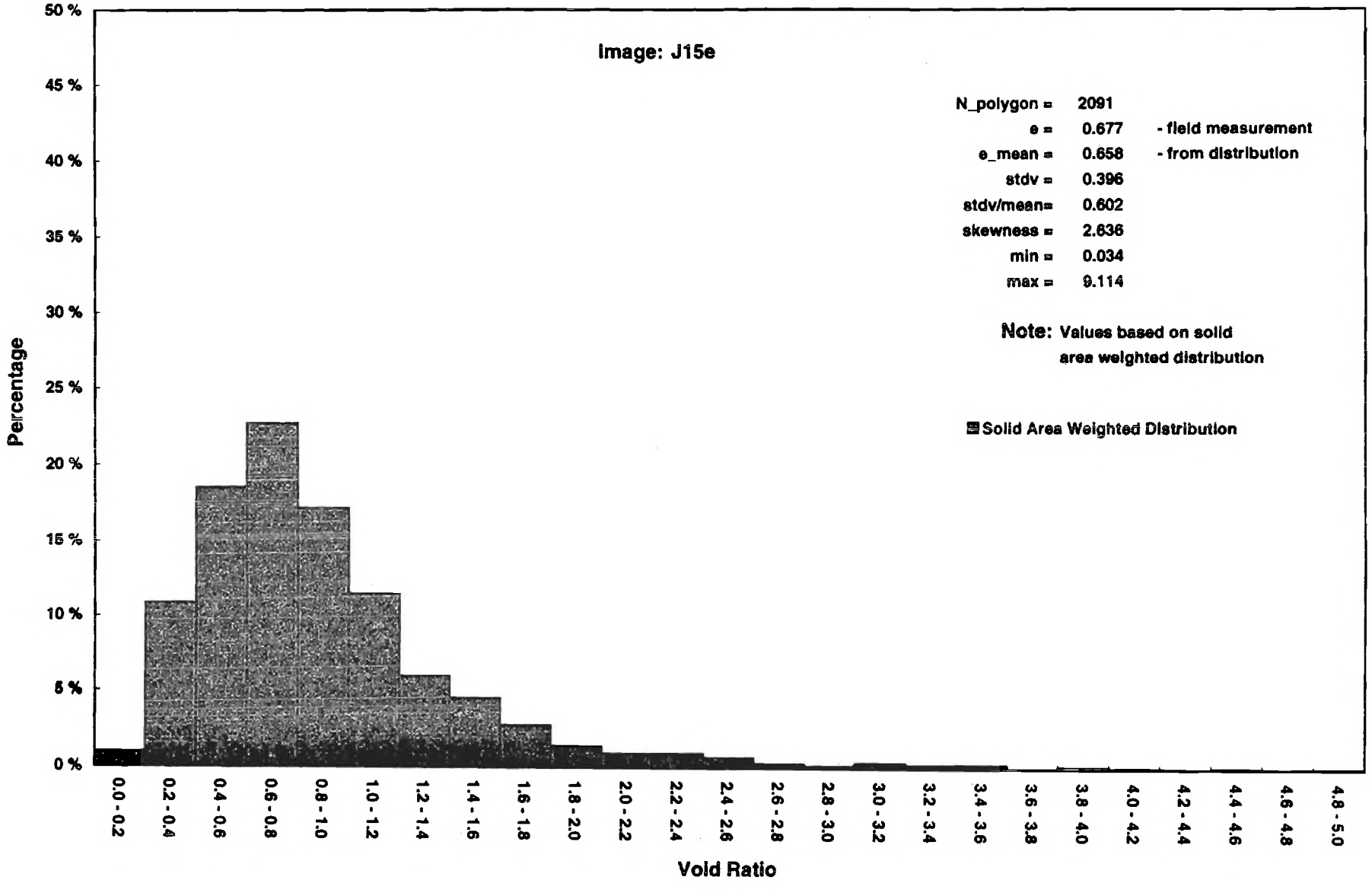

Local Void Ratio Distribution

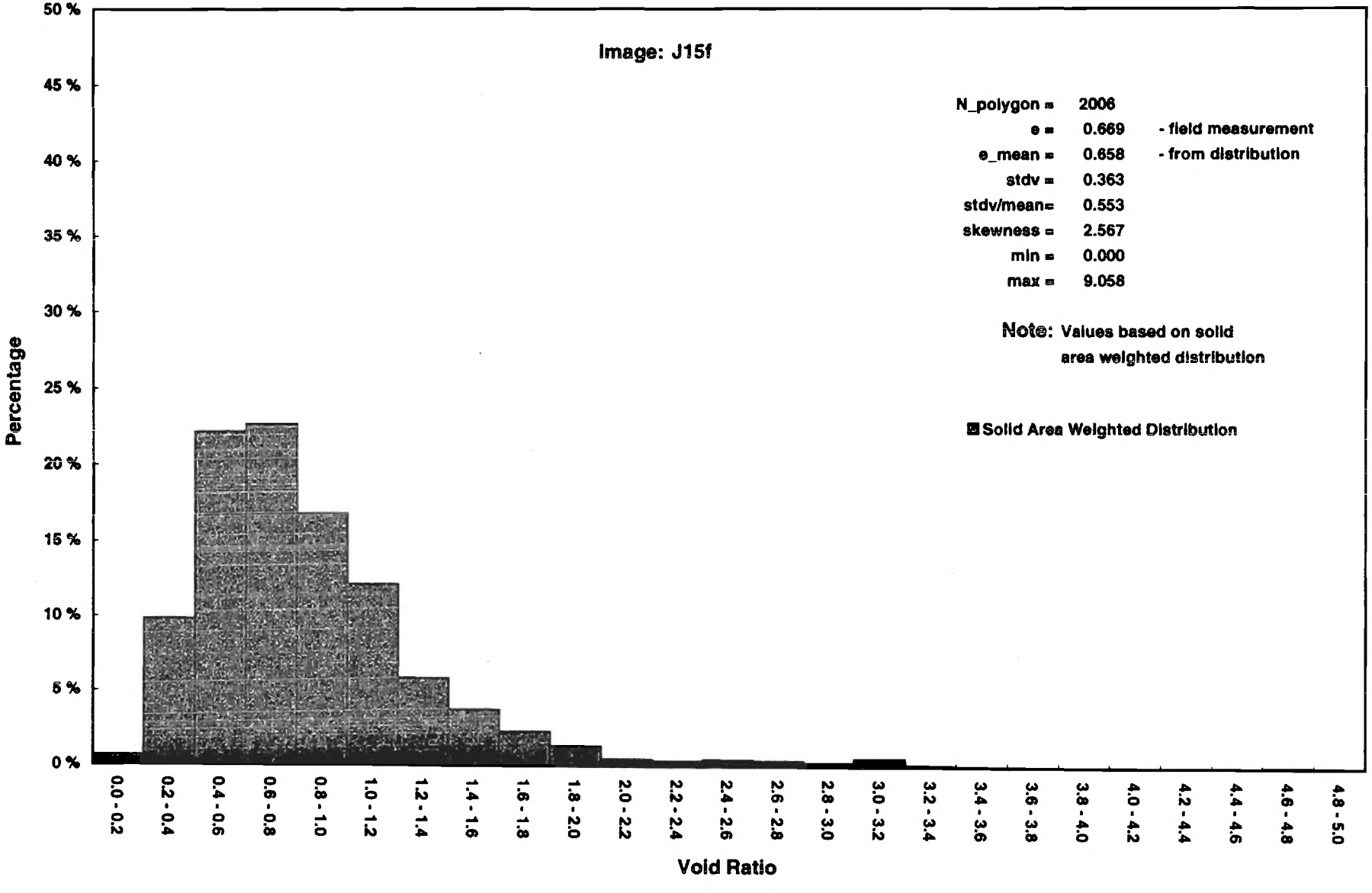

Local Void Ratio Distribution